



Successful First Light for the VLT Interferometer

C. CESARSKY, ESO Director General

Another momentous event took place recently at Paranal when the “First Fringes” were obtained for the VLT Interferometer, more than two weeks in advance of the planned schedule. As will be known, everything went extremely well and it was possible to do right away some real physical measurements as a most visible proof to the scientists and the public of the effectiveness of the VLTI concept. (See the article on page 2 and ESO Press Release 06/01.)

In fact, it seems that we have become used to this kind of positive experience at ESO, following the effective start-up of the four Unit Telescopes during the past years. We must not forget, however, that to do interferometry means to enter into an entirely new world where state-of-the-art astronomical technology is pushed to its utmost limits. I doubt that many people outside the inner circle fully appreciate what kind of skills and efforts it has taken to reach that momentous event when, on March 17, 2001, the first light from the bright star Sirius was directed through the complex VLTI optics to the VINCI instrument in the Interferometric Laboratory. This would never have been possible without the enormous dedication of a large number of people at ESO, in collaborating astronomical institutes and, not least, within European industry. All astronomers should be thankful for their hard work which led to the beautiful performance of all elements, in particular the Delay Lines and VINCI, already at the moment of VLTI First Light.

It gives us all great confidence to see how these first observations were immediately followed up by on-line determinations of angular diameters of several other stars, including – I guess not quite by chance – for the first time ever of that of one of the stars in the Southern Cross that is depicted in the ESO logo!

European astronomy can be proud of these early achievements and I have little doubt that interferometric observations will in due time become as common and easy to perform as normal observations are now at the VLT and other ESO telescopes, thanks in particular to the implementation of very user-friendly VLTI software. Indeed, I believe that this now opens fantastic perspectives in virtually all fields of modern astronomy and that we are now entering an era in which “stars will never be point sources anymore”!



Celebrating the moment of “First Fringes” at the VLTI. A number of people have, with their talent and determination, made this achievement possible. See the list of authors of the article on page 2 and the names in this caption. At the VLTI control console (left to right): P. Kervella, V. Coudé du Foresto, P. Gitton, A. Glindemann, M. Tarenghi, A. Wallander, R. Gilmozzi, M. Schoeller and W. Cotton. Bertrand Koehler was also present and took the photo.

Light at the End of the Tunnel – First Fringes with the VLTI

A. GLINDEMANN, B. BAUVIR, F. DELPLANCKE, F. DERIE, E. DI FOLCO, A. GENNAI, P. GITTON, N. HOUSEN, A. HUXLEY, P. KERVELLA, B. KOEHLER, S. LÉVÊQUE, A. LONGINOTTI, S. MÉNARDI, S. MOREL, F. PARESCHE, T. PHAN DUC, A. RICHICHI, M. SCHÖLLER, M. TARENGHI, A. WALLANDER, M. WITTKOWSKI, R. WILHELM

1. Introduction

On March 17, 2001, at 10 p.m. local time, the VLT Interferometer project reached a major milestone by observing the first interferometric fringes on a star, using two siderostats and the test camera VINCI. After almost 10 years of planning, analysing, simulating and

Parameter	Specification	Achieved
Transfer Function	0.25	0.87
Stability	±5% over 5 hours	±1% over 3 days
Measurement accuracy for a star diameter	±5%	±2%

Table 1: The criteria for First Fringes as specified and as achieved.

lay Line System moving a Cat's Eye reflector system with micrometre precision.

Early in 2000, activities started on a large scale. Containers arrived in front of the VLTI control building and equipment disappeared inside, like in the hold of a cargo ship. Inside the tunnel, hundreds of holes were drilled, cables were installed and the computer network was configured. An ante room was built at the entrance of the VLTI beam combination laboratory to properly seal off the tunnel and the laboratory as clean rooms. With the installation of computers and telephones the VLTI control building looked more and more like a real control centre.

In the middle of the year, the first piece of high-tech equipment arrived when the installation of the Delay Lines started. After the Delay Line Integration Team had spent the better part of last year in the tunnel, the first three Delay Line Systems were commissioned (see Fig. 2). For the installation of the rails of

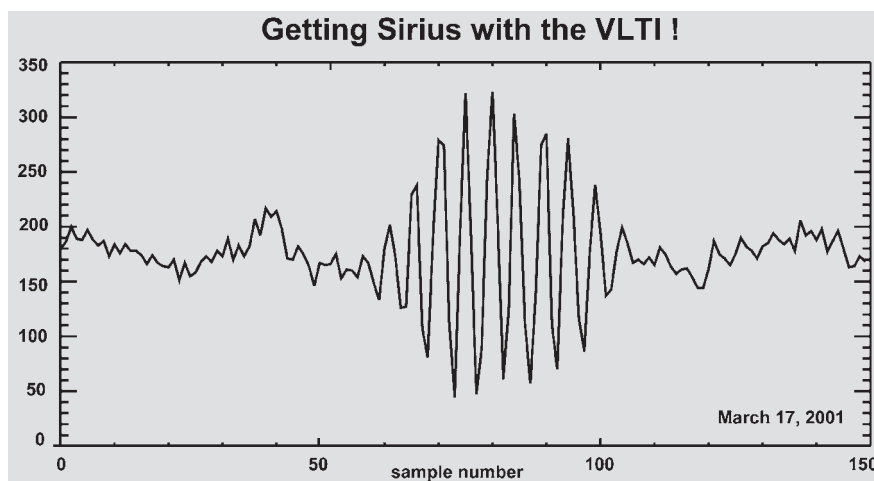


Figure 1: The very first fringe pattern of the VLTI observing Sirius.

testing, this was a memorable moment especially because the quality of the first fringes was truly outstanding (see Fig. 1). In the following commissioning phase, several sources in the sky were observed to verify the performance of the VLTI. We found that all specifications were met or exceeded (Table 1). However, numerous tasks are still ahead of us before science operations can start. We are now looking forward to the next major milestone combining the light from two Unit Telescopes in November this year.

2. The Last Two Years

At the time when the last *Messenger* article on the VLTI [1] was written, only 18 months ago, the Delay Line Tunnel was a rather deserted place. It was empty and clean but there was not a single one of those dozen mirrors that are now in place, aligned with sub-millimetre precision. And there was no De-



Figure 2: The Delay Line Integration Team with staff from ESO, Fokker, TPD/TNO and S&B after integrating the second Delay Line on November 22, 2000.

the Delay Lines, a sophisticated measurement system with water level gauges was used providing a flatness of less than $25 \mu\text{m}$ over the full length. The Delay Line System is one of the most spectacular subsystems of the VLT, moving the 2-m-long carriages with the Cat's Eye reflector at speeds up to 0.5 m/sec in the 130-m-long tunnel. While moving the carriage, the reflected beam is tilted less than 1.5 arcsec at all times, the absolute position accuracy is $30 \mu\text{m}$ over the full range of travel of 65 m and the position error is of the order of 20 nm. Fulfilling the specifications, the contract with Fokker was closed a few weeks ago.

At the same time, the 40-cm siderostats were tested close to the Mirror Maintenance Building. The VLT control software was installed to make them "look" the same as the Unit Telescopes when using the VLT Supervisor Software. They were moved up to the summit early in 2001 and tested successfully shortly thereafter.

Meanwhile in Europe, the test camera VINCI was put together at Paris Observatory in Meudon, and the observing software was produced by the Observatory of Toulouse. Only one year after the signature of the contract, the instrument was delivered to ESO Garching for integration with the infrared camera LISA provided by the Max-Planck-Institute for Extraterrestrial Physics in Garching. It proved extremely useful to have a three-month test period in Garching, allowing us not only to put together the individual pieces of hard- and software under laboratory conditions, but also to rehearse the integration of the complete system after transporting it from Paris to Garching. With this experience, the integration, testing and commissioning of VINCI at Paranal was a swift and seamless exercise in the first two months of 2001 (see Fig. 3), supported by the VINCI team from Meudon.

At the beginning of 2001, the Delay Line Tunnel and the beam combination laboratory at Paranal saw some heavy pieces of equipment arriving: five optical tables each weighing around a ton. Solid optical alignment units were also installed providing a reference mark at every turn of the beam.

Finally, towards the end of February 2001, all mirrors, tables, benches, and detectors were installed and tested, and the tunnel and the laboratory were closed for normal access to ensure the clean-room conditions and the stable

γ Cru:	24.7 ± 0.35 milliarcsec
α Cen:	9.6 ± 0.5 milliarcsec
δ Vir:	10.4 ± 0.6 milliarcsec
R Leo:	24.3 ± 0.4 milliarcsec

Table 2: Star diameter measurements with the VLT in April 2001.

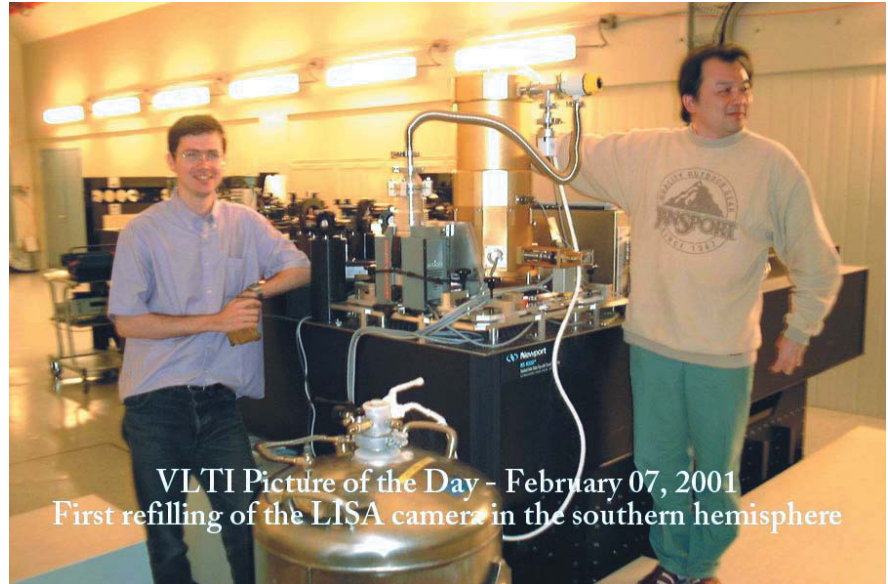


Figure 3: VINCI in the VLT beam combination laboratory. On February 7, 2001, the opto-mechanical alignment was finished and the LISA camera was cooled down for the first time at Paranal.

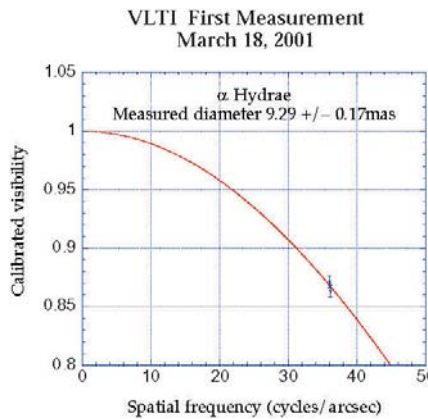


Figure 4: Three individual measurements were taken to determine the first diameter of a star, α Hydras. The best fit of the visibility curve and the three measured points, almost on top of each other, together with the error bar of 0.17 milliarcsec are displayed. The measured diameter of 9.29 milliarcsec is well within 15% of indirect (photometric) estimates of about 9 milliarcsec.

thermal environment required for First Fringes.

3. First Fringes

Planning for First Fringes a few years ago, we decided to specify criteria asking for more than just catching fringes in passing for a lucky moment. We defined that the VLT should reliably provide fringes with a contrast of 0.25 for a non-resolved star (when it is 1 in the perfect case) and with a contrast stability of 5% over 5 hours. In addition, a star diameter should be determined within 15% of a former measurement of the diameter. Choosing these numbers was somewhat arbitrary; it was a measure of our confidence in what could be achieved in reasonable time.

In the project schedule, the second half of March was available to fulfil the First Fringe criteria. We chose a baseline of 16 metres for the first attempt to



Figure 5: The First Fringe Team after having measured the first star diameter.

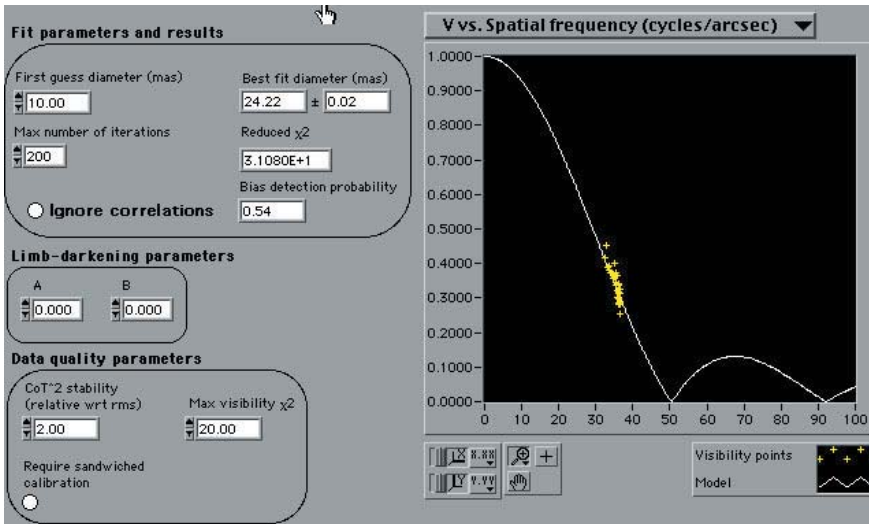


Figure 6: The best fit of the visibility curve of R Leo and individual points on the curve measured over several hours. This result illustrates very nicely the change of effective baseline (from 13.7 m to 16 m, i.e. from ≈ 30 to ≈ 36 cycles per arcsec) with the sidereal motion of the star. As expected, the measured contrast is going down for longer effective baselines. This computer display is part of the data analysis software provided by the Jean-Marie-Mariotti Centre for Interferometry in France.

see fringes. The tension was intense when star light was guided for the first time from the primary mirror of the siderostats, through the light ducts, the tunnel and the beam combination laboratory to the detector of VINCI. And, after a few nights, the result was spectacular. The very first result, the fringe pattern of Sirius, is shown in Figure 1.

This was a joyful moment and the champagne corks were popping. But it was also a touching moment when we kept a minute of silence remembering Jean-Marie Mariotti who was one of the fathers of the VLTI and who died much too early three years ago.

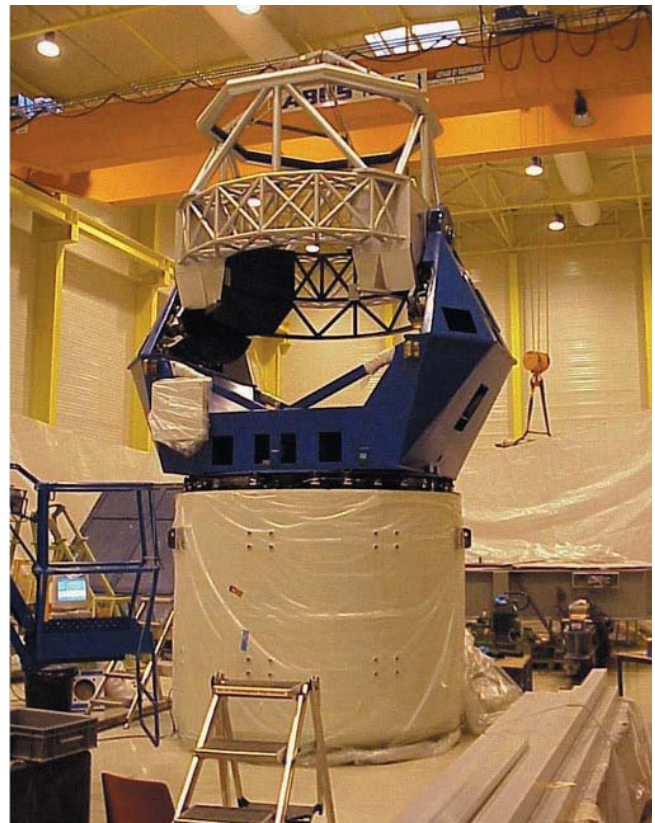
In the following nights, more stars were observed. We fulfilled all First Fringe criteria on March 18, 2001, by determining the diameter of α Hydrae to 9.29 ± 0.17 milliarcsec (see Fig. 4). This measurement is within 15% of indirect (photometric) estimates of about 9 milliarcsec. The next day saw a very happy and exhausted First Fringe Team (Fig. 5). After three nights, the criteria for stability were fulfilled in an impressive manner: The equivalent point source contrast, i.e. the interferometer transfer function, was measured to be 0.87 and to be stable to within 1% over three days what is far better than the required 5% over five hours (see Table 1).

After the first week of commissioning, the performance can be summarised as follows: Fringes were found on any bright star in the specified field of view (60 degrees of zenith) within $500 \mu\text{m}$ of the nominal zero optical path difference position. In one case, Sirius was observed only 10 degrees above the horizon without difficulties. The smallest visibility that was measured was around 5%. No contribution from internal tunnel seeing could be detected. The limiting magnitude of VINCI, with

the siderostats effectively stopped down to 100 mm, is about $K \approx 1$. It is possible to guide with the siderostats on stars down to $V = 9$, and to do blind acquisition in VINCI.

During the first few nights we had the benefit of a benign atmosphere providing rather slow seeing and, thus, slow fringe motion. The mean value of the Paranal atmosphere is a factor of two faster, either reducing the sensitivity about one magnitude due to shorter integration times for the same signal-to-noise ratio (SNR) of the measured visibility, or reducing the SNR for the same sensitivity. The latter requires averaging over more observations in order to improve the SNR.

Figure 7: The telescope structure of the first Auxiliary Telescope (AT) during final integration at AMOS in Belgium. The 1.8-m telescope with an Alt-Az mount, like the Unit Telescopes, provides a collimated beam 1.2 m underground that is sent towards the Delay Line Tunnel through insulated light ducts. The ATs are relocatable on 30 stations using special transporters moving on rails. The transporter structure is not shown on the photograph.



It is also worthwhile noting that even in this early phase of commissioning the VLTI was run in complete remote control. Except for refilling the VINCI dewar and some other day-time activities, not a single visit of the tunnel or the beam combination laboratory was required during operation at night. For data reduction, a first version of the pipeline was in operation providing visibility values of the fringe pattern and storing the data in the archive. A more sophisticated data analysis software package to determine stellar diameters was provided by the Jean-Marie-Mariotti Centre in France. In the meantime, most of this software is implemented in a second version of the ESO pipeline.

In the course of April, some interesting results were achieved, demonstrating the potential and the reliability of observations with the VLTI. Some more stellar diameters were determined (see Table 2), e.g. of γ Cru (the star on the right of the ESO logo), of α Cen (our closest neighbour in the universe), of δ Vir and of R Leo. Due to the sidereal motion of R Leo, the effective baselines changed by about 10% over three hours. Observing R Leo over this period of time means that different points on the visibility curve can be measured. Figure 6 illustrates very nicely the effect of the change in baseline on the fringe contrast.

It is planned to have a few periods of about 8 days of science observations later this year. All scientific results will become public in the ESO archive as it was done with the UT science data during UT commissioning.

4. The Next Steps

The next major milestone in 2001 will be First Fringes with UT1 and UT3 in November. The installation of the coudé optical trains and of the relay optics in the Unit Telescopes is progressing – the coudé focus of UT3 had its First Light in May – as well as of the beam compressors in the VLTI Beam Combination Laboratory. The beam compressors are required to convert the 80 mm collimated beam from the UTs into a 18-mm input beam for the instruments and to improve the sensitivity when observing with the siderostats. In addition, tip-tilt sensor units (STRAP) will be installed in the coudé foci of the UTs improving the beam feeding into the optical fibres of VINCI.

This wraps up the VLTI activities for this year. A complete summary of the

subsystems and of the instruments of the VLTI can be found in the proceedings of the SPIE conference on Interferometry in Optical Astronomy [3].

In 2002, the science instruments MIDI and AMBER and the fringe sensor unit FINITO will arrive, and the integration of the Auxiliary Telescopes will start. Figure 7 shows the erected mechanical structure of AT1 at AMOS in Liège, Belgium. Once the ATs and the science instruments are functional, regular science operations can start. The following article by Francesco Paresce [2] gives a taste of the science programmes that are planned with the VLTI.

5. Acknowledgements

In addition to the authors of this article, about twice as many ESO staff have contributed to the VLTI. Un-

fortunately, there is not enough room to name them all. Fortunately, we did have the support of such a large and experienced team, and we would like to thank all of them for their enthusiasm and their hard work.

The results presented in this article were produced with the software provided by the Observatoire de Paris for the Jean-Marie-Mariotti Centre for Interferometry in Grenoble.

References

- [1] Glindemann, A., et al. 1999 *The Messenger* **98**, 2–7.
- [2] Paresce, F., et al. 2001, *The Messenger* – This volume.
- [3] 32 papers in the SPIE Proceedings on Interferometry in Optical Astronomy, Session 1 *VLTI: Its subsystems and its instruments*, 2000, *Proc. SPIE* **4006**, 2–307.

Scientific Objectives of the VLT Interferometer

F. PARESCE, ESO

Astronomers have long sought to improve the sensitivity and spatial resolution of their observations in order to see as far back in time and as sharply as possible. As the photon-collecting power scales as the telescope diameter D^2 and spatial resolution as D^{-1} , the solution of the problem has always been in the form of ever larger collecting-aperture telescopes. Unfortunately, although this solution did indeed increase dramatically the sensitivity of astronomical observations, it still was far from ideal in terms of spatial resolution owing to the negative effects of the earth's atmosphere. On the ground, the improvements were mainly due to finding the proper location where the seeing was best (California, Hawaii and Chile) and, more recently, to the technique of adaptive optics as shown schematically in Figure 1.

Apart from the development of a ~100-m-diameter telescope, the foreseeable breakthroughs in optical/IR resolution in the near future are essentially only two: operating in space (HST and, in the future, NGST) and aperture synthesis interferometry. In essence, even going to space with a simple filled aperture telescope of 6 m diameter (NGST) still does not approach the potential of the latter technique even on the ground. This is especially true in the infrared at 2.2μ where very high sensitivity can be coupled to very high angular resolution of ~1 milliarcseconds (mas).

Because of these considerations, in-

terferometry has begun to play a central role in ground-based high-resolution astronomy, and numerous instruments have been completed or are in the process of construction (see Table 1 for a summary of the present situation in this regard). Several large-aperture interferometers will come on-line in the next few years. The impending presence of these new instruments represents an important incentive both for clarifying the scientific cases for various VLTI implementation plans and for ensuring VLTI's competitiveness in the international context over the next 10–20 years.

It has always been ESO's aim to operate the VLT in an interferometric mode which allows the coherent combination of stellar light beams collected by the four 8-m-diameter

telescopes (UT) and by several smaller 1.8-m-diameter auxiliary telescopes (AT). Thus, the VLTI has the unique advantage of being the only large telescope facility together with the LBT designed from the very start as an interferometer. This means that it will have three main characteristics that are unprecedented for this type of array:

- very high precision visibilities (up to $\Delta V/V=10^{-4}$) for moderately bright sources,

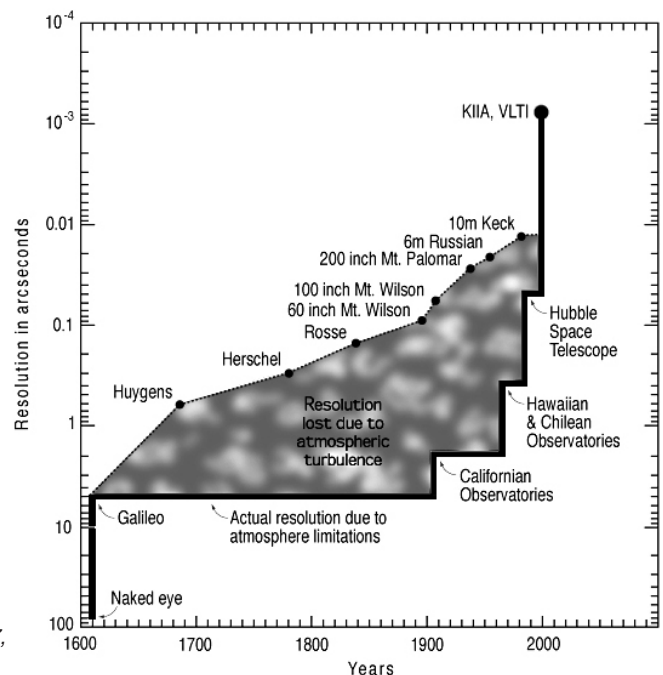


Figure 1. Spatial resolution as a function of historical time since Galileo. Adapted from P. Bely (ESA SCI(96)7, 1996).

Table 1. Current ground-based optical long-baseline interferometer projects

Programme (Nation)	No. of simultaneous baselines (ultimate)	Maximum baseline [m]	Telescope diameter [m]	Status or year of first fringes
GI2T (F)	1	65	1.52	Operational
ISI (USA) ³	1	35	1.65	Operational
COAST (GB)	3 (6)	100	0.40	Operational
SUSI (AUS)	1	640	0.14	Operational
IOTA (USA)	1 (3)	45	0.45	Operational
NPOI (USA)	3 (6,15)	250	0.35	Operational
ASEPS (USA)	1	100	0.45	Operational
CHARA (USA)	10	350	1.00	2000
KIIA (USA)	1/6/15 ¹	75/180 ²	10/1.8	2001
VLTI (EUR)	6/3/21 ¹	128/200 ²	8 /1.8	2001
LBT(USA/I/D) ⁴	1	20	8.4	2005
MAGELLAN (USA)	1	20	6.5	>2005

Notes: ¹Beam combination: main / auxiliary / hybrid. ²Between main / auxiliary telescopes. ³Heterodyne, to be changed into a homodyne interferometer. ⁴Monolithic array.

- excellent (u,v) coverage (a synthesised beam of 1–2 mas FWHM at 2 μ),
- very high sensitivity to faint sources (down to K \sim 20 with a brighter reference).

Of course, it has to be realised that, in practice, these capabilities will be acquired over a period of time in various phases starting with the easiest to implement and progressing to ever more demanding capabilities. The dates listed in Table 1 represent the start of operations in the various facilities with the most basic of capabilities. In general, these phases can be broken down into the following periods:

Phase 1: two-beam combination to measure fringe visibility leading to the amplitude of the object's Fourier transform. This phase usually includes the gradual development of additional capabilities leading to a significant improvement in sensitivity like on-source fringe tracking and wave-front reconstruction using adaptive optics (AO) techniques. In this phase, earth rotation and relocation of telescopes over a grid of different positions ensure a reasonable coverage of the (u,v) plane in order to obtain a well behaved point spread function for moderately bright objects (K–14). These capabilities allow one to reconstruct several components of the object's Fourier transform and, by fitting to a few-parameter model, to invert the transform and extract useful astronomical information at resolutions of several mas for simple objects with the main arrays and moderate spectral resolutions in the 1–20 μ range.

Phase 2: maintaining equal optical paths in the two beams to within a fraction of a wavelength or co-phasing the interferometer. Fringes can be tracked on a bright reference star, allowing long integrations on the fainter target source located an atmospheric coherence length away (\sim 1' at K). This allows phase-referenced imaging of sources of brightness up to K \sim 20 with the UT (main array, VIMA) and very accurate

astrometry with precisions up to 10 microarcseconds (μ as) with a dual beam instrument such as PRIMA for the VLTI with the AT (auxiliary array, VISA). This phase will follow the first by a few years for the VLTI.

Phase 3: combining beams from more than three telescopes, ideally up to eight for a measurement of visibilities on 28 baselines simultaneously yielding a closure phase for 21 triangles. This would determine the exact fringe position as a measure of the phase of the Fourier transform of the object's brightness distribution. Combined with the visibility measurements, this allows, in principle, model-independent reconstruction of an image of the object. This phase requires developing a complex 8-way beam combiner and using many delay lines implying an advanced sophistication in the management of many highly complex and extremely sensitive components working simultaneously. The final outcome is an instrument capable of generating images on suitable sources of a few tens to a few hundred non-zero intensity mas spatial resolution elements or as many as the number of independent measurements in the (u,v) plane. This phase might also include more sophisticated AO techniques to allow expansion into the visible range and higher spatial and spectral resolutions.

Phase 4: enlarging the instantaneous field of view of the array from a single telescope Airy disk (\sim 0.1–1") to several arcseconds as required for imaging of complex extended sources such as a dense cluster of stars. This can be accomplished with a Fizeau-type interferometer with homothetic mapping over a large field. Attaining this capability, in essence, would place the VLTI at the pinnacle of human achievement in its attempt to resolve or distinguish very faint and distant astronomical objects as shown in Figure 1.

ESO is defining and prioritising the key science drivers for each phase of

the programme and the technical specifications that flow from them. This article briefly presents these science goals as they currently stand. The list is not meant to be frozen or complete, but rather is intended to stimulate community reflection and comment. As already evident from the position of VLTI in Figure 1 with respect to all other facilities currently available, the kind of data which interferometry will access is so far beyond our current experience that it is inherently difficult to specify a definitive science justification. Indeed, much of the prospects are more in the nature of the unexpected. Although optical interferometry carries within it the potential to revolutionise whole areas of astronomy, it suffers currently from the difficulty to exactly foresee the details of the revolution. No one yet has peered into the very core of an AGN, for example, as the VLTI surely will and one can only speculate by engaging in risky extrapolations as to what one might find there. This is especially true since interferometric performance is still not well understood for a large class of sources which are extended on the scale of a few Airy disks.

In any case, it is still relatively straightforward to foresee, at least in general terms and on the basis of the expected VLTI performance parameters just described, the areas of research where VLTI is most suited to providing the kind of potential breakthroughs that we currently require in order to better understand our universe. Although the VLTI targets are mainly located in our relatively local universe due to the limitations in sensitivity inherent in high spectral and spatial resolution interferometry even with large telescopes, the impact of these breakthroughs on our knowledge of the furthest reaches of the observable universe cannot be underestimated. This is especially true when one considers that much of the universe consists of stars and fundamental information on stellar formation,

the IMF, binarity, ages and distances are crucial in unravelling the mysteries of galaxy and structure formation, the reionisation of the IGM by the first stars, etc.

These research areas are the following:

- The structure and composition of the outer solar system.
- The mass function of low mass stars, brown dwarfs (BD) and planets.
- The direct detection and imaging of extra-solar planets.
- The formation mechanism of stars and planetary systems.
- The formation of star clusters and their evolution.
- The surface structure of stars.
- The accurate distance to galactic Cepheids, the Large Magellanic Cloud and globular clusters.

- The baryonic composition of the galaxy's spheroid.

- The physical mechanisms responsible for stellar pulsation, mass loss and dust formation in stellar envelopes and evolution to the Planetary Nebula and White Dwarf stages.

- The structure and evolution of stellar and galactic nuclear accretion disks and associated features (jets, dust tori, Narrow-line Regions, Broad-line Regions, etc).

- The nature of the Milky Way nucleus surrounding the central black hole (BH).

- Interacting binary evolution and mass transfer mechanisms.

- The structure of the circumstellar environment of stellar BH and neutron stars.

- The evolution of the expanding shells of novae and supernovae and

their interaction with the interstellar medium and its chemical enrichment.

- The mass distribution of the galaxy beyond the solar circle.

- The internal dynamics of star clusters and tidal interactions with the galactic potential.

Naturally, as the VLTi evolves in this time interval through the four development phases briefly outlined above, the quality and volume of information to be garnered in most areas will grow allowing fainter, more distant and/or more complex objects to be studied with greater accuracy.

This is the executive summary of a report with the same title prepared by the author for ESO in February 2001. The complete text can be found at: <http://www.eso.org/projects/vlti/science/VLTscienceMarch2001.pdf>

2p2 Team News

H. JONES, E. POMPEI and the 2p2 Team

Personnel Movements

Team member Patrick François returned to the Observatoire de Paris after several years with the team, his last of which was as Team Leader. We wish him continued success back in France. Patrick's responsibilities have been taken over by John Pritchard, who joined the 2p2 Team in April. Before joining ESO, John was a New Zealand Science and Technology Post-Doctoral Fellow, hosted by Copenhagen University Observatory. John has interests in Magellanic Cloud Eclipsing Binaries and was already a frequent visitor to La Silla before commencing work at the observatory.

In April we were also joined by Ivo Saviane and Rainer Madejsky. Ivo previously held a postdoctoral position at UCLA, studying stellar populations in dwarf galaxies, globular clusters, and the chemical evolution of galaxies. Rainer is a part-time team member and EIS Visitor, presently on leave from his university in Brazil, the Universidade Estadual de Feira de Santana. His scientific interests include interacting galaxies and the evolution of galaxies.

News from the 2.2-m

It has been a busy time at the 2.2-m telescope and there are three articles in this issue of *The Messenger* that cover recent activities at the 2.2-m in detail.

In March, Fernando Selman, Lutz Wisotzki and Alain Gilliotte commissioned two grisms (red and blue) for use with the Wide Field Imager (WFI). They offer a combined wavelength cov-

erage of around 400 to 900 nm with dispersions of around 0.7 nm per pixel. For more details, see their special article about the new grisms and the possibilities they open for wide-field slitless spectroscopy with the WFI.

The 2.2-m telescope has been running under the VLT-style Observing Software for nearly half a year. This means that Observing Blocks are prepared and executed in a manner similar to that at the VLT, NTT and 3.6-m tel-

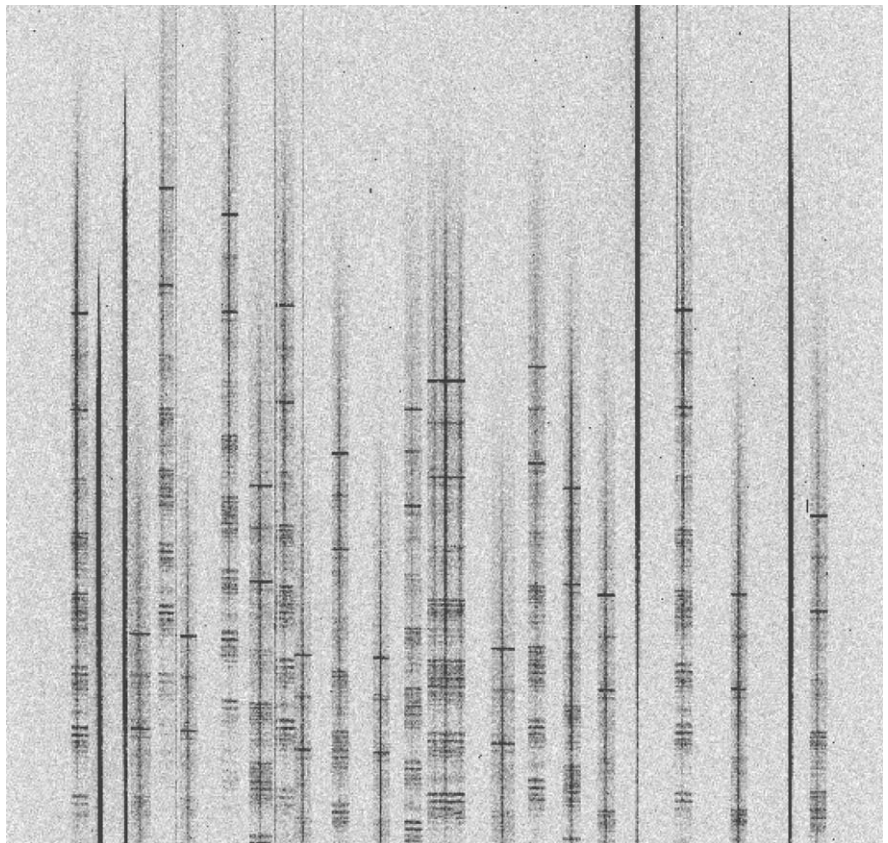


Figure 1. Twenty-minute exposure of galaxy spectra from the EIS 61 field, taken with the Danish 1.54-m in multi-object spectroscopic mode.

escopes. An article by Selman et al. describes the development of this software and how it was put in place over the existing control software.

Recent work by J. Manfroid and F. Selman has demonstrated that the amplitude of the flat-field calibration error plays a significant role in photometric accuracy with the WFI at the level of a few per cent. The accompanying article by Manfroid, Selman & Jones describes a dithering technique that allows observers to correct for this, with examples demonstrating its effect on some photometry. Any observers requiring WFI photometry to better than a few per cent are encouraged to look into this procedure.

Multi-Object Spectroscopy at the Danish 1.54-m

Multi-Object Spectroscopy (MOS) was recently performed successfully with DFOSC at the Danish 1.54-m tele-

scope. The observational procedure requires one to take a pre-image of the required field(s), send the image files to Copenhagen (where a punching machine creates the mask), and finally to ship the mask(s) back to La Silla in time for the spectroscopic observations. The mask is placed in the DFOSC slit wheel and aligned on the sky using a MIDAS procedure (kindly made available by P. Leisy of the NTT Team and modified for use at the Danish 1.54 by E. Pompei). The procedure calculates the offsets between the object centres and those of the corresponding slitlets, correcting for the alignment by applying a fine rotation to the DFOSC slits wheel.

To make this possible, it is necessary to bypass the DAISY acquisition system, through a C-shell script that accepts direct input from the instrument workstation to the PC controlling DFOSC. The new mode was tested during February 2001 in Danish time,

with Prof L. Hansen (Niels Bohr Institute, Copenhagen University). Long slit spectra of galaxies in the EIS field 61 were successfully acquired: Figure 1 is a 20-min exposure of a field full of spectra. A new flat-field lamp will soon be installed in the sky baffle, to allow the acquisition of flats without the need to change telescope position, hopefully expediting calibration.

The effectiveness of this system will be checked when it is installed. The final implementation was the result of interaction between the Copenhagen University (in particular Per Kjaergaard Rasmussen, Michael I. Andersen, Morten Liborius Jensen and Anton Norup Soerensen) and the 2p2 Team.

The MOS mode has been offered since the beginning of March this year but is only available in Danish Time (not ESO Time). Any observer wishing to use it must include the time for pre-imaging time in the estimate of the total time requirements.

Commissioning the Spectroscopic Mode of the WFI at the MPG/ESO 2.2-m Telescope at La Silla

L. WISOTZKI¹, F. SELMAN², A. GILLIOTTE²

¹Universität Potsdam, Germany, lutz@astro.physik.uni-potsdam.de

²La Silla Observatory, European Southern Observatory, Chile, fselman@eso.org, agilliot@eso.org

1. Introduction

For Period 68, the Wide Field Imager at the MPG/ESO 2.2-m telescope at La Silla will offer, in addition to the imaging mode, a spectroscopic mode. This will be accomplished by the installation of a grism in front of the WFI triplets to allow for slitless spectroscopy. The combination of the wide field of view, the grism, and the simultaneous availability of the whole set of WFI filters, make this a unique instrument in the southern skies. The instrument will be operated in VLT mode, with the instrument package with the spectroscopic templates already released.

In a preliminary ESO internal report by Hermann Boehnhardt, now at Paranal, the following case was made for the spectroscopic mode of the WFI. This mode will allow survey work for stellar, nebular objects, and galaxies with special characteristics. The main goal would be the registration and identification of such sources by their spectral signatures to establish population and distribution statistics and to prepare in-depth follow-up investigations by dedicated research programmes with other telescopes and instruments.

A rough estimate of the gain in sensitivity for the WFI at the MPG/ESO

2.2-m telescope as compared to objective prism spectroscopy at Schmidt telescopes gives: gain in aperture by a factor of 4–5, gain by CCD sensitivity as opposed to photographic emulsion

by a further factor of 20 or more, for a total factor of 100 in sensitivity gain. The advantage of the WFI in spectroscopic mode with respect to standard CCD spectrographs at 2–4-m-class tel-

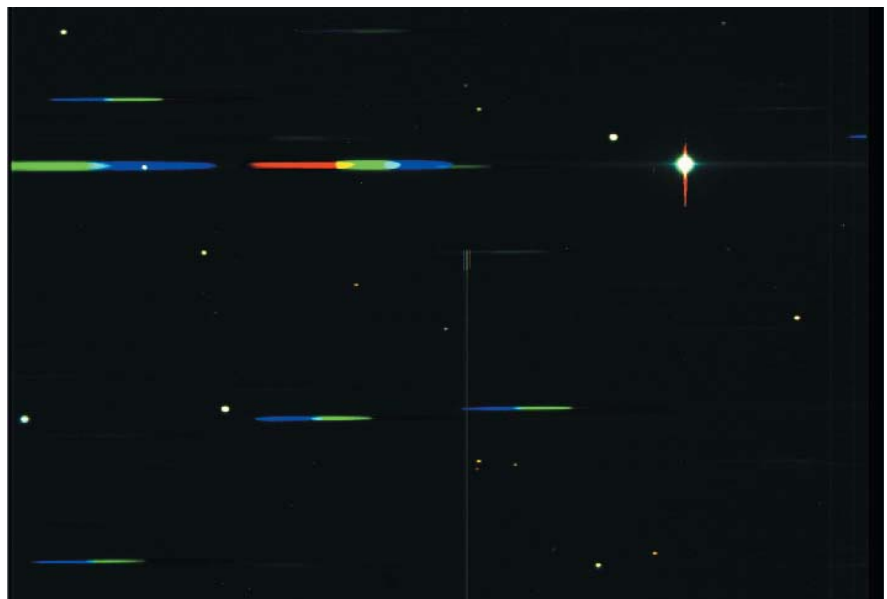


Figure 1: Portion of chip 51 showing the spectra of several stars taken using the WFI and grism B50. Notice the large amount of flux going into the 0th and negative orders. Also notice the white, 0th order image on top of one of the spectra; from its colour it is obvious that this is not an emission feature.

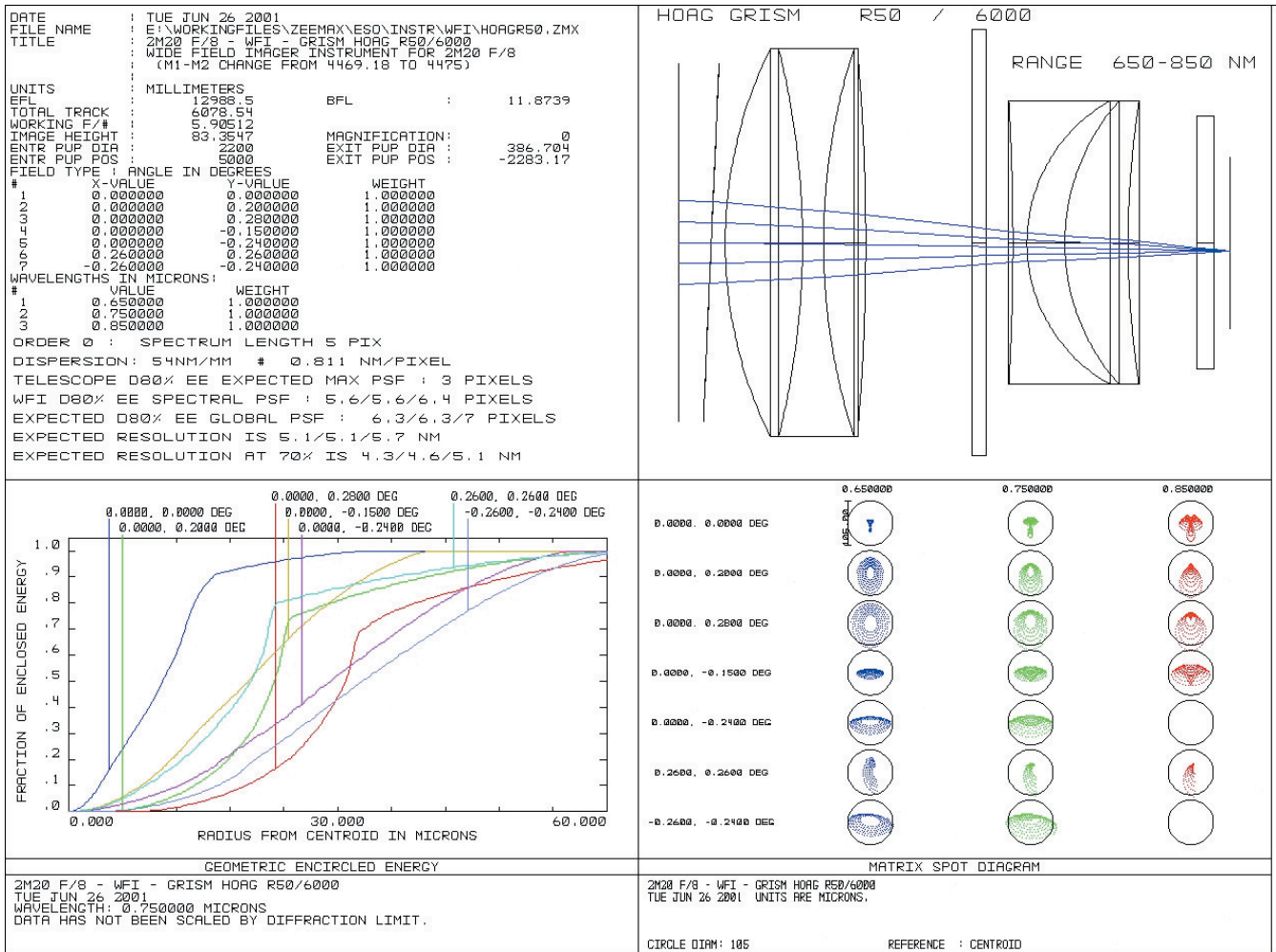


Figure 2: Optical simulation of the WFI with the R50 grism. First quadrant: optical data such as field sizes, wavelengths and resolutions. Second quadrant: layout of the WFI; the light comes from the left and the filter (thin large rectangle) is between the two lens triplets in a converging $f/5.9$ beam. Third quadrant: encircled energy of the telescope/WFI. Fourth quadrant: spot diagrams at different points (X, Y) in the field.

scopes is its much larger field of view, and its ability to obtain spectra of all objects therein at once.

In the preliminary draft mentioned above, the following areas of research were identified:

- search for stars with emission lines,
- search for stars with peculiar molecular lines,
- search for white dwarfs,
- detection of stars with strong magnetic fields,
- detection of $H\alpha$ emission-line stars in dark clouds,
- search for Herbig-Haro objects,
- search for stars at large distances above the galactic disk,
- detection of extragalactic HII regions and planetary nebula,
- detection of objects without obvious spectral lines,
- membership in distant galaxy clusters,
- search for emission-line galaxies and quasars,
- detection of galaxies with peculiar continuum at high redshift,
- search for lensed quasars.

The potentialities of the instrument can be gauged by looking at the survey results by Schneider, Schmidt, and

Gunn (1994). These authors, using the 4-shooter in scanning mode at the Hale 5-m telescope at Palomar Mountain, covered a 61-degree area of the sky with an effective exposure time per strip ranging from 34s to 63s (the WFI in 10 hours integration covers an equivalent volume): they obtained spectra for 600,000 objects, with approximately 800 emission-line galaxies, and 90 quasars. The same authors in a deeper survey, with 300 s effective exposure time, and 1.10 square degrees effective area, find approximately 50 low-redshift emission-line galaxies, 9 high-redshift $z > 2.7$ quasars (Schneider, Schmidt, and Gunn 1999).

Here we describe the instrument configuration for spectroscopic observations, and summarise the results of two commissioning runs done during March 2001.

Table 1: Summary of properties of the WFI grisms.

Grism	Blaze wavelength nm	Wavelength Range		Dispersion		IQ Resolution	
		nominal nm	measured nm	nominal nm/pix	measured nm/pix	pix	nm
B50	400	400–650	380–740	0.807	0.701	4.5	3.1
R50	600	650–850	420–900	0.811	0.691	6.3	4.4

2. Image Quality and Calibration

In Table 1 we present a summary of simulated and measured properties of the two available grisms. The wavelength range has been defined as that portion over which the efficiency is above 25% of the measured peak efficiency, and has been read directly from the measured response curves for the B50 and R50 grisms. As we discuss below, the B50 grism is so much inferior compared to the R50, even in the blue, that we will concentrate the discussion on the red grism.

2.1 Simulated Optical Properties

Because of the geometry of the WFI instrument, the dispersing elements have to be placed in the converging

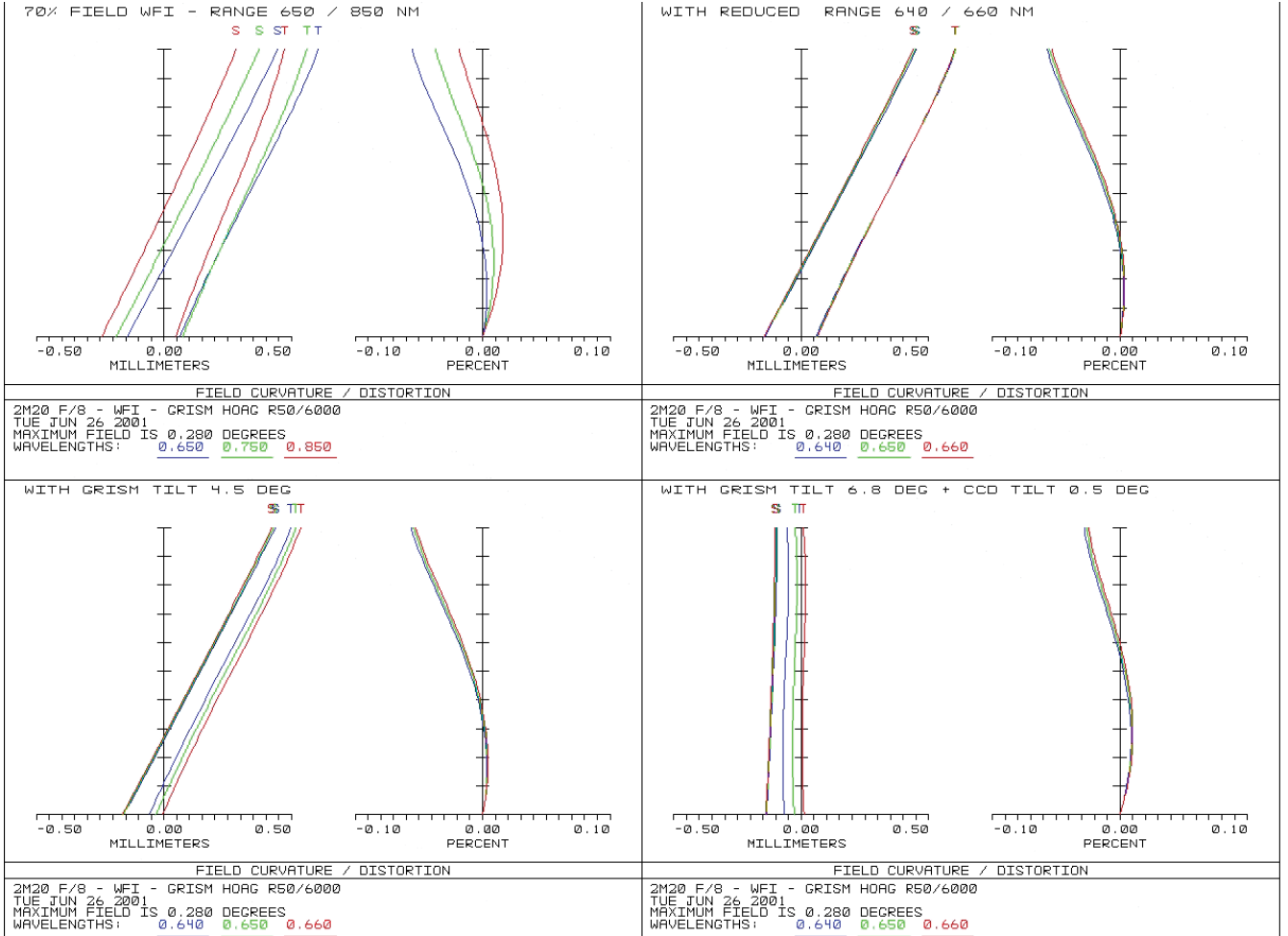


Figure 3: Optical simulation of the field curvature and distortion for several configurations of the WFI + R50 grism. Top left, full wavelength range, and top right, restricted wavelength range centred at $H\alpha$. Bottom panels: restricted wavelength range centred at $H\alpha$ with left, tilted grism, and right, tilted grism + tilted CCD, a combination which minimises the defocus.

beam where they induce larger aberrations (see the classical papers by Hoag and Schroeder 1970 and by Bowen and Vaughan 1973). Thus, a careful optical analysis had to be conducted.

A technical/feasibility study was performed by one of the authors in 1998 (*WFI Grism Spectroscopy*, LSO-TREESO-75441-001, Gilliotte 1998). It contains simulations of the optical properties expected with the different available grisms. Because of its superior efficiency and order rejection properties, we concentrate below in a description of the R50 grism.

R50/6000 Grism

The dispersion of this grism was calculated to be 54 nm/mm, or 0.811 nm/pixel. The geometric encircled energy plots show a predicted 80% monochromatic imaging quality of 5.6, 5.6 and 6.4 pixels, for each wavelength, to be convolved with an assumed telescope PSF of 3 pixels. The global image quality will amount to 6.3, 6.3, and 7.0 pixels respectively when the external seeing is 0.65 arcsec. The nominal spectral resolution is then around 5.1, 5.1, and 5.7 nm for $\lambda = 650$ nm, 750 nm, and 850 nm, respectively (in general,

the resolution in slitless spectroscopy depends on the seeing and will be degraded in case of poor seeing conditions). Notice that the actually measured dispersion is slightly lower than the nominal value.

Technical data:

- corning B1664 prism of 2.49 degrees
- replica 53.33 gr/mm with 3.42 blaze angle
- triplet properties: 54 nm/mm with blaze wavelength at 590 nm

Figures 2 and 3 show the field curvature, distortion, and the spot diagram plots obtained under the following four instrumental set-ups: (1) 70% of the full field; (2) after reducing the wavelength range around $H\alpha$; (3) after tilting the grism alone; and (4) after both grism

and CCD tilt. Grism tilt reduces longitudinal astigmatism by a factor of 1.5, but final image quality does not improve much (coma). Only CCD tilt improves the image quality drastically, with image below 2 pixels, meaning 2.9 nm over the full field. However, as of this writing there are no plans to offer a set-up with a tilted CCD for Period 68.

2.2 Measured optical properties

The simulations described in the previous section established that the best image quality of the R50 grism can be obtained with a tilt of the grism itself and also of the CCD. Because we did not tilt the CCD, we thought it important to perform actual measurements regarding the degradation of image quality.

Table 2: Efficiencies of the WFI + grisms (counts in first order).

Filter	ETC counts e^-	B50 counts e^-	R50 counts e^-
U 350	19	12	
B	222	81	108
V	248	68	150
R	543	111	429
I	371		176
White	1729	387	≈ 1100

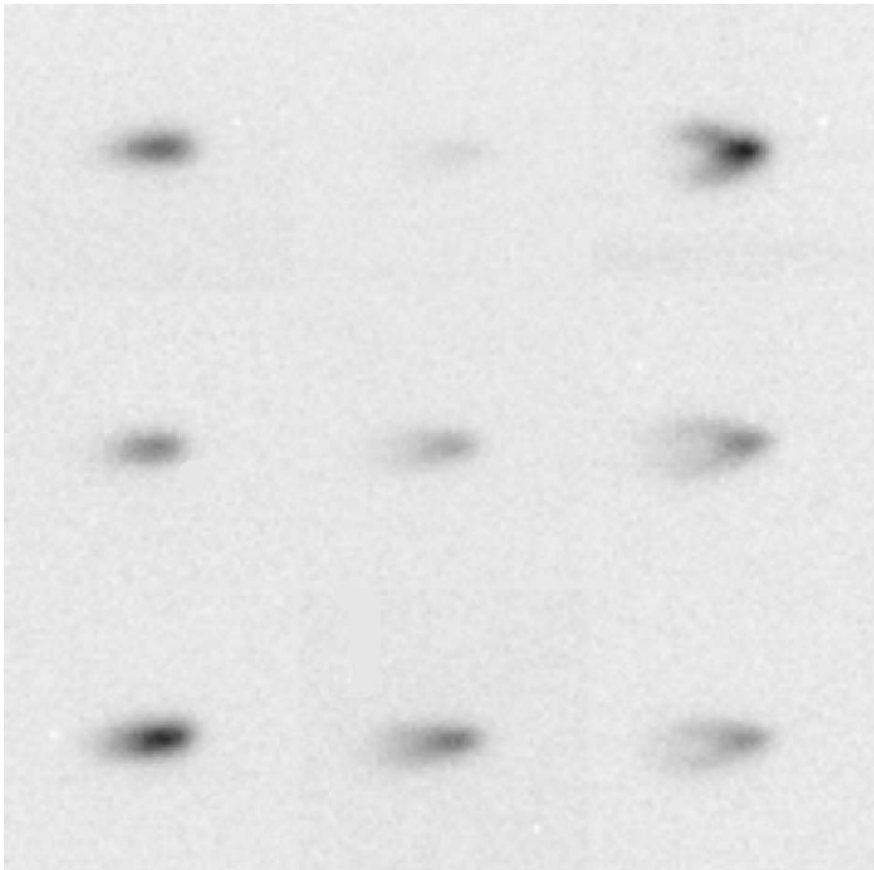


Figure 4: Shape of the zeroth orders in different parts of the mosaic as measured with the R50 grism and the B filter. The scale is such that the vertical and horizontal distances between images correspond to 60 pixels or 14 arcsec.

Figure 4 shows the image quality with the R50 grism together with the B filter. Although what we show is the shape of the 0th order, and not that of an emission-line feature in the first order, we can see that the simulations did a good job at predicting the effect. The nine images are extractions of 0th orders in different parts of the mosaic: the top row shows images extracted in the upper parts of chip 51, 52, and 53; the middle row shows images extracted at the bottom of the same chips; and the bottom row shows images extracted at the bottom of chips 56, 55, and 54.

Figure 5 shows a better example of the achievable quality. It shows extracts from a 900 s image through the R50 grism and the medium-band filter MB516. The arrangement in the montage is as before. The numbers are the FWHM of the vertical distribution of light at the centre of each spectra, measured in pixels (1 arcsec = 4.2 pix).

Another important property is the ability to superimpose dithered images. What we did was to use the astrometry tasks of the IRAF astrometry package, mscred, to superimpose the zeroth orders, and then see how well the first orders matched. We produced an animation that you can see in the web version of this document, at <http://www.lis.eso.org/lasilla/Telescopes/2p2T/E2p2M/WFI/grism>.

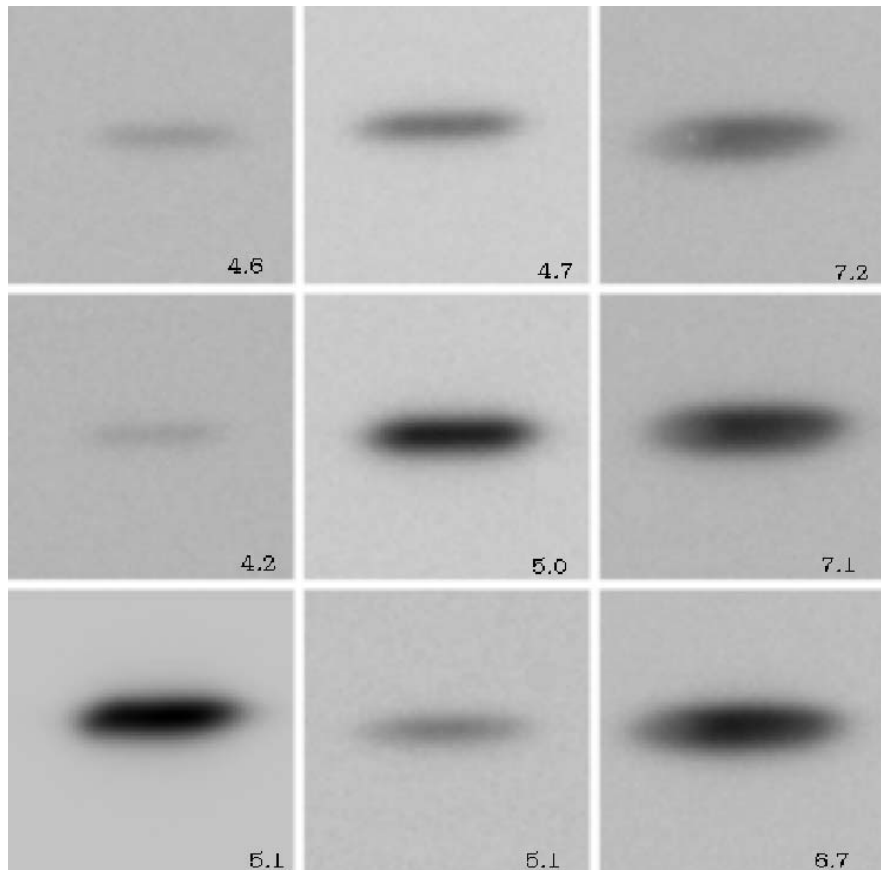


Figure 5: Shape of the first order as measured with the R50 grism and the MB516 filter. Scale set in same way as in previous figure.

The animation shows a portion of three dithered images centred on a bright quasar. One can see that the emission lines superimpose rather well.

2.3 Flux calibration and efficiencies

Table 2 summarises the data on the overall response of the telescope plus grism plus WFI. The numbers reported are the integrals over the response curves. They assume a source having a flat spectrum with $f_{\lambda} = \text{const.} = 1 \times 10^{-16} \text{ erg s}^{-1} \text{ cm}^{-2} \text{ \AA}^{-1}$ (corresponding to a Vega magnitude of $V = 18.83$), observed with an exposure time of 1 s. For comparison, we list also the count rates estimated by the WFI exposure time calculator for direct imaging in each filter; the ratio between these and the grism counts gives directly the efficiency losses due to the grism.

Figures 6 and 7 show the response curves of the two grisms obtained by observing the HST flux standard GD108. The units of the ordinates are electrons/pixels/seconds. Notice that even in the blue the R50 grism has a much higher response than the B50. The main reason for this unexpected behaviour are the substantial flux losses to other than the first spectral order in the B50 grism, discussed in more detail below.

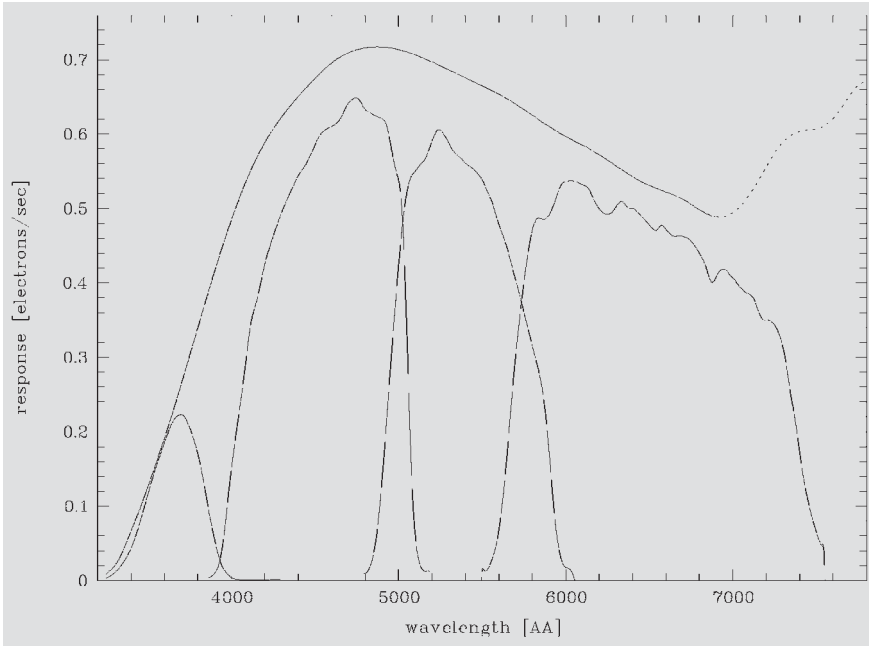


Figure 6: Response curves for the B50 grism with no filter, and with the U 350, B, V, and R filters.

Notice that above 690 nm for the B50, and 640 for the R50, the curves for no filter (“white”) are heavily contaminated with light from the second order (dotted lines). As soon as filters are used, no such contamination occurs since the orders will always be spatially well separated.

Diffusion of flux into adjacent orders

Table 3 shows the relative flux distribution among the different orders. The 1st order has always been set to 100. The R50 grism has a much better characteristic than the B50: while the latter allows more than 50 % of the flux to spill over into unwanted orders, the former concentrates more than 90% of the flux in the first order (in the *R* band). This results in an almost total lack of 0th-order images when observing with some red medium-band filters, a fact that could somewhat complicate the wavelength calibration (but see our suggestions below on observing strategies). Indeed, the better suppression of unwanted orders by the R50 makes it outperform the B50 even in the *B* band, despite the latter’s nominal “blue” classification.

2.4 Wavelength calibration

Table 4 summarises the measured dispersions of the two available grisms. The wavelength calibrators used were the Seyfert 1 galaxy Mrk 1239, which shows several emission lines over the entire spectral range, and a number of M-type stars with prominent TiO absorption bands. The object was placed near the centre of the array, and in several positions near the corners and edges. In the absence of accompany-

ing direct images, the 0th order centroids were used to define the wavelength zero points. We found that the true zero points varied substantially, up to ~ 3 pixels between different locations on the array in a nontrivial manner, probably as a result of optical distortions induced by the grism. Unless a much more detailed investigation shows how to model these distortions, this effect ultimately limits the achievable wavelength calibration accuracy to $\sim \pm 15$ Å or so.

The dispersion relations of both grisms are well described by 2nd-order polynomials (see Fig. 8). Given the

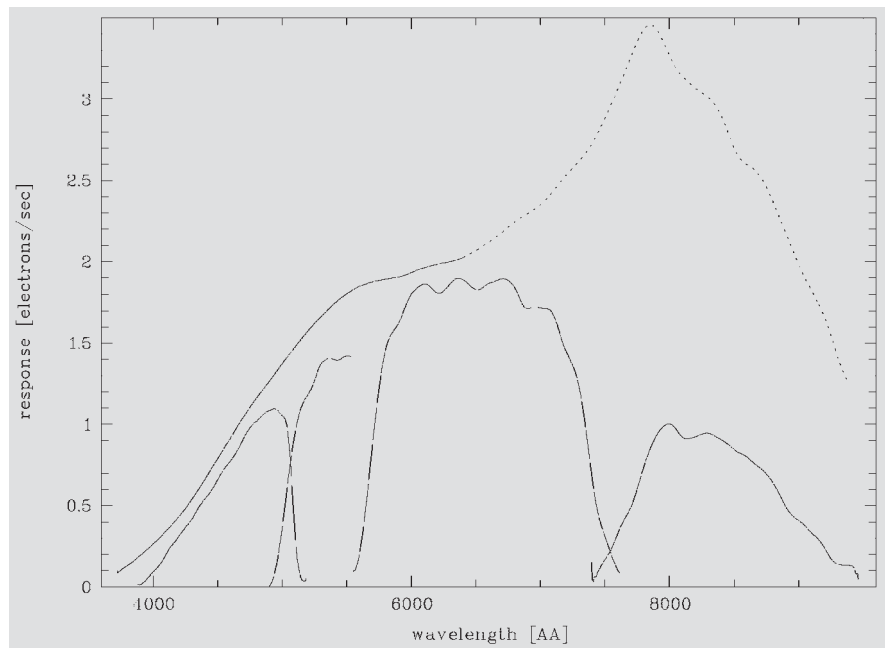


Figure 7: Response curves for the R50 grism with no filter, and with the B, V, R, and I filters. Notice the different scale between this graph and that of the B50 grism: the R50 grism is better than the B50 even in the blue.

Table 3: Distribution of flux among orders.

Order	Grism B50		Grism R50	
	B	B	B	R
-4	3			
-3	6		0.1	
-2	9		0.4	0.8
-1	16		2	1.6
0	42		7	2.3
+1	100		100	100
+2	4		29	0.4
+3	1		2	
+4			0.4	
+5			0.1	

substantial zero point uncertainties, in most practical cases it is probably sufficient to work with a linear dispersion relation, as the maximum systematic error will be substantially less than the zero-point variations except for white light (no filter) images, which we strongly discourage anyway.

3. Observing

3.1 Example spectra

We present in this section a few real extracted and calibrated spectra so that future users obtain a better idea of the capabilities of the instrument.

Flux standard star

Figure 9 shows the HST flux standard GD 108, a hot subdwarf with distinct Balmer absorption lines, observed with the WFI R50 grism and the *B*, *R*, and *I* broad-band filters. Integration time for each of these exposures was 100 sec.

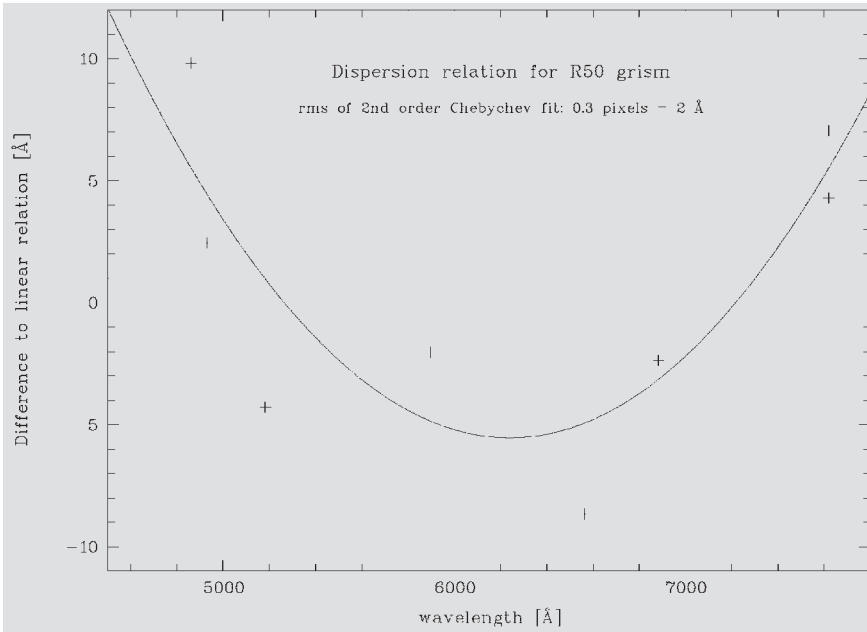


Figure 8: Quadratic dispersion solution for the R50 grism.

Table 4: Global dispersions of the WFI grisms.

Grism	Measured Dispersion nm/pix	Spatial Variation	
		%	pix
B50	0.701	1	2–3
R50	0.691		N/A

Slitless spectroscopy has one rather obvious property which is nevertheless worth recalling: Slit losses are naturally avoided as there is no slit, and the extracted spectra are therefore easily placed onto a proper (at least relative) flux scale.

Comparison between a slitless and a slit spectrum

Figure 10 shows the extracted slitless spectrum of our wavelength calibrator, the Seyfert galaxy Mrk 1239 (plotted in black), obtained with the B50 grism in white light. This is contrasted with a slit spectrum of the same object taken in 1997 with the ESO 1.52-m telescope and the Boller&Chivens spectrograph (upper spectrum plotted in red). The original B&C spectrum has somewhat better spectral resolution, and we therefore smoothed it to approximately the same resolution as the WFI spectrum. The resemblance of the two datasets is striking and illustrates the fidelity by which spectral information can be extracted from WFI slitless spectroscopy.

3.2 Hints for observing

The Wide Field Imager in its slitless spectroscopic mode is a powerful and almost unique instrument to conduct surveys for objects with characteristic spectral signatures. This final section

is meant to help interested potential users planning such a survey, and to provide some guidelines for data reduction.

Always observe with a filter

Without filter, there are several substantial drawbacks that will severely reduce the usefulness of your data:

The background would be prohibitively high for deep surveys as all the sky contributions over the entire spectral range go into each pixel.

2. The spectra are much longer, and the losses because of overlapping spectra will be substantially increased.

3. Contamination by 2nd-order spectra limit the exploitable spectral range to below ~ 650 nm.

Always obtain a direct image of your field

Although it is technically possible, in principle, to use the 0th orders to define objects and determine wavelength calibration zero points, we *strongly* recommend to use paired direct images for this purpose. This recommendation is based on the experience collected in the course of the Hamburg/ESO survey, a large quasar survey based on digitised objective-prism Schmidt plates (Wisotzki et al. 2000; see also Reimers & Wisotzki 1997). These papers also outline a working strategy for object definition, extraction and wavelength calibration for slitless spectroscopy in general.

The suggested approach has important advantages:

1. Object definition and classification is much easier and more reliable on proper direct images with no interference from spectra. Photometry and astrometry are also more accurate.

2. Once an astrometric transformation from direct to spectroscopic image is established, one can *a priori* identify spectra that suffer from contamination from other objects (either 1st or other orders). In particular, the superposition of 0th and first orders from different sources can mimic emission line objects; this can be easily recognised with a direct image.

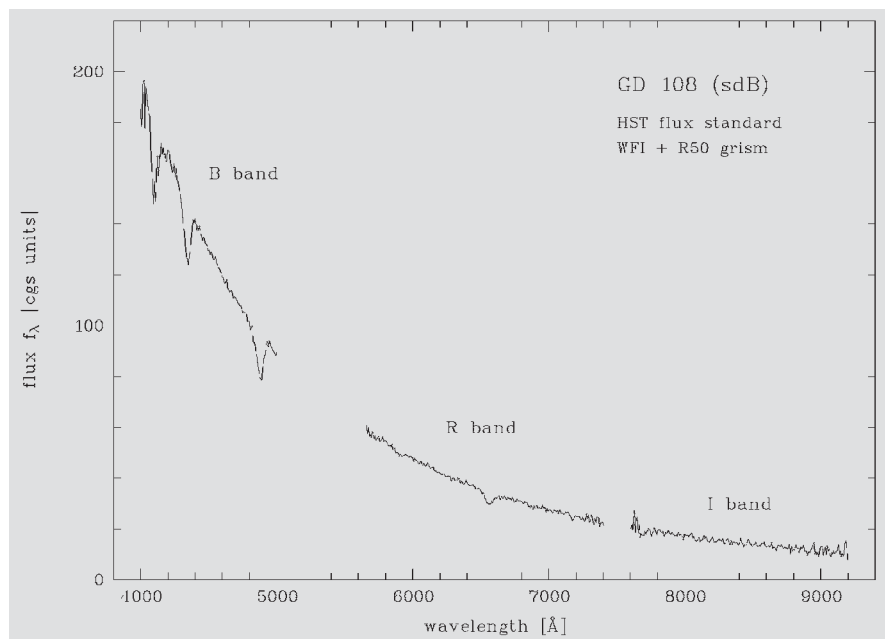


Figure 9: Spectra of the HST standard GD108.

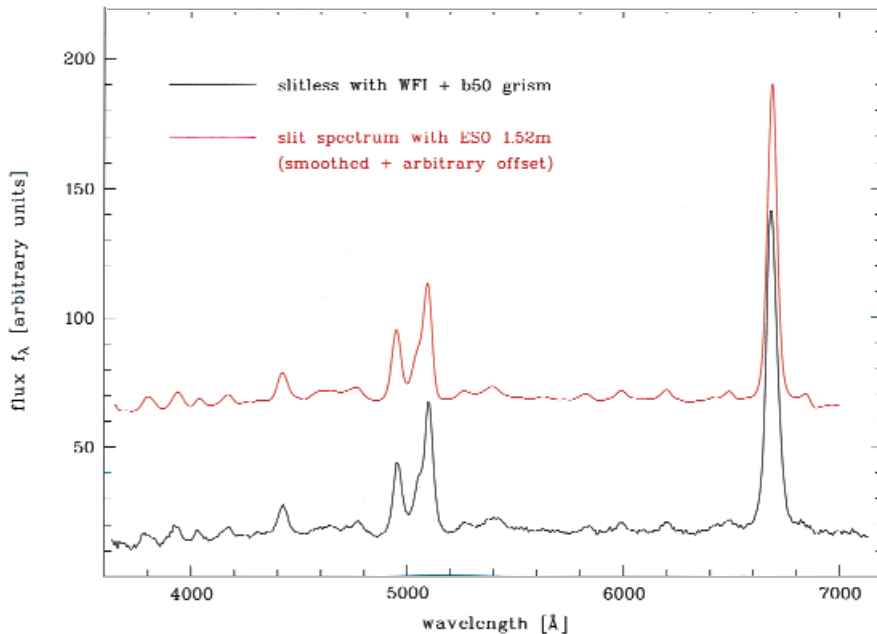


Figure 10: Spectra of the Seyfert 1 galaxy Mrk 1239. Lower spectrum in black: WFI slitless plus B50; upper spectrum in red: slit spectrum taken with ESO 1.52-m telescope.

3. Especially with certain medium-band filters, the 0th order can be so faint that it is barely detectable except for the brightest sources.

The direct image should be sufficiently deep as to allow the detection of all objects of interest. In certain applications, this may require a pretty long integration in the same filter band(s) selected for spectroscopy. Consider for example a search for continuum-free

emission-line objects with medium-band filters. Such objects are effectively point sources in the spectral images, so in order to reach similar depth in the direct image, almost comparable exposure times are needed.

Take flat fields in all filters

At the same time that the direct images are taken, one should obtain flat

fields in all the filters that will be used. The flattening of this kind of observations is an unsolved problem which will require further experimentation: the pixels exposed by the spectrum of an object each receive a different wavelength, monochromatic light, due to the object. When a flat field is obtained, those same pixels are illuminated by broad-band, or at best medium- or narrow-band light of the same spectral composition throughout.

Take rotated images in crowded fields

It is important to obtain images in at least two rotations if source crowding is important. Currently, the system allows only small rotations, less than 10 degrees, but this is more than enough to move zeroth and higher orders of neighbouring objects from the areas of interest.

References

- Bowen L. S., Vaughan A. H., 1973, "Non-objective" gratings, *PASP* **85**, 174.
- Hoag A. A., Schroeder D. J., 1970, "Non-objective" grating spectroscopy, *PASP* **85**, 174.
- Reimers D., Wisotzki L., 1997, *The Messenger* **88**, 14.
- Schneider D. P., Schmidt M., Gunn J. E., 1994, *AJ* **107**, 1245.
- Schneider D. P., Schmidt M., Gunn J. E., 1999, *AJ* **117**, 40.
- Wisotzki L., Christlieb N., Bade N., et al., 2000, *A&A* **358**, 77.

VLT-Style Observing with the Wide Field Imager at the MPG/ESO 2.2-m Telescope at La Silla

C. URRUTIA¹, T. PAZ¹, E. ROBLEDO¹, F. GUTIERREZ¹, D. BAADE², F. SELMAN¹, F. SANCHEZ¹, J. BREWER³, and M. SCODEGGIO⁴

¹La Silla Observatory, ESO, Chile; ²ESO, Garching; ³University of British Columbia, Canada; ⁴Istituto di Fisica Cosmica G. Occhialini, Italy

1. Introduction

The Wide Field Imager instrument of the MPG/ESO 2.2-m Telescope has been operating with the VLT-style Observing Software (OS) since the beginning of the year. Users can now prepare Observation Blocks in the same manner as for the VLT and other La Silla instruments. This uniformity of the user interface will make the system even more easy to use than before. This work is the result of the efforts of a large number of people: the sequencer scripts were written with extensive help from Paul Lesaux of the NTT team, and Emilio Barrios of the 3.6 team at La

Silla. Figure 1 shows the control room with the new system in place.

Testing and development was done during the normally scheduled idle times around full moon, having thus little impact on the functioning of the telescope. This was possible only because of the dedication of all persons involved. Special thanks to the Team's Telescope and Instrument Operators (TIOs), Roberto Castillo, Francisco Labraña, Mauricio Martinez, Jorge Araya, Jose Cortes, who had to suffer during the initial times before the system achieved stability. We would also like to gratefully acknowledge the patience of those users of the system

whose programmes were compromised by the initial teething problems.

2. Software Design

It was decided early on to keep the existing low-level subsystems and to build an interface layer from the existing Telescope Control System (TCS), Data Acquisition Integrated System (DAISY), which commands the instrument, and the WFI-specific installation of the FIERA control software, to the VLT compliant OS (for details on the TCS see *The Messenger*, No. 93, p.19, and No. 94, p.12). The resources available at the time did not permit the de-



Figure 1: The new control room layout. The Telescope Instrument Operator Jorge Araya in front of the new instrument workstation at the 2.2-m telescope control room.

velopment of a fully VLT compliant TCS. The hybrid solution for the TCS required us to write many interface functions between the upper VLT compliant layer, and the existing TCS. Thus, a good part of the functionality of a TCS was implemented as an integral part of the Sequencer scripts library (see below). These include the focusing (with temperature compensation and filter-specific offsets) and the autoguider functions. It is evidence of the power of the VLT software that such a “fake”, but nevertheless functioning, TCS could be implemented with those tools. We are currently studying the possibility of updating the TCS to a fully VLT compliant one. If this is done we will be able to simplify the sequencer scripts (and thus bring them if not to full VLT compliance, at least closer to the VLT spirit).

Figure 2 shows a schematic view of the software layout with all its subsystems. To place the above diagram in the proper perspective, it is useful to think in terms of the following observing metaphor: The *Broker of Observation Blocks*, BOB, is the main programme, in charge of *executing* the observations. It runs on top of another layer which in this case is the Observing Software (OS). With the help of the p2pp tool, the Visiting Astronomer gives values to the parameters of an observing sequence, such as exposure time, number of exposures, filter, offsets, etc. These values, and their legal ranges are defined in what is called a *Template Signature File*. These are the files in the *instrument package*. p2pp has a graphical form editing interface which presents to the user all the variables that must be filled so that the sequence can be executed. An observing block can contain data for several sequences, stored in an *Observation Block Description* file (*.obd), which is just a file with the names of the sequences composing the OB, together with their variables and the values as-

signed to them by the visiting astronomer.

When the OB is executed, BOB calls the Tcl procedures coded by the 2p2 Team in a *sequencer file* and submits to them the values of the variables as entered by the Visiting Astronomer. The Software Team at La Silla wrote the modules in gray in the diagram; they are required to translate the instructions in the sequencer files into tasks understandable by the existing system. The beauty of the system is that it gives to the team in charge of the telescope/ instrument the power and responsibility of writing the appropriate template signature and sequencer files, and it is precisely here where familiarity with the system is needed. It is also here where quick response to requests by observers could be accommodated, like the survey modality, described below, implemented at the WFI upon request from a group of observers at the Max Planck Institute in Heidelberg.

2.1 Observing efficiency

As of this writing the system stability has allowed observations to be conducted with a median efficiency of

66%. That is, during about two-thirds of the night time useful for observations the shutter was open (this has been monitored for only one month). The best value so far, for a whole night of observations, is 79%. If we keep in mind that the above figures include observing programmes with typical integration times of only 30 seconds, this is a rather positive result, as the single frame overhead can be anything from 1 minute to 2 minutes for filter changes and telescope re-positioning. We have just implemented a *fast* mode which will have a positive impact on the above figures.

2.2 The flow of the data

Because of the large size of the images involved (140 MB), it was not possible with the available resources to adhere strictly to the current VLT-style data-flow system. Among the modifications we had to implement are the incorporation of direct saving to DLTs in several of the workstations, and the separation of the dhs/oh workstations, which in the latest versions of the VLT data-flow system were merged into a single “dhs” machine (dhs = data handling system, oh = observation handling). Without this latter modification we experienced many freeze-outs of the system which were (to the relief of every one) alleviat-

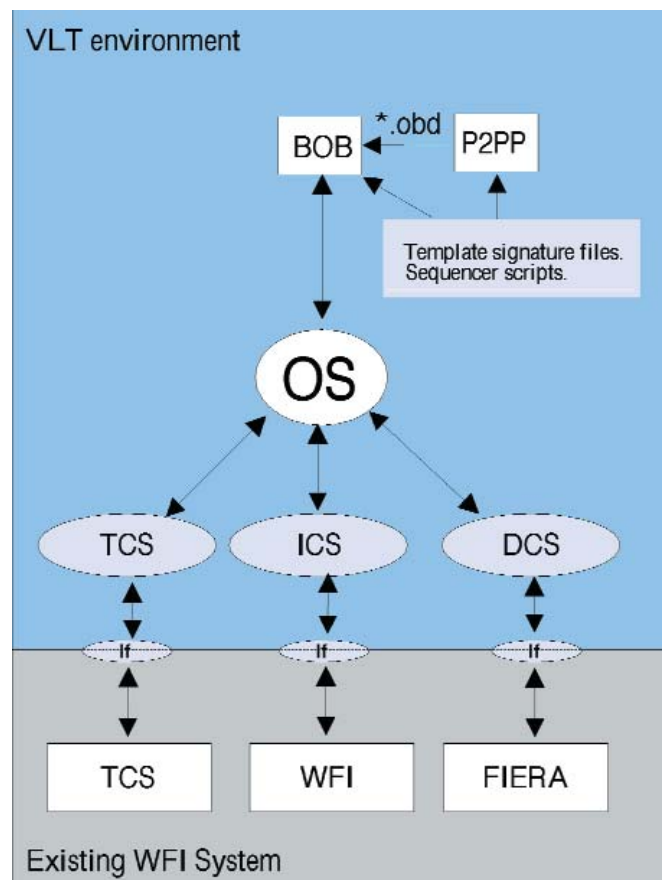


Figure 2: Schematic view of the observing software system for the WFI. The gray modules were written by the Software Team at La Silla. All others are original VLT software.

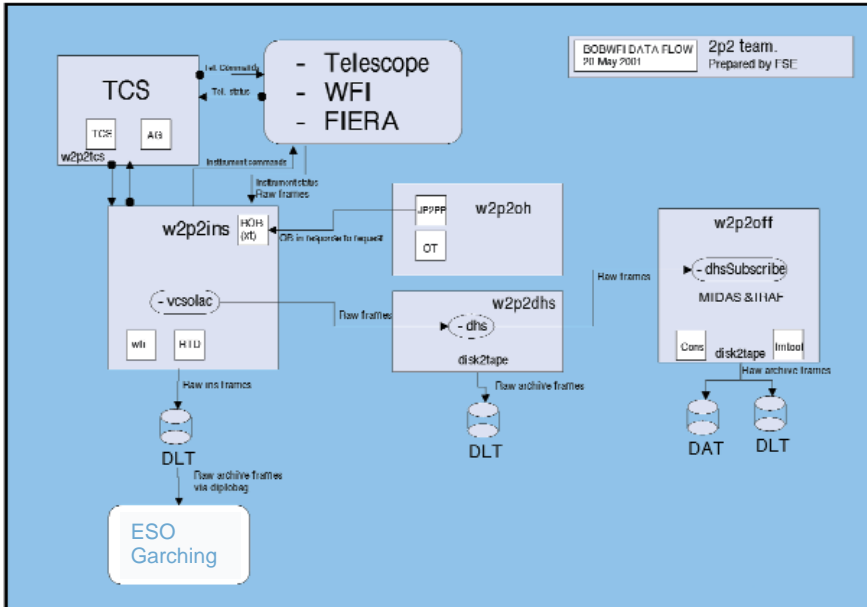


Figure 3: Data flow for the BOB@WFI system.

ed once p2pp was run on a different computer than the one where dhs runs.

Data saving continues to be a problem as it consumes a large amount of resources because we have not been able to automate it yet. This will change in the future, once the proper data flow for archiving is implemented.

Figure 3 shows the scheme which we are currently using. The data are backed up every morning from the instrument workstations (w2p2ins) to two DLTs (operations that, together with data verification, take many hours and extend into the early afternoon). One of the DLTs is sent to Garching, while the other is kept at La Silla. Once the tape is "ingested" by the archive in Garching it is returned to La Silla for its reuse (together with the copy that was kept at La Silla). The backup for the Visiting Astronomer is made on DAT tapes from the w2p2off machine. It must be requested daily as there is no room for backlogs. Only raw data are backed up for the Visiting Astronomers.

The backing up of reduced data is their responsibility.

The team is working on an automatic scheme to save data on the w2p2dhs and the w2p2off machines simultaneously to the taking of the data. The main routine has been written and is in the process of debugging. Once they have been fully tested out we will need to assess their impact on the observing efficiency.

3. The future

Among the immediate tasks of the 2p2 Team is the improvement of the Sequencer scripts by making them more efficient and versatile. To this end we are engaged in an effort to parallelise some of the observing tasks, so that the overhead per observation could be reduced. Recent experiments show that without guiding and without filter change, the best we can achieve is 55 s overhead per observation (as opposed to 68 s with the current system). This *fast* mode has resulted in

over 340 frames per night for a programme with a constant integration time of 30 s and no guiding. Such data rates put extreme stress on the operation, and more efficient data archiving methods are urgently needed.

We have also recently experimented with a survey modality of observation, which allows the Visiting Astronomers to align their offsets along lines of constant declination and right ascension for an equinox of their choice, and to specify offsets of any size in their templates. This modality, together with the proper rotation of the instrument will allow for the very precise repetition of previous observations of a large field. We expect to offer these improvements for P68.

One of the main motivations and driving forces behind the development of the VLT-style OS for the WFI is the decision of bringing the WFI to full service mode for period 68. As of this writing (beginning of Period 67), 20% of the assigned time is for service-mode observations. During this time the Team is gaining practice in the use of observing tools such as BOB, P2PP, and OT, to carry out the observations, and it is still getting some of the bugs out of the system.

As mentioned above, among the challenges that we face is the proper data archiving. ESO's Data Management Division is planning to install during July this year the first prototypes of their Next Generation Archive System Technologies, NGA, units at the 2.2-m telescope. This prototype uses swapable SCSI-IDE magnetic disk technology based on a Linux PC system.

The next period with full service mode will be quite challenging, and if it is to succeed it will need the close collaboration between the team in charge of the WFI, the other support teams at La Silla, and the Data Management Division of ESO at Garching. These have certainly been challenging and interesting times and we are motivated by the support of the user community, and of everybody involved.

Achieving 1% Photometric Accuracy with the ESO Wide Field Imager

J. MANFROID (Univ. Liège), F. SELMAN (ESO Chile), H. JONES (ESO Chile)

Introduction

Characterising the accuracy and the precision of photometric observations is notoriously difficult. Although photon statistics, readout noise and other basic parameters offer useful insight into the lower limit of the achievable precision,

actual observations suffer from many additional problems: vagaries of the atmosphere, mismatch between instrumental and standard systems, uncertainties in the standard system, non-linearity of the detectors, and the like. Each source of error has special characteristics with different consequences

for the observations, as is summarised in Table 1.

The highly successful Wide Field Imager (WFI) on the ESO/MPG 2.2-m telescope offers the possibility of undertaking photometry over a half-degree field. Here we discuss findings concerning the photometric perform-

Table 1: Comparison of common sources of photometric errors dependent on colour, intensity, space, time.

Error source	dependent on				possibility for correction	affects		
	colour	intensity	space	time		CM diag.	C index	diff. phot.
Flat field	(x)	–	x	(x)	x	x	(x)	x
Turbulence	(x)	–	–	x	–	(x)	(x)	(x)
Transparency	(x)	–	(x)	x	–	x	x	(x)
Non linearity	(x)	x	(x)	–	x	x	x	x
System mismatch	x	–	–	–	(x)	x	x	–
Photon statistics	–	x	–	–	–	x	x	x

ance of the camera. In particular, we describe strategies for dealing with the flat-field calibration error, which is often underestimated by observers.

Calibration Errors

A recent study by Manfroid et al. (2001) of four telescopes at both ESO and Haute-Provence shows that the amplitude of the flat-field error over the camera area can be of the order of 0.05 mag. Hence, the calibration error must be considered as one of the major sources of uncertainty in CCD photometry.

A component of the flat-field calibration error can be a non-uniform illumination (e.g., a non-uniform twilight sky). However, usually the major contribution comes from scattered light and ghost reflections inside the instrument. Much of this light originates from within the field of view, and even the most careful baffling cannot eliminate the effect.

The insidiousness of the effect is due to the fact that it is a redistribution of light that affects both the science and the flat-field exposures in the same manner. Thus, after dividing the science exposure by the flat-field, one ends up with an image with a very flat sky level, which is what most observers are looking for. However, because the illumination at the mosaic plane was not constant, the result should actually be an image which shows an uneven illumination. Therefore, in this case, a flat sky is a sign of a bad flat field.

The Photometric Super-Flat

We present below two methods for the correction of the data. The first method has been thoroughly tested and has the advantage that one can use the same science observations, if there are enough of them with the proper dithering pattern, to find the correction; the second one, still under development at La Silla, was designed as a quick way to get the *zero-point correction map* (or *photometric super-flat*) with very simple special purpose observations.

Those procedures do not require standard stars and they work with any filter. Obviously, a third, direct, method

can be used if suitable standards can be found all over the camera field. The analysis of a single frame yields the zero-point map. Such standard fields are being set up for the major photometric bands of the WFI.

Method 1. The calibration error can be evaluated – and corrected – by comparing the photometry of stars on dithered exposures (see Manfroid 1995, 1996; Andersen et al. 1995). This procedure yields a purely photometric calibration which has exactly the same purpose as the usual night-sky super-flat: namely, addressing the large-scale trends. Instead of relying on pure background data in median-filtered, blank-sky night frames, the photometric super-flat only uses stellar photometric data and is clearly more suitable.

Suppose we have a number of stars ($s = 1, \dots, S$) recorded on a series of dithered frames ($f = 1, \dots, F$), obtained with various amounts of translation and/or rotation. We assume the frames have been corrected with some high-S/N flat-field calibration (dome or sky), so that high-frequency variations have been removed.

Let $\Psi_{\text{star}}(\mathbf{x})$ be the actual correction needed for stars, and m_s their actual magnitudes. The instrumental magnitudes are $m_{0,f,s}(\mathbf{x})$ and $\mathbf{x} = (x, y)$ is the position on the CCD.

We write

$$m_{0,f,s}(\mathbf{x}) = m_s + a_f + \Psi(\mathbf{x}; \mathbf{b})$$

The parameters a_f are zero-point frame corrections.

$\Psi(\mathbf{x}; \mathbf{b})$ is considered to be dependent on a series of parameters $\mathbf{b} = \{b_i\}$. It can be developed as a finite series of independent functions $\psi_i(\mathbf{x})$ such as polynomials, but more complex functions can be used. This choice may be crucial. When substantial rotations of the camera are considered, (e.g., alt-az telescopes) the instrumental settings are changed and an angular dependency may have to be introduced.

The parameters a , b and m can be determined by minimising a chi-square function

$$\chi^2 = \sum_{f,s} \sigma_{f,s}^{-2} |m_{0,f,s}(\mathbf{x}) - m_s - a_f - \sum_i b_i \psi_i(\mathbf{x})|^2$$

where $\sigma_{f,s}$ is the precision on the magnitude measurement (f, s).

Under even limited photometric conditions (a_f constant for at least three frames), simple dithered sequences suffice to yield a robust solution. Otherwise it is necessary to know the precise photometry of at least three stars. Combining rotations and translations is an alternative, not always feasible, and which introduces instrumental changes.

In order to get the best accuracy, one can combine all available photometric data from dithered frames observed during an observing run. The observations must have been obtained under similar instrumental conditions and processed with the same flat field calibration. This means that tens or hundreds of frames can be used in each band.

Method 2. This second method, just a variation of the previous one, was developed by one of the authors (Selman 2001), because it was important for the La Silla team in charge of the 2.2-m telescope to have a procedure that could be carried out as part of the standard calibration plan. The requirements for such a procedure are that it should use as little telescope time as possible, and that the data analysis should be straightforward. As mentioned above, it is possible to do a quick calibration with the use of only three dithered exposures per filter. We have developed a method that, if used with three exposures of an adequately dense stellar field, taken in quick succession, permits an adequate calibration (residual errors $\approx 1\%$). The three exposures should be a central exposure, a second exposure with a right ascension offset, and a third exposure with a declination offset. One should cross identify stars in the frames and perform aperture photometry on them. The photometry is then corrected for any overall zero point shifts that could be caused by transient atmospheric transparency fluctuations between exposures. Then, the mosaic is divided in sub-areas numbered 1 to N. The areas are chosen such that their sizes correspond to the amplitude of the offsets. Thus, each star has its magnitude measured in at least two areas, with an observed magnitude difference dm_{obs} .

If we knew the difference in zero points between the different sub-areas,

we could calculate the magnitude differences measured above. Even if we do not know the zero point differences, we can calculate them with the following procedure: assign to sub-area i , a zero point z_i , and estimate for each dm_{obs} , a corresponding dm_{calc} . In matrix notation, if each row of a *design* matrix represents a single magnitude difference, and the columns represent the different sub-areas, we can write $dm_{\text{calc}} = A \cdot z$, where z is a vector with the zero points for each sub-area, and A is the design matrix, with as many columns as the number of areas in which the mosaic has been subdivided, and as many rows as stellar magnitude differences that have been measured. This matrix is made of mostly zeros, and has the values of 1 and -1 at the two positions corresponding to the areas where the magnitude difference is being computed. One can then determine the values of z which minimise $\|dm_{\text{obs}} - dm_{\text{calc}}\|^2$. The solution to this least-square problem is given by the *normal equations*

$$(A^T \cdot A) \cdot z = A^T \cdot dm_{\text{obs}}$$

This linear system is ill-defined unless we design the observations properly. That is why we need offsets in both directions. We also need to fix the value of the zero-point in one of the mosaic sub-areas. For the details on how to solve these equations, see Selman (2001).

Results with the WFI

Figure 1 shows contour plots of *UBVR I* flat-field corrections obtained over a two-night observing run with the ESO WFI, using the first method described in the previous section. Figure 2 shows perpendicular profiles through the CCD. The results presented here correspond to a particular set of dome flat fields. The screen was illuminated with a lamp except for the *U* flats which were obtained with day light.

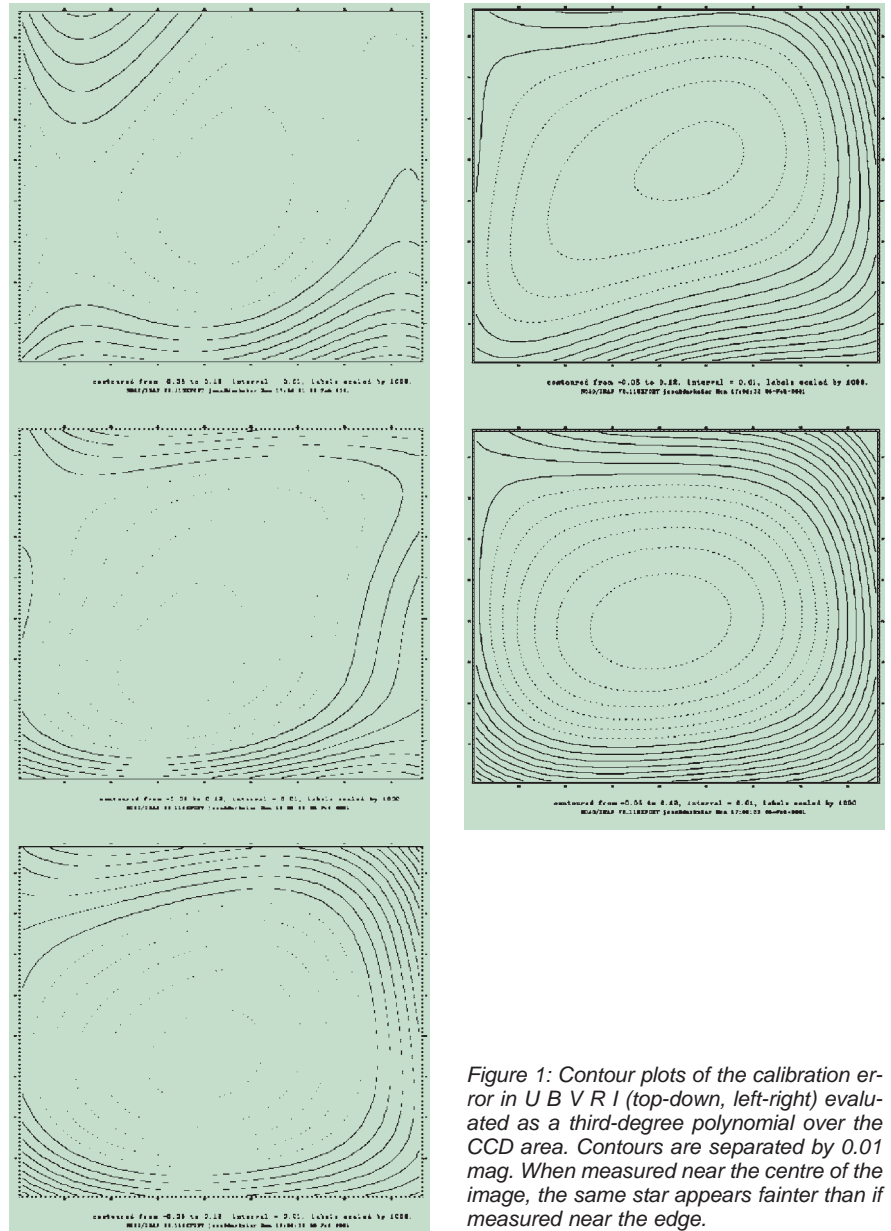


Figure 1: Contour plots of the calibration error in *UBVR I* (top-down, left-right) evaluated as a third-degree polynomial over the CCD area. Contours are separated by 0.01 mag. When measured near the centre of the image, the same star appears fainter than if measured near the edge.

The illumination conditions were therefore quite different and this explains the peculiar characteristics of the *U* calibration correction. The correction that

must be applied to the regular dome, twilight, or super sky-flats, always results in a relative dimming of their central areas with respect to the areas

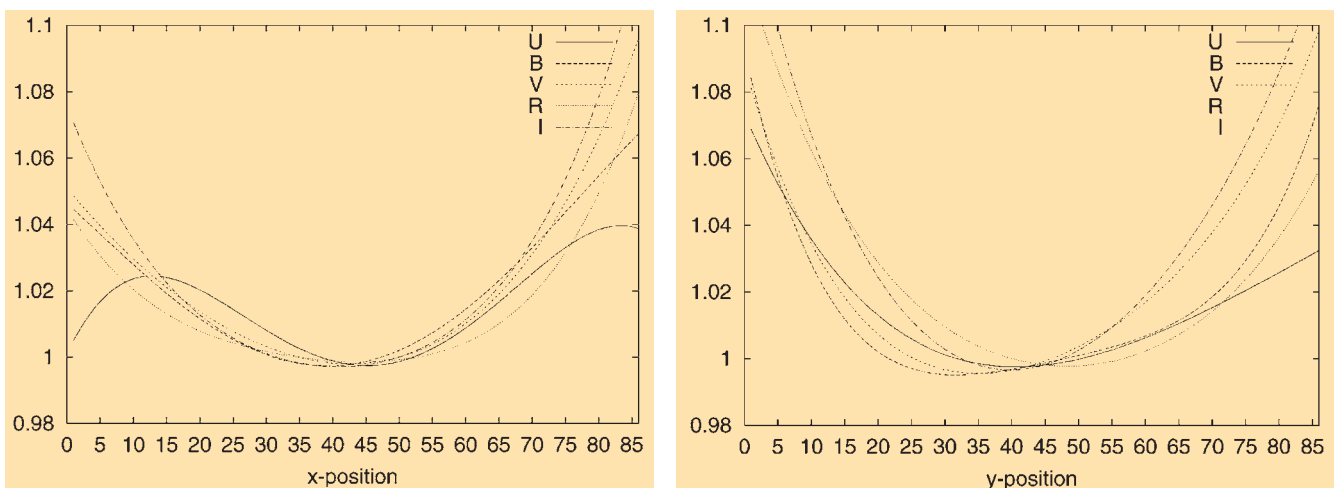


Figure 2: Central cross section of the calibration correction in RA (left) and dec (right). The correction is normalised to unity in the central area.

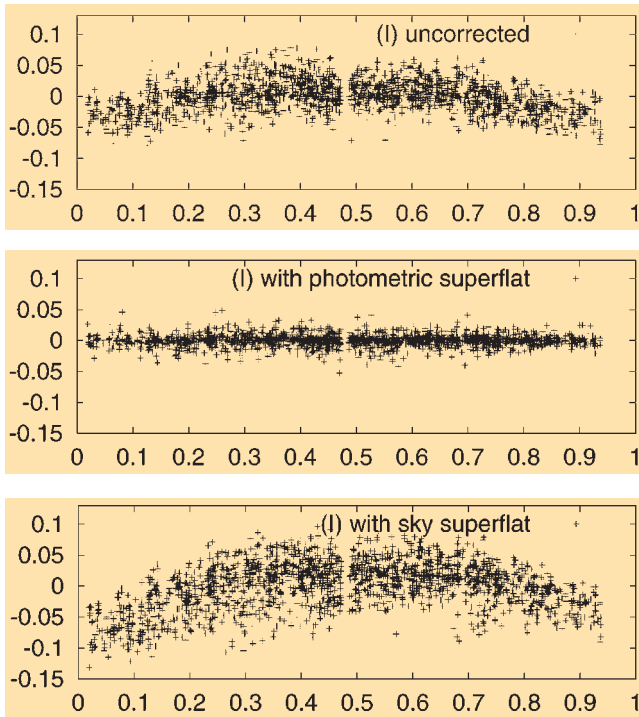


Figure 3: Observed deviations to the average I magnitude as a function of position (declination in relative units) for 400 stars observed on 34 exposures in 7 distinct fields. The upper plot shows data processed through the usual flat-field technique. In the middle plot the correction (“photometric super-flat”) has been applied. The lower plot shows the same results when a night-sky super-flat calibration is used instead.

away from the centre. This will result in a brightening of the sky background in the central areas of the science images, together with a brightening of the stars in the same areas (see Figs. 2 and 3).

Figure 4 shows the results of applying the second method to a totally independent data set. The points depict the local V magnitude differences with an offset of only 30 arcsecs. The solid line is a solution zero point curve, that is, it is the magnitude that has to be added to each stellar magnitude as a function of position on the mosaic. This solution corresponds to a one dimensional analysis of a strip 1000 pixels wide, along the declination direction of the mosaic. A cursory look to the data shows that the agreement with the results from method 1 is roughly at the 1% level.

The correction tends to be larger at longer wavelengths. Scattering and/or reflections by the optical elements may be less important at shorter wavelengths. Another explanation is that the contrast between the screen and the surrounding surface of the dome may be higher in the blue and UV, hence the relative amount of scattered light decreases.

It is logical to expect that sky flats contain a larger proportion of scattered light than dome flats obtained with a correctly-sized screen. Indeed, this is what has been observed at various telescopes (Manfroid et al. 2001), including the WFI. Images processed with

twilight or night sky flats need larger corrections. This is illustrated in the lower panel of Figure 3 which shows that the worst photometric results are obtained with a night-sky super-flat – a technique that is often claimed to offer the best calibration. However, when using dome flats with the WFI, it is advisable to check each new set against an old one, since variations in the illumination pattern have been noted on rare occasions (Jones et al. 2000). We have also found for the WFI that although dome flats taken with a lamp do not do a good job at removing features such as *dust donuts*, dome flats with Sun light do.

Stray Light Contribution

All optical systems exhibit the effects of stray light at some level. Usually it is

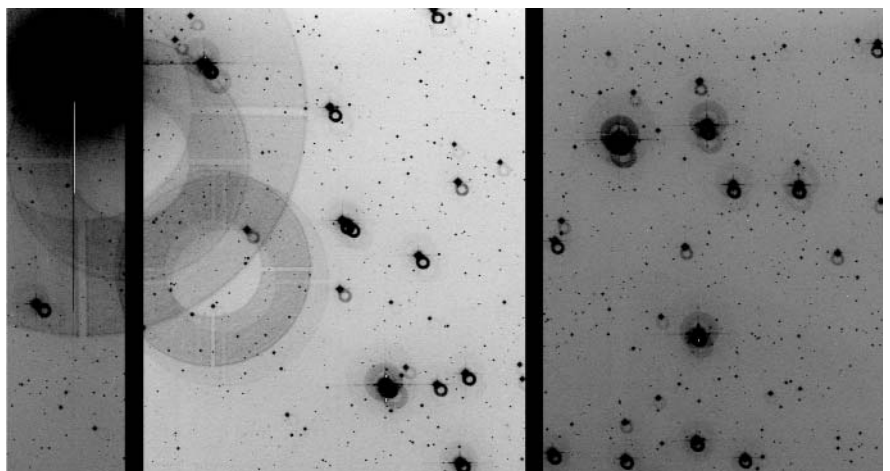


Figure 5: Ghost reflections seen in the $H\alpha$ filter on a portion of the WFI mosaic. Most stars show a primary reflection (smallest and nearest to the star). Secondary and tertiary reflections are also visible on a few of the brighter stars while the very bright star in the top left shows ghost images almost as large as an entire CCD, due to multiple internal reflections, many times over.

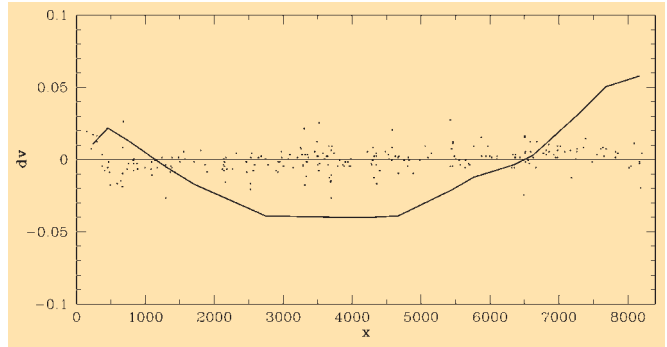


Figure 4: The points show the differences in magnitude between measurements performed on the same stars, but separated by 30 arcseconds in RA. The solid curve shows the zero point difference as a function of position in the mosaic, obtained with the second method described in the text. It is noteworthy that the stars used to make the graph are extremely bright, with DAOPHOT estimated errors much smaller than 1 mmag; nevertheless, the scatter in the magnitudes is only slightly less than 10 mmag.

seen in the form of spurious reflections (“ghost images”) originating between different combinations of optical surfaces. It is commonly a problem in imaging instruments such as focal reducers, that carry several air-glass surfaces. It is not uncommon to see families of ghost reflections following distinct exponential or diametric patterns, depending on the geometry of the optics (see e.g. Jones, Shopbell & Bland-Hawthorn 2001). Such internal reflections can be largely minimised (< 1%) through suitable anti-reflection coatings, typically consisting of a quarterwave layer of MgF_2 , or multi-layer coatings of alternating MgF_2 and TiO_2 . Alternatively, silica sol-gel coatings have recently been demonstrated to give superior performance over traditional coatings (Stilburn 2001), and they are now being used in place of MgF_2 for some astronomical instruments with many air-glass surfaces.

The ESO WFI consists of two lens triplets and the filter is located between them in a converging $f/5.9$ beam. There are nine air-glass surfaces, including

the CCD dewar entrance window and the surface of the CCD itself. The most obvious spurious reflections in WFI images are out-of-focus ghost images of bright stars (Fig. 5). The effect is at least partly filter-dependent – multiple reflections are much more prevalent in the H α and [S II] narrow-band filters compared to other narrow-bands or *UBVR I*. Individual ghost reflections in *BVR I* contain 1.5 to 2% of the unreflected starlight; the reflections in H α and [S II] are even stronger than the others because the first reflection is nearer to focus, and the light more concentrated, even though the total reflected content is virtually the same. Removing these ghosts from sky frames is somewhat problematic, since the offset between ghost and object varies symmetrically with object distance from the optical axis. Hence, telescope dithering and median-filtering strategies such as those described in Jones, Shopbell & Bland-Hawthorn (2001) are not effective.

Ghost reflections are just one contributor to stray illumination in the flat-field. Other components such as diffuse scattered light (across the full field), focal concentration and side illumination also contribute, giving rise to flat-field errors discussed earlier. These are not as readily identifiable as the ghosts, and so at best, the observer needs to correct for their influence through the offset technique described above. The bottom line is that the combined contribution is more than a few per cent, and observers desirous of

photometric precision better than a few per cent need to correct for these effects.

Conclusions

Considering the field size of the WFI camera, the flat-field errors are not unusually large. This bears testimony to the quality of the optics. However, for many observers, the amplitude of the effect might come as a surprise since it is often claimed in the literature that cameras in general can be flat-fielded to within a few millimagnitudes (particularly when using median filtered night-sky frames as super-flat calibration). A perfect calibration should *not* leave a flat sky background if the illumination at the detector plane is not uniform, hence this should not be considered as a valid test of the achieved accuracy. We have shown that if we use just the standard flat-field correction, the achievable accuracy is of the order of 5%. Nevertheless, this number does not contain the whole truth because the same star placed at different parts of the mosaic could show systematic variations in its measured brightness of almost 10% peak-to-valley. This is quite devastating for programmes that attempt to find spatial correlations in quantities directly derivable from the fluxes. Thankfully, the colours appear to be much less affected.

One may wonder why such errors are rarely accounted for. It is simply not easy to detect the 2-D effect unless you specifically look for it, and have suitable

dithered frames to analyse. It is reassuring to see that with the proper procedures the systematic errors can be reduced down to 1%.

Because of a fast readout and the large area – hence, the large number of measurements per frame – WFI observations can easily include the dithered exposures needed for computing the calibration correction. This procedure will still be easier when accurate wide-field standard fields are available.

References

- Andersen M.I., Freyhammer L., Storm J., 1995, in “Calibrating and understanding HST and ESO instruments”, Ed. P. Benvenuti, ESO Conference and Workshop Proceeding No. **53**, 87.
- Jones, D. H., Shopbell, P. L., Bland-Hawthorn, J., 2001, *MNRAS*, submitted (http://www.sc.eso.org/hjones/WWWpubl/detect_meas.ps.gz).
- Jones, D.H. and the 2p2 Team, 2000, “Inspection of Flatfields from the Decontamination Monitoring Programme” (<http://www.lis.eso.org/lasilla/Telescopes/2p2T/E2p2M/WFI/documents/Decontam/FFofWFI.ps.gz>).
- Manfroid J., 1995, *A&AS*, **113**, 587.
- Manfroid J., 1996, *A&AS*, **118**, 391.
- Manfroid, J., Royer, P., Rauw, G., Gosset, E. 2001, in *Astronomical Data Analysis Software and Systems X*, ASP Conference Series, in print.
- Selman, F. J., 2001, “Determining a zero-point variation map for the WFI.” (<http://www.lis.eso.org/lasilla/Telescopes/2p2T/E2p2M/WFI/zeropoints>).
- Stilburn, J., 2000, in “Optical and IR Telescope Instrumentation and Detectors” Eds. M. Iye and A. F. M. Moorwood, *Proc SPIE* 4008.

SCISOFT – a Collection of Astronomical Software for ESO Users

R. HOOK, ST-ECF

There are active astronomers, visitors and students at all four ESO sites who need a wide variety of software to work efficiently. Much of this scientific software has been developed in the community and is not normally used in non-astronomical establishments. Examples are software to reduce, display, analyse and visualise astronomical data.

If there is no co-ordination, there is a strong tendency for such software to be installed at the different sites only when requests come from users and there is no simple way, or enough human resources, to make updates or ensure compatibility between sites. As a result it was common for visitors to ESO sites to be unsure what software they could expect to be available and in the case of offline data manipulation at the tele-

scope such uncertainty could lead to inconvenience and possibly inefficient use of observing time.

To try to avoid these problems the Scisoft project was established at the beginning of 2000. It is a joint effort between the author from the ST-ECF, the ESO scientific community represented by an advisory board with delegates from each ESO site, and the ESO IT group which is part of the Technology Division. Recently, the Data Management and Operations Division has also become an active member by supporting external distribution.

Scisoft maintains a uniform, documented and tested collection of software for the three main ESO computer platforms – Solaris, HP-UX and Linux – and makes regular distributions internally on CD-ROM. This collection is the

standard one for users and visitors at all four sites. It is also distributed from Garching to Chile using mirroring so that updates propagate automatically. The items included on the three platforms are close to identical. At each release the policy is to have only one version of each package, the most recent available. Installing a single collection takes far less effort than locating and installing many individual items and testing them and hence leads to a major reduction in the total effort required for scientific software support throughout ESO.

The content of the collection is driven by the needs of ESO users which are expressed by representatives of all four ESO sites at a board meeting before each new release. At present the collection contains IRAF with many lay-



ered packages, ESO-MIDAS, Eclipse (for ISAAC and other data), IDL (although a license must be bought to allow full operation, not just the demo mode), GILDAS, Difmap, Terapix tools including SExtractor, image display programmes such as Skycat, ds9, SAOimage, ximtool, etc, and many other things. A full list is available at <http://www.eso.org/scisoft>. Anyone planning observing at an ESO telescope in Chile can expect to find this collection on site for their immediate off-line data analysis. The contents are biased towards the needs of the ESO optical and near-IR communities so, for example, there is no X-ray software included.

Although some ESO software items (ESO-MIDAS, Eclipse and Skycat for example) are included in Scisoft, most are not as they typically are linked to other deadlines such as proposal submission and maintained and supported independently. These items should be obtained via the ESO web pages as at present.

Scisoft releases occur at approximately six-monthly intervals and there have so far been two, in June and November 2000. The next one will be in July 2001. Originally, this collection was just intended for internal ESO use but in spring 2001 it was decided to also allow external distribution without support.

Although now available to external users, it is intended that the Scisoft collection will remain focused on the ESO internal needs and will develop accordingly. Nevertheless, we are interested in hearing comments from the external community.

The external ("EXPORT") version lacks some of the items in the internal version because of copyright questions but is otherwise close to identical. Anyone wishing to request a copy is encouraged to send their postal address and the name of the version they would like to receive (Linux, Solaris or HP-UX) to "scisoft_request@eso.org" and we will post them a CD (see picture at right of title).

LATEST NEWS

ESO High-Level Presentation in Porto

C. MADSEN, ESO

In connection with the meeting of the ESO Council in Porto on June 18–19, ESO invited a number of representatives from important groups in Portuguese society, including academia, industry, politics and the media for a presentation at the Centre for Astrophysics of the University of Porto (CAUP). At the meeting, presentations were given by the Portuguese Minister for Science and Technology, Prof. J.M. Gago, the ESO Council President, Dr. Arno Freytag, the Director General of ESO, Dr. Cathrine Cesarsky, Prof. Teresa Lago, Head of CAUP and Portuguese delegate to the ESO Council, and finally Dr. João Alves, ESO. This was followed by a



live video conference with Paranal, where Damien Hutsemékers discussed current observations done with the VLT telescope ANTU. A cocktail and a short planetarium show completed the event, which also marked ESO's first public appearance in Portugal since the formal accession of this country to ESO. ESO will continue its high-level presentations in its member states with the next event planned to take place in Brussels in November this year, at the time of the Belgian EU Presidency.

Prof. Gago's speech about the development of science in Portugal and the importance of international collaboration drew great applause among the invited guests.

SOFI and ISAAC Pierce the Obscured Core of SBS 0335-052

L. VANZI, ESO, Chile; L. HUNT, CNR, Italy; T. THUAN, University of Virginia, USA

1. Introduction

In the list of Blue Compact Dwarf (BCD) galaxies known to date (Izotov & Thuan 1998, Kunth & Östlin 2000) SBS 0335-052 shows one of the lowest abundances, $Z = Z_{\odot}/41$, and is second only to I Zw 18 with $Z = Z_{\odot}/50$. Though new BCDs with low metallicity have been recently discovered (van Zee 2000, Kniazev et al. 2000), the two aforementioned galaxies keep holding the record. It is a general result that all star-forming low-metallicity galaxies are BCDs.

The study of such unevolved systems is extremely important to understand galaxy formation. It is believed that galaxies began to form at redshifts larger than 3 (Steidel et al. 1996) but all high- z galaxies discovered so far appear to be substantially enriched in heavy elements. Hence with these young nearby systems, we can study the star-formation process in environments which are sometimes much more pristine than those in known high-redshift galaxies. The star-formation process in primordial environments is very poorly understood but the metallicity obviously plays a fundamental role, nevertheless other parameters must be important as suggested by the variety of properties displayed by BCDs (Kunth & Östlin 2000).

SBS 0335-052 belongs to the handful of galaxies with abundance below $Z_{\odot}/20$ (Melnick et al. 1992), as such it is a candidate “local primordial galaxy” according to Izotov & Thuan (1999) who argued from the constancy of the N/O and C/O abundance ratios with O/H that galaxies with such low metallicity are younger than ~ 100 Myr. This idea however has been challenged by the recent observations of an evolved stellar population in I Zw 18 by Aloisi et al. (1999) and Östlin (2000).

HST observations of SBS 0335-052 have evidenced star formation occurring in six Super-Star Clusters (SSCs) not older than 25 Myr and located within a region smaller than 2 arcsec, or 520 pc at a distance of 54.3 Mpc (Thuan et al. 1997). Further observations obtained with ISO have shown a flux at $15 \mu\text{m}$ much brighter than expected and a spectral energy distribution that, at these wavelengths, is well

fitted by a highly absorbed modified black-body (Thuan et al. 1999 – hereafter TSM). From their fit, TSM deduce a visual extinction in the range 19–21 mag. and suggest that most of the star formation in SBS 0335-052 might be optically obscured. With this in mind we have started a programme aimed at a better understanding of the physical conditions in low-metallicity BCDs. In particular, the near-infrared (NIR) spectral region can help resolve the age controversy because of the uniformity of NIR colours in evolved stellar systems (Frogel 1985). Dust can be best targeted in the NIR, its thermal emission becoming evident above $2 \mu\text{m}$. The effects of extinction are reduced by roughly a factor of 10 in K band and by almost 20 in L band relative to the optical bands. Finally, NIR spectroscopy gives unique probes on the physics of the gas and constrains the star formation history of the galaxy through features like $\text{Br}\alpha$, $\text{Br}\gamma$, H_2 , $[\text{Fe II}]$ and CO in absorption.

2. Observations

We have observed SBS 0335-052 on several occasions. Images in the J and Ks bands were obtained with SOFI at the NTT. These images were not very deep, only 300 sec. each, but had a good spatial resolution ($0.5''$). In addition we obtained a Ks image in the high-resolution imaging mode of SOFI during 400 sec. of integration; on this image we measure 0.3 arcsec seeing on a field star. This high-resolution image is shown in Figure 1 with the HST V contours overplotted. Previously we had obtained very deep exposures at UKIRT in J, H and K. The objective was to use the NIR colours to resolve the age issue since they are extremely effective indicators of stellar population ages and they allow to break the age-metallicity degeneracy when coupled with optical observations. However, colours of strong line-emitting galaxies are not representative of the stellar populations unless they are corrected

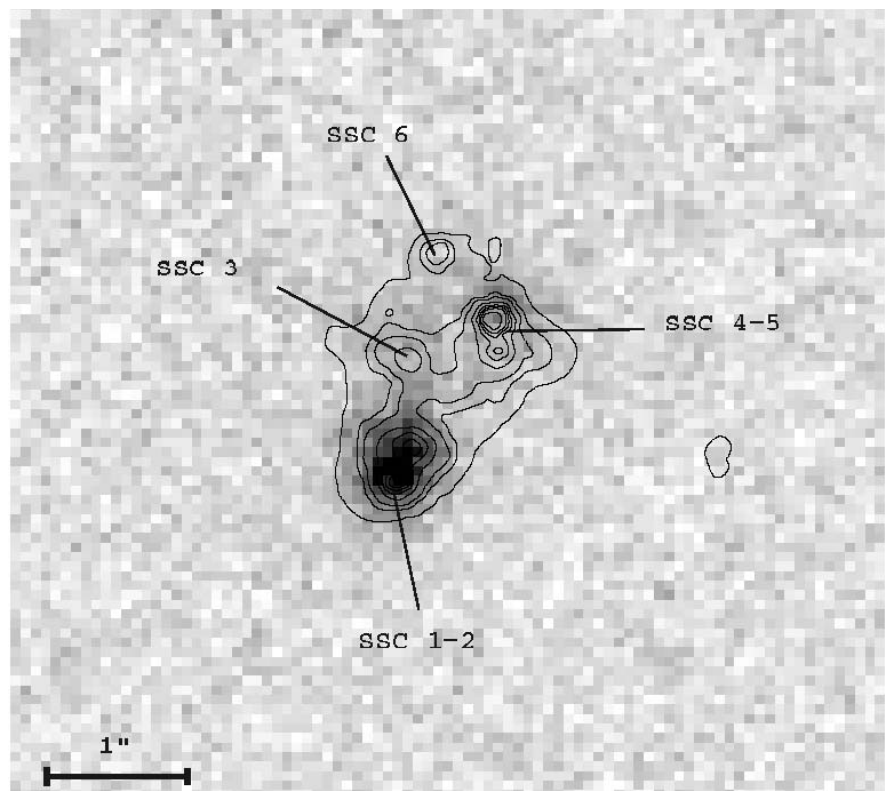


Figure 1: Ks image of SBS 0335-052 observed with SOFI at the NTT under $0.3''$ seeing. Contours in V band from the HST are overplotted.

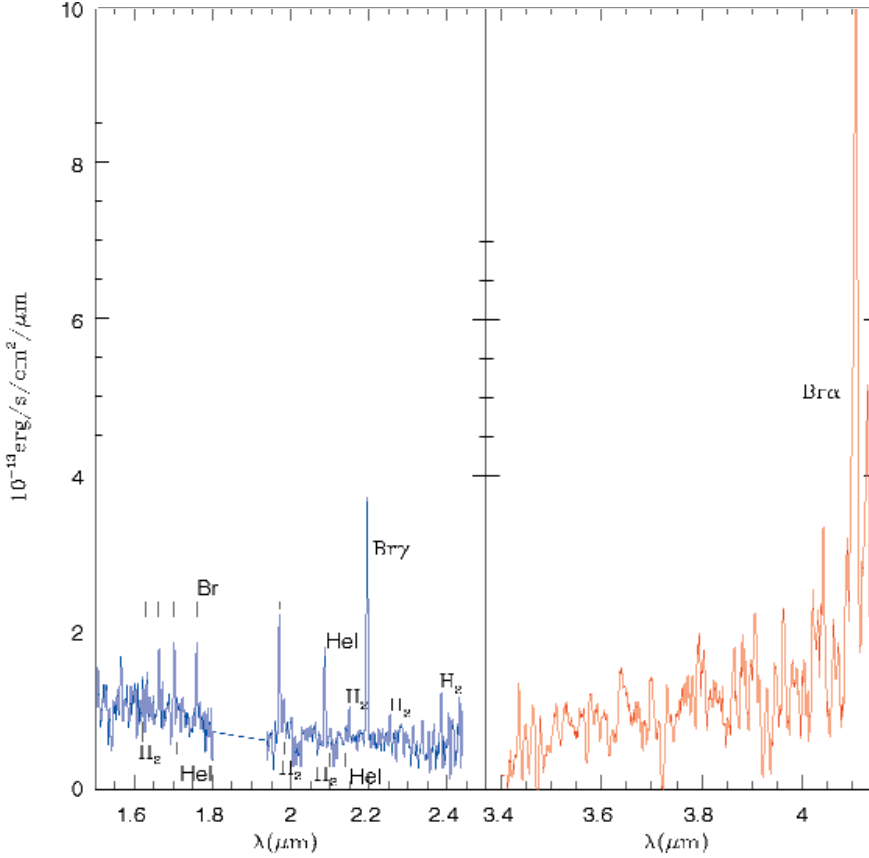


Figure 2: Low-resolution SOFI (blue) + ISAAC (red) infrared spectrum of SBS 0335-052.

for the nebular contribution. For this reason we also obtained a low-resolution spectrum ($R = 600$) covering the H and K NIR bands integrating 1 h 30 m and a medium-resolution ($R = 1400$) spectrum in the Ks band, 1 hour integration with SOFI at the NTT. The medium-resolution spectrum was observed under good seeing conditions ($0.5''$). In both cases we used a 1 arcsec wide slit and $PA = 145$. Finally, to better probe the high extinction found by TSM, we obtained a long wavelength ($2.7\text{--}4.2\ \mu\text{m}$) low resolution ($R = 360$) spectrum with ISAAC at the VLT-UT1 ANTU. A first observation with 30 minutes integration revealed a prominent $Br\alpha$ but with a too low S/N. Thanks to a Director discretionary time (DDT) approved programme we were able to integrate this first observation with 2 more hours of spectroscopy and a 30-minute L image before the galaxy set this year. Observations at these wavelengths are critical to probe the thermal regime and to check for the presence of dust and extinction. Figure 2 shows our low-resolution spectrum from 1.5 to $4.2\ \mu\text{m}$.

3. Results

3.1 Extinction

We measured the fluxes in the $Br\gamma$ and $Br\alpha$ recombination lines with an aperture of 1×1.5 arcsec. From Izotov et al. (1997) we have the flux in $H\alpha$ and $H\beta$ in the same aperture and can there-

fore attempt a multi-wavelength measure of the extinction by comparing the line ratios observed with the theoretical values. From the $Br\gamma$ measure, which was the first available to us, combined

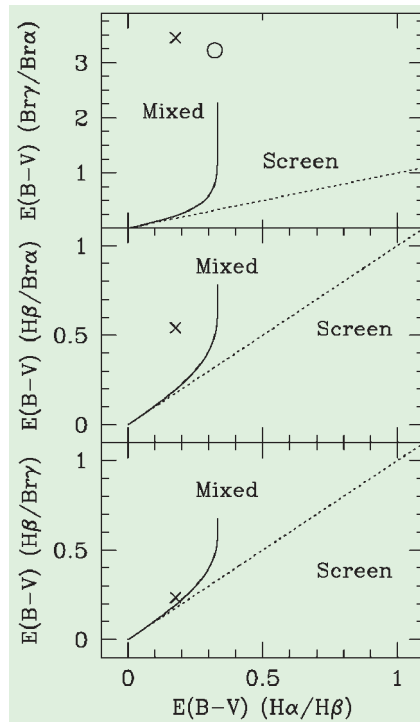


Figure 3: Colour excesses compared with a foreground screen and a mixed ISM. X is SBS 0335-052, O is NGC 5253.

Table 1: Values of the visual extinction measured with different recombination lines.

	$H\alpha/H\beta$	$Br\gamma/H\beta$	$Br\alpha/H\beta$	$Br\alpha/Br\gamma$
A_V	0.55	0.73	1.45	12.1

with $H\beta$, we obtained $A_V = 0.73$. This value was in agreement, within the errors, with the optical estimate of $A_V = 0.55$ showing little evidence, if any, for the heavily obscured star formation proposed by TSM. The recent measure of $Br\alpha$, however, gave a different result. Its comparison with $H\beta$ and $Br\gamma$ gives $A_V = 1.45 \pm 0.11$ and 12.1 ± 1.8 respectively. The values of optical extinction derived using different lines are summarised in Table 1. In Figure 3 we compare the corresponding values of $E(B-V)$ with a foreground screen of dust and a homogeneously mixed medium of dust and gas. Neither model gives an adequate description of the observations, although the mixed model is a better representation. Since the optical lines give very low extinction, a more likely picture consists of a dust free region responsible for most of the optical emission surrounding a highly obscured central core. In Figure 3 we also show the point corresponding to the blue dwarf galaxy NGC 5253 considered by Rieke et al. (1988) to be the youngest starburst known.

3.2 Stellar Population

Our NIR images achieve a spatial resolution that almost matches HST; in particular the regions corresponding to the SSC 1+2 and 4+5 are clearly resolved. Combining the NTT and HST images we have been able to build an optical-NIR colour-colour diagram including different regions of the galaxy. In Figure 4 we plot the points corresponding to the SSC 1+2 and 4+5, the global emission (E) and the north-west extended component (Ex) of the galaxy. The green solid line is the output of Leitherer et al. (1999, SB99) for a metallicity $Z_{\odot}/20$. Though SB99 includes the contribution of the nebular continuum emission, it does not reproduce the colours observed. This can be due to different reasons: (1) the metallicity of SBS 0335-052 is significantly lower than the model; (2) the high contribution of the emission lines to the broadband magnitudes. To investigate this we constructed a new model using the stellar SED for $Z_{\odot}/50$ – blue dotted line – and including nebular continuum and emission lines (see Vanzì et al. 2000 for details). The blue dots of Figure 4 correspond to ages of 3 and 5 Myr for this new model with the gas contribution included. The colours of the SSC 1+2 and 4+5, though not perfectly, are better reproduced than with SB99 and are consistent with a very

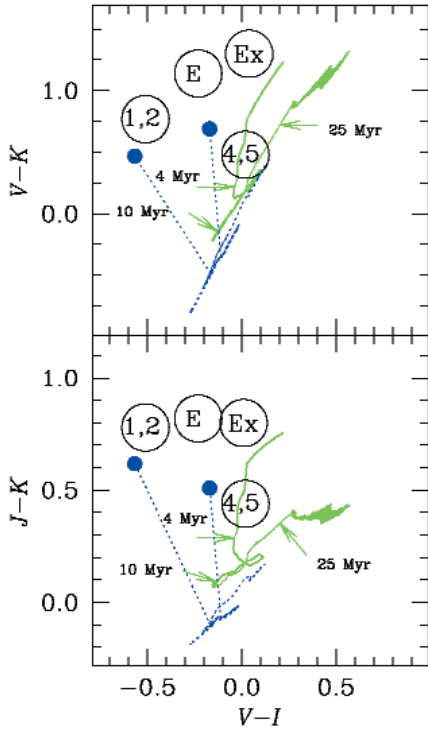


Figure 4: Optical-NIR colour-colour diagram of different regions in SBS 0335-052, mainly SSC1+2, 4+5, the whole galaxy (E) and north-west extended region (Ex). The green curves are the SB99 model with 4, 10 and 25 Myr indicated by arrows. Blue dotted curves represent the colours of a $Z_C/50$ stellar population, dotted lines connect the points of age 3 and 5 Myr to the points that include the nebular contribution.

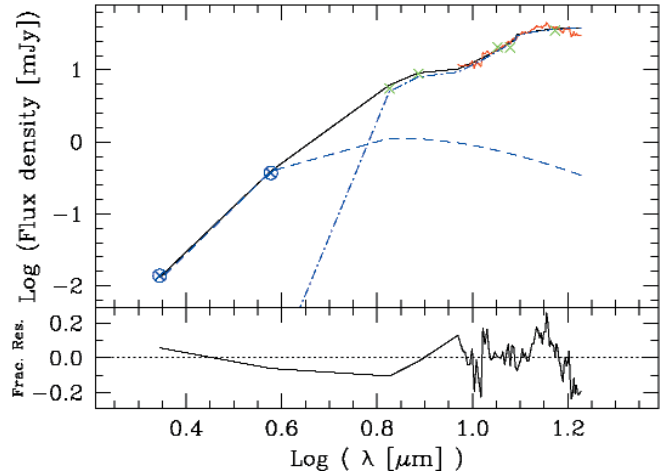
young population. Neither globally nor in the extended emission down to 23 K-mag/arcsec² do we find evidence for an evolved population. By including the colours of an evolved population in the model we can estimate what fraction of old stars can be present. Since we detect no evolved stars in our observations, the limit is set by the photometric errors and turns out to be $\sim 15\%$. This finding is supported by the non-detection of stellar absorption features in our NIR spectra. Though the S/N ratio on the continuum is never higher than 5, the CO bands at 2.3 μm should be prominent and observable if a population older than 10 Myr were dominating the K continuum. However, the non-detection of CO in absorption could also be attributed to the low metallicity of the galaxy.

We detect the helium recombination lines $4^3D - 3^3P^0$ at 1.700 μm and the blend of $4^1S - 3^1P^0$ and $4^3S - 3^3P^0$ at 2.113 μm . Their intensities relative to Br10 and Br γ respectively are consistent with the presence of stars more massive than 35 M_\odot (Vanzi et al. 1996, Vanzi et al. 2000) and therefore with the very young age of the galaxy.

3.3 Dust and Gas Content

The presence of dust in SBS 0335-052 has been inferred directly through

Figure 5: Fit of the IR SED. The green crosses are the photometric points from ISO, the blue circled crosses are the measures from SOFI and ISAAC and the red spectrum is from ISO. The blue dashed lines represent the modified black bodies and the dark line the best fit to all observations. In the lower panel the fitting residuals are displayed.



infrared observations, it is the only BCD observed in the mid-infrared along with He 2-10 (Sauvage et al. 1997) whose metallicity is not as extreme. The K-L colour is unusually red for a non Seyfert galaxy and has an average value of about 2. In Figure 5 we show the IR Spectral Energy Distribution built from the ISO observations of TSM and our K and L points after correcting for nebular and stellar emission. The data have been fitted by the superposition of two modified black bodies, one with $T = 192$ K obscured by $A_V = 16$ and the other with $T = 459$ K and no extinction. From the extinction observed we derived a total amount of dust of about $5 \cdot 10^3 M_\odot$. Such an amount would not have been expected in a BCD, but it is consistent with the expected production of type II supernovae. From the Br α flux and using the starburst model of Rieke et al. (1993) we derive a SN rate of about $6 \cdot 10^{-4} \text{ yr}^{-1}$ that, integrated over the present burst lifetime after onset of SN, gives about $2 \cdot 10^3$ SN. Each massive SN is expected to produce about 1 M_\odot (Todini & Ferrara 2001) which would produce about $2 \cdot 10^3 M_\odot$ of dust, roughly consistent with what is observed.

For what concerns the gas, most BCDs are undetected in the CO (1-0) transition (Taylor et al. 1998). This finding contrasts with the relative brightness of these objects in HI at 21cm (Thuan et al. 1999) and was initially interpreted as due to the

large ratio of neutral to molecular gas produced by the unusually high star-formation efficiency of these galaxies. However, recent evidence suggests a high H_2/CO ratio rather than a molecular gas deficiency (Taylor & Klein 2001). Our H_2 detection in the NIR spectrum of SBS 0335-052 supports the idea that molecular gas is actually present in BCDs though difficult to detect in the CO. At least 4 H_2 lines are clearly detected in our K spectrum. The comparison of the relative strength of these lines with the models support UV fluorescence as the main excitation mechanism.

3.4 Star Formation and Geometry

Our medium-resolution 2 μm SOFI spectrum was acquired under very good seeing conditions. The spatial profile of the emission lines is similar, and clearly distinct from the continuum. While Br γ and H_2 have a single-peaked spatial profile, the continuum shows a double peak. This is clearly shown in Figure 6. The main peak of the continuum and the emission lines are spa-

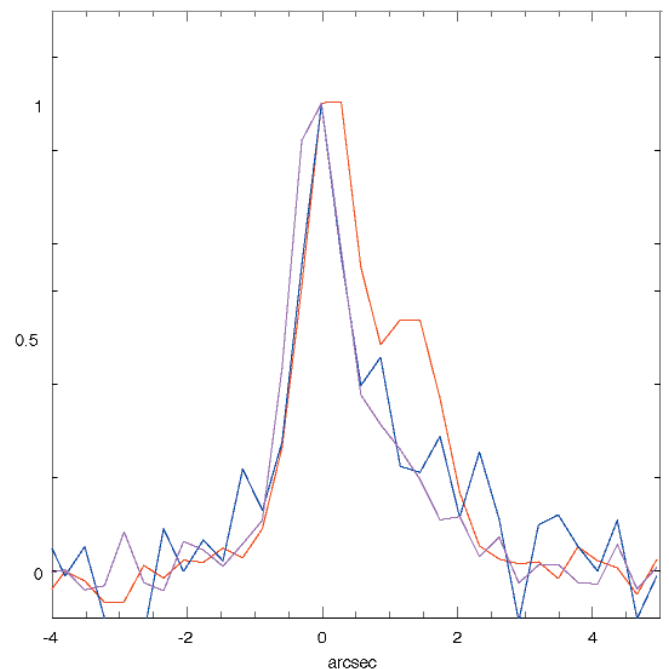


Figure 6: Spatial profile of Br γ – magenta – H_2 – blue, and 2 μm continuum – red.

tially shifted by about 60 pc meaning that the site of the most recent star formation is not located at the peak of the continuum. The same is detected by Izotov et al. (1997) in the optical but, in this case, the spatial shift is larger and about 200 pc. We interpret this as due to the larger contribution from the ionised gas to the NIR continuum than to the optical one, but it could also be partly an effect of extinction.

The L image, observed at the VLT with 0.5" seeing, reveals a very compact source at the position of the SSC 1+2. It is difficult to compare the location of this object with respect to the spectral profiles due to the lack of a reference point in the latter but, on the basis of this observation and the extinction derived at different wavelengths, we can envision the following picture.

Star formation occurs in a heavily obscured central core that contributes most of the IR emission. This core lies behind a dust-free region that instead emits the bulk of the optical radiation observed. The central burst produced a number of supernovae that polluted the interstellar medium with dust. Assuming that all the H α flux observed

is generated in the external shell and using standard line ratios we derive that the outer region contributes 50% of Br γ and only 25% of Br α . In other words, 75% of the star formation in SBS 0335-052 is only observable at 4 μ m! (see Hunt, Vanzi & Thuan 2001 for details). These results open a new view on SBS 0335-052 and possibly on star formation at high redshift. If the hidden star formation in SBS 0335052 is typical of young galaxies at high redshifts, then the cosmic star formation rate as derived from UV-optical observations would be underestimated by a factor 2–3. ISO surveys of distant galaxies (Flores et al. 1999) suggest that this is the case.

References

- Aloisi, A., Tosi, M., Greggio, L. 1999, *AJ*, **118**, 302.
 Flores H., Hammer F., Thuan T.X., Cesarsky C. et al. 1999, *ApJ* **517**, 148.
 Frogel J. 1985, *ApJ* **298**, 528.
 Hunt L.K., Vanzi L., & Thuan T.X. 2001, *A&A*, submitted.
 Izotov Y.I., Thuan T.X. 1998, *ApJ* **500**, 188.
 Izotov Y.I., Thuan T.X. 1999, *ApJ* **511**, 639.

- Izotov Y.I., Lipovetsky V.A., Chaffee F.H. et al 1997, *ApJ* **476**, 698.
 Leitherer C., Schaerer D., Goldader J.D. et al. 1999, *ApJS* **123**, 3.
 Kniazev A.Y., Pustilnik S.A., Masegosa J., Marquez I. et al. 2000, *A&A* **357**, 101.
 Kunth & Östlin 2000, *A&A Rev.* **10**, 1.
 Melnick J., Heydari-Malayeri M., Leisy P. 1992, *A&A* **253**, 16.
 Östlin, G. 2000, *ApJ* **535**, L99.
 Rieke G.H., Lebofsky M.J., Walker C.E. 1988, *ApJ* **325**, 687.
 Rieke G.H., Loken K., Rieke M.J., Tamblyn P. 1993 *ApJ* **412**, 111.
 Sauvage M., Thuan T.X., Lagage P.O. 1997, *A&A* **325**, 98.
 Steidel C.C., Gialalisco M., Pettini M., Dickinson M., Adelberger K.L. 1996, *ApJ* **462**, L17.
 Taylor C.L., Kobulnicky, H.A., Skillman E.D. 1998 *AJ*, **116**, 2746.
 Taylor C.L., Klein U. 2001, *A&A* **366**, 811.
 Thuan T.X., Izotov Y.I., Lipovetsky V.A. 1997, *ApJ* **477**, 661.
 Thuan T.X., Sauvage M., Madden S. 1999, *ApJ* **516**, 783.
 Thuan T.X., Lipovetsky, V.A., Martin J.M., Pustilnik S.A. 1999 *A&AS* **139**, 1.
 Todini P., Ferrara A. 2001, *MNRAS*, submitted.
 van Zee L. 2000, *ApJ* **543**, L31.
 Vanzi L., Rieke R.H., Martin C.L., Shields J.C. 1996, *ApJ* **466**, 150.
 Vanzi L., Hunt L.K., Thuan T.X., Izotov Y.I. 2000, *A&A* **363**, 493.

Eigenvector 1: An H-R Diagram for AGN?

J. W. SULENTIC¹, M. CALVAN², P. MARZIAN²

¹Department of Physics and Astronomy, University of Alabama, Tuscaloosa, AL, USA

²Osservatorio Astronomico di Padova, Padova, Italy

Abstract

Observations with 1.5-m-class ESO telescopes have contributed significantly to a much clearer understanding of the phenomenology of Active Galactic Nuclei (AGN) that has emerged over the past seven years. Long-slit spectra of good resolution and high s/n enable us to accurately measure emission-line parameters for a significant number of AGN. Combined with soft X-ray and UV line measures from Hubble Space Telescope, the data reveal a parameter space that distinguishes between the diverse classes of AGN and organises them in a way that promises to redefine the input to physical models. We suggest that this Eigenvector 1 (E1) parameter space may be as close as we will ever come to finding an H-R diagram for quasars. Several arguments suggest that the ratio of AGN luminosity to black hole mass ($L/M \propto$ accretion rate) convolved with the effects of source orientation drives the principal E1 correlation. While L/M sustains, in a sense, the H-R analogy beyond phenomenology, the

role of orientation reflects the greater complexity inherent in the lack of spherical symmetry for AGN.

1. Introduction

The H-R Diagram is well known as the most fundamental correlation space for stars. A plot of surface temperature vs. luminosity effectively discriminates between the diversity of normal and "abnormal" stellar types. Main-sequence stars show a strong correlation in the space while stars in other evolutionary stages are identified by their different domain space occupation. The fact that a 2-D correlation space is so effective reflects the simplicity of the law of hydrostatic equilibrium that governs stellar structure. Thus the principal driver of the correlation space is stellar mass. It is possible that after less than 50 years of study we might see a similar correlation space on the horizon for Active Galactic Nuclei (AGN). ESO spectroscopic observations have made a significant contribution to the work that has led to the Eigenvector 1 concept. The fundamental parameters of

an AGN correlation space might be expected to be more numerous than those for a stellar diagram because we are observing a combination of primary continuum and secondary line and continuum emission components in a structure with complex geometry. In fact, the 2-D optical (for low z quasars) parameter plane reveals much of the correlation power. In its present evolution our 4-D Eigenvector 1 correlation space shows a phenomenological discrimination in several ways comparable with that of the H-R diagram for stars. The veracity and implications of that statement will likely be the subject of much research in the next decades.

A defining characteristic of AGN involves the presence of broad emission lines (usually FWHM H $\beta \geq 10^3$ km/s). This definition encompasses Seyfert 1 nuclei, QSO's, broad line radio galaxies and quasars. BLLACs (in low continuum phase) and Seyfert 2 nuclei (in polarised light) also sometimes show broad lines. Although the first AGN (quasars) were discovered because of their radio-loudness, it is now known that the bulk of AGN are radio-quiet.

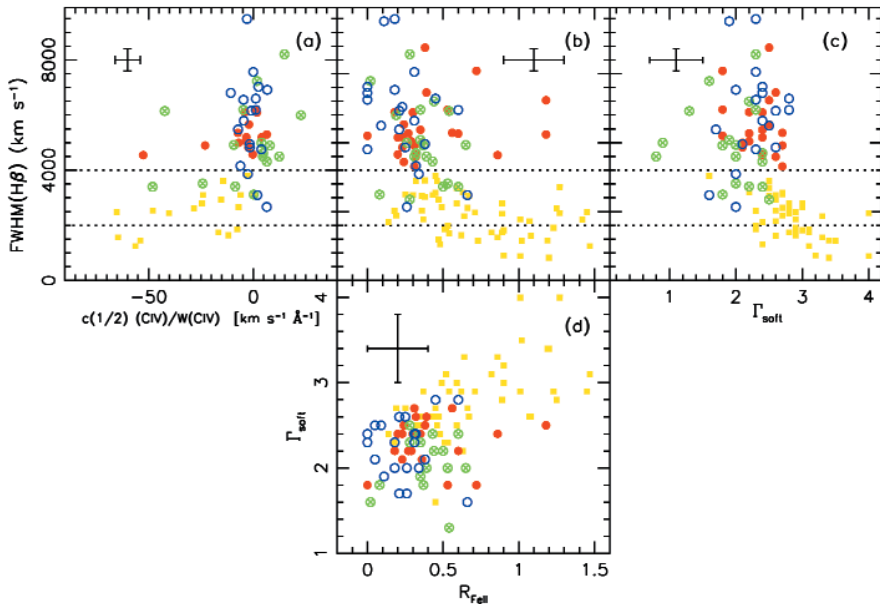


Figure 1: Principal correlates of the E1 parameter space. The central panel (b) shows the optical E1 plane: $FWHM(H\beta)$ vs. RFE. RQ Population A sources (yellow squares), RQ population B (red circles), core-dominated RL (green circles) and lobe-dominated RL (blue open circles). Other E1 panels shown are: (a) $FWHM(H\beta)$ vs $CIV\lambda.1549$ shift normalised by rest frame equivalent width; (c) $FWHM(H\beta)$ vs Γ_{soft} and (d) Γ_{soft} vs. RFE. Horizontal lines mark the approximate FWHM upper limits for NLSy1 (2000 km/s) and RQ population A (4000 km/s) sources.

Radio-loudness in this context involves sources with a radio continuum flux $SR > 100$ times larger than an optical continuum value (see e.g. Kellermann et al. 1989). Various unification schemes have been proposed to unite all of the AGN phenomenology under the umbrella of a model that assumes: (1) the ultimate energy source as gravitational accretion onto a supermassive black hole and (2) an obscuring torus that prevents us from observing broad lines in sources inclined within $\approx 45^\circ$ of edge-on to our line of sight.

2. Eigenvector 1 Parameters

We currently define Eigenvector 1 in terms of four parameters:

1. Full width half maximum of the low ionisation broad lines (LIL: $H\beta$ is the current favourite because it is reasonably strong, not impossibly contaminated by other lines and yields optical measures for sources out to a redshift of $z \sim 1.0$) ($FWHM(H\beta)$).

2. The equivalent width (EW) ratio of the optical FeII emission (usually the FeII Ångstrom 4570 blend) and broad line $H\beta$ (RFE).

3. The soft X-ray photon index which is thought to measure a thermal emission feature seen in the 0.1–2.4 keV range for many AGN (Γ_{soft}).

4. The FWHM centroid velocity shift of the high ionisation broad lines ($CIV\lambda.1549$ is the easiest to measure) ($C(1/2)_{CIV}$).

We focus on the first two (optical) parameters and indeed the H-R analogy is obvious there. The optical parameters first appeared in a correlation

analysis of LIL emission-line data for PG bright quasars (Boroson & Green 1992). Our ESO observations helped to double the number of sources with such measures. Γ_{soft} measures come from numerous ROSAT observations (e.g. Wang et al. 1996; Brinkmann et al. 1997) while $C(1/2)_{CIV}$ emerged from the first large sample comparison of HIL and LIL in the same sources (Sulentic et al. 1995b; Marziani et al. 1996). Figure 1 shows the four most studied planes of E1. We plot data for sources with spectra having (in most cases) $s/n > 30$ (continuum near $H\beta$) and resolution better than 10 \AA (see Sulentic et al. 2000a,b for details). We find that addition of data with lower resolution and s/n quickly blurs all important structure and correlation in E1. There is no substitute for high s/n and moderate/high-resolution spectra. Many, of these sources ($n = 128$) have matching X-ray and UV data ($n = 76$). At this point our sample is mixed with major data components from the reasonably complete PG bright quasar sample and a heterogeneous sample of sources with HST archival UV spectra. The latter element results in an over-representation of radio-loud (RL) sources. The results so far suggest that E1 organises the AGN phenomenology better than any previous result.

3. Domain Occupation and Correlation in Eigenvector 1

Narrow-line Seyfert 1 (NLSy1) galaxies occupy one parameter domain extremum in E1. They show: (a) the narrowest broad line (down to 800 km/s)

LIL profiles; (b) largest RFE; (c) strongest soft X-ray excess and (d) a systematic CIV blueshift with values as large as 4–5000 km/s. At the opposite extremum we find steep spectrum (lobe dominated) radio-loud sources with: (a) the broadest LIL profiles (up to $FWHM = 23,000 \text{ km/s}$); (b) smallest RFE, (c) no soft X-ray excess and (d) a stochastic distribution of red and blue CIV centroid shifts (a mean near 0 km/s). Aside from the difference in domain space occupation for RL and RQ sources, we find that both radio and optical continuum luminosity appear to be uncorrelated with E1 parameters. We tentatively identify two radio-quiet populations in Figure 1: “Pure RQ” Population A (yellow) with $FWHM(H\beta) \leq 4000 \text{ km/s}$ and Population B (red) with the same domain occupation as the majority of RL sources (flat spectrum – green and steep spectrum – blue). The few RQ sources in the “forbidden zone” of the optical E1 plane (large FWHM and RFE) generally show broad absorption lines, excess IR emission and ultra strong FeII emission – this may be the domain of type 2 (obscured) quasars. Population A sources show significant intercorrelation between all parameters (a “main sequence”?) which breaks down in the RL/RQ population B domain. It is not yet possible to say if this reflects larger uncertainties for measurements of the broader line sources.

Figure 2 shows ESO spectra for two RQ sources (population A NLSy1 Ton 28 and population B RQ Seyfert 1 NGC 3783) that illustrate well the extreme differences found between AGN in the RQ population A and B domains. The ESO data alone show the full optical phenomenological differences revealed by E1. The days are clearly gone when one can say that all quasars look alike spectroscopically! Figure 3 shows the matching $CIV\lambda.1549$ line profiles obtained through ESO-ST-ECF. We also show our ESO spectrum of Pictor A which further emphasises the line profile differences across E1. This RL source is typical of the most extreme lobe-dominated RL sources that show the broadest observed LIL Balmer lines. It is a true opposite extreme from Ton 28 in all the E1 parameters. Table 1 provides a summary of average parameter values across E1.

4. Towards a Physical Interpretation

Attempts to model E1 have so far focused on the optical plane where the ESO observations have played an important role. This is also where the “H-R” analogy is most compelling. It is the plot of line width versus the intensity ratio of two different atomic species that can be easily measured for a large number of quasars. Absorption line widths and line intensity ratios vary

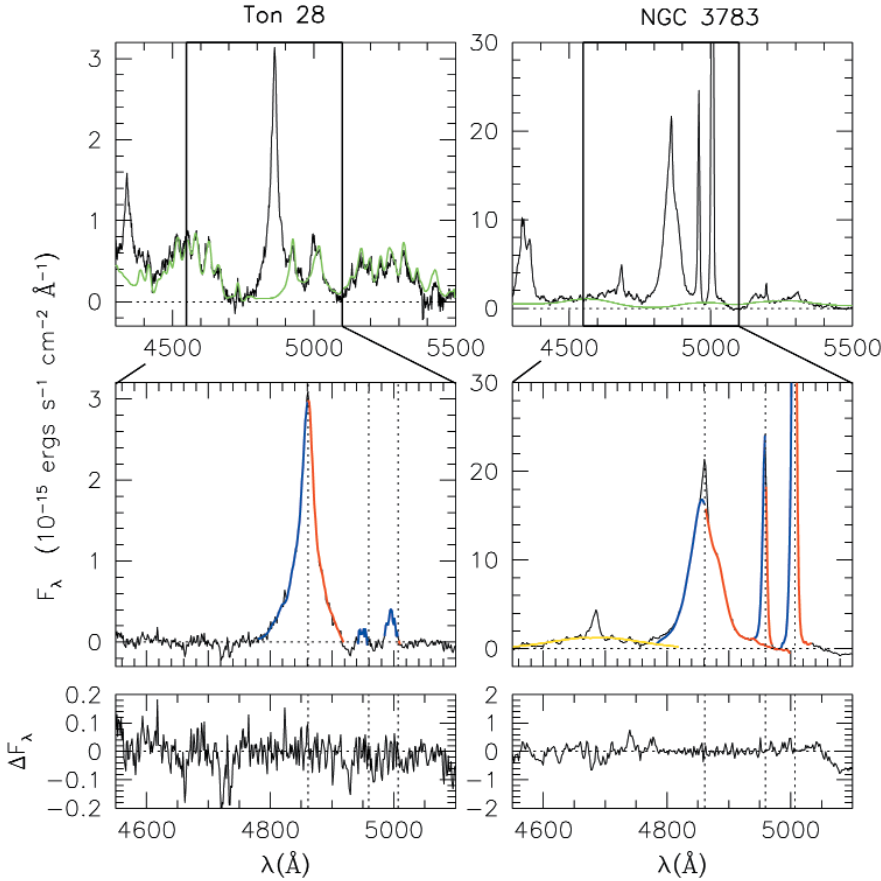
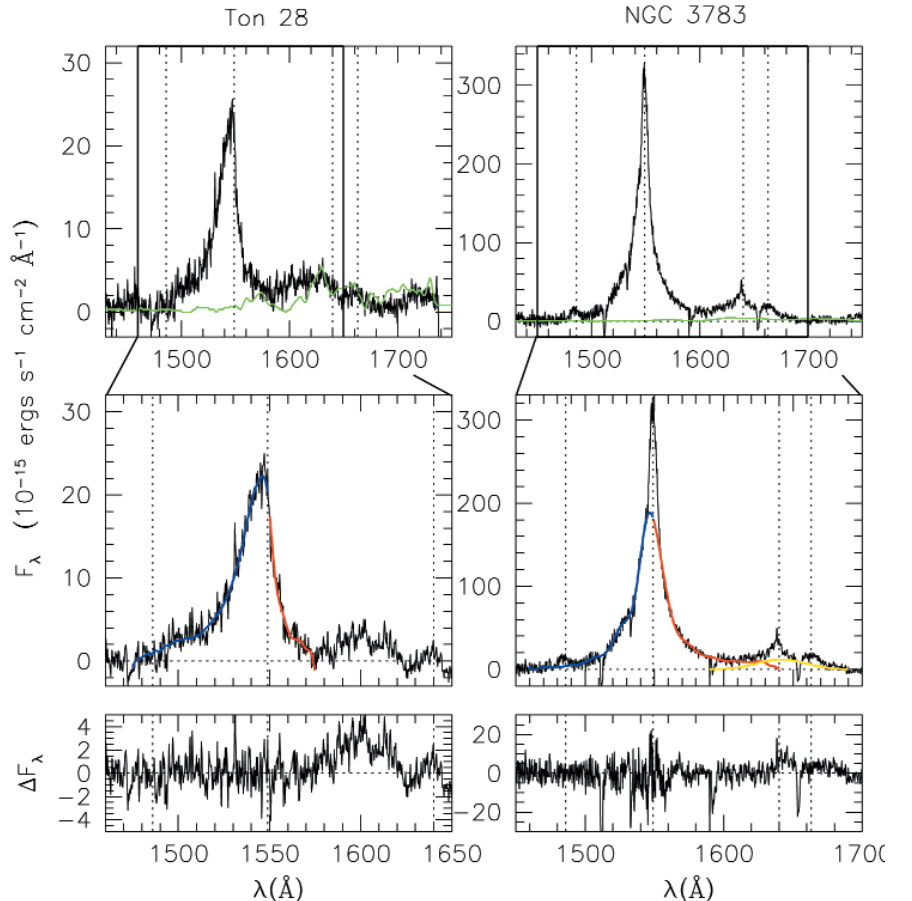


Figure 2: Comparison of ESO spectra for the $H\beta$ region of a NLSy1 Population A source (Ton 28) and a RQ Population B source (NGC 3783). Upper panels show the continuum subtracted, flux-calibrated spectra. We superimpose the adopted FeII emission model (green). The middle panels zoom the wavelength range around $H\beta$ in order to better show the line profile. The vertical dotted lines indicate the rest-frame wavelengths of $H\beta$ and the $[OIII]\lambda\lambda 4959, 5007$ lines. Blueward and redward wings of the broad component of $H\beta$ and the $[OIII]$ lines are traced in red and blue to better emphasise profile asymmetries and shifts. The thick yellow line shows a gaussian fit to a very broad $H\beta$ emission component. The lower panels show the residual spectrum after subtraction of continuum, FeII, and all identified lines.

across the H-R diagram and are central to our understanding of stellar physics. In fact, the optical plane of E1 illustrates well the role of the principal physical drivers in E1. The X-ray and CIV $\lambda 1549$ measures provide additional and strong support for our interpretation with the latter, our best hope for decoupling the effects of source orientation. Independent studies which interpret the soft X-ray excess as a thermal feature and the UV CIV blueshift as a wind or outflow motivate the suggestion that they are directly related to an accretion disk surrounding the central black hole. Thus we begin our inter-

Figure 3: Comparison of ST-ECF archival data for the CIV $\lambda 1549$ spectral regions in Ton 28 and NGC 3783. Spectra are displayed in the same manner as for $H\beta$ (Figure 2). Note the large CIV profile blueshift in NLSy1 Ton 28.



pretation of the optical plane with the assumption that NLSy1 sources are the class of AGN with the highest accretion rate.

A long-standing problem for BLR models has involved explaining the strength and dispersion of FeII emission observed in AGN. The optical FeII lines arise from collisional excitation, and therefore assumptions of high density and large column density are required to model them. The presence of strong FeII emission, especially in population A sources, makes an accretion disk origin for FeII production an attractive possibility. A medium that favours strong FeII emission may, at the same time, collisionally suppress $H\beta$ emission. Perhaps this combination explains why the EW ratio RFE is so extreme in NLSy1 and shows such a large dynamic range across E1. At the same time FWHM ($H\beta$) in such a scenario is likely to be orientation sensitive. The narrow FWHM measures found for many NLSy1 argue that at least some of them are seen near face-on (this argument is supported by the short time-scale high amplitude X-ray variability seen in some NLSy1). We have developed a model where we express the E1 parameters and the model physics in terms of the AGN luminosity to black hole mass ratio ($L/M \propto$ Eddington ratio = the dimensionless accretion rate). This allows us to predict the expected values of the optical E1 parameters for a typical black-hole mass convolved

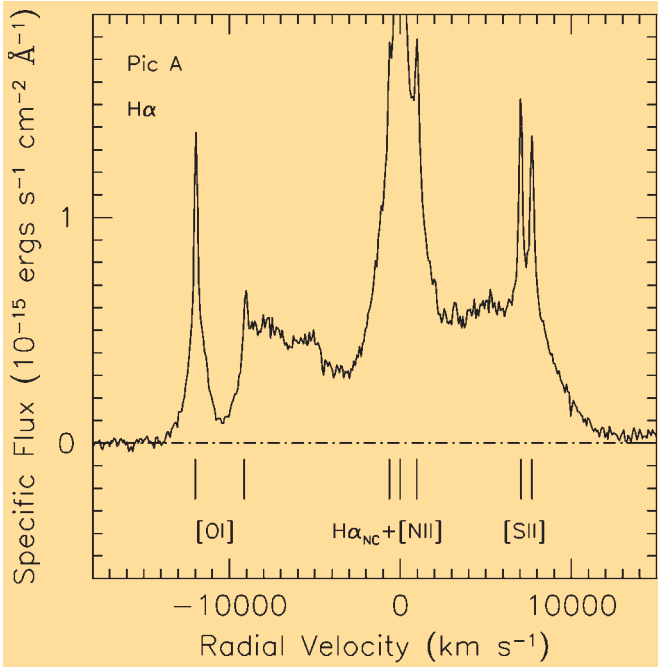


Figure 4: ESO spectrum of the complex and ultra-broad $H\alpha$ profile of Pictor A. This records its appearance on December 18, 1993. The source was single peaked and much narrower 5–10 years before this date.

with a range of source orientation from near face-on (10°) to near torus obscured (40°). In Figure 5 our model fits are superimposed on the optical E1 plane and appear to predict the principal zone of occupation/correlation quite well. The analogy to the “main sequence” is apparent except that L/M is convolved with source orientation while M is an orientation independent physical driver of the main sequence. In this interpretation NLSy1 sources with the hottest disks and strong wind outflows suggest an analogy with the hottest main sequence OB stars.

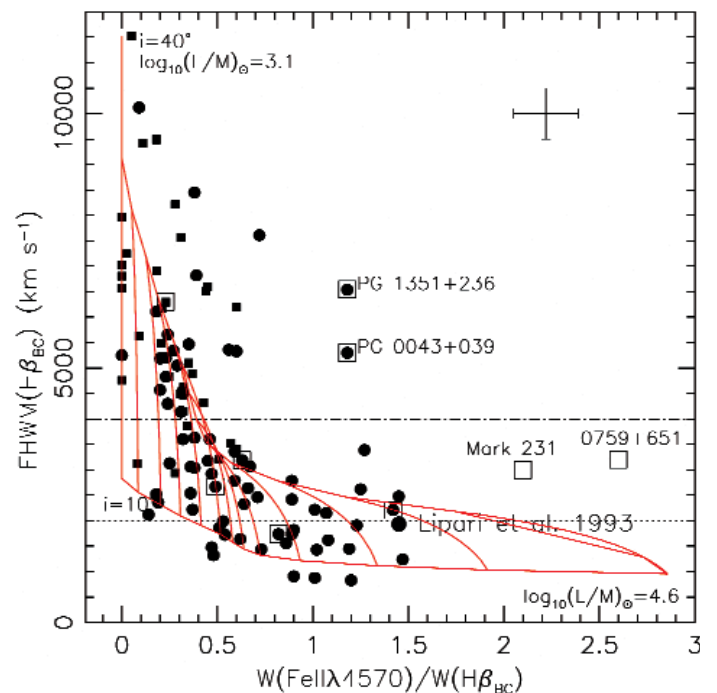
Our model is focused on the population ARQ sources and suggests that E1 is measuring several accretion disk properties that reflect a high accretion rate. Ironically the RL sources that were argued, just a few years ago, to be the best candidates for disk line emission may be the lowest accreting AGN. We are exploring the possibility that RL and RQ population B sources lie below a critical accretion threshold where the disk could be optically thin, transient or nonexistent. The line profile of Pictor A (Figure 4) has indeed shown dramatic changes over the past 15 years (Sulentic et al. 1995a). Several properties of these low-accreting sources are consistent with line production in a bi-conical outflow.

5. Conclusion

How is it possible that potentially fundamental results about AGN could emerge from observations with telescopes with small/moderate aperture? The first response is that a significant number of quasars are brighter than $V = 16.0$ so that excellent spectra can be obtained with investments of 0.5–

2.0 hours. The second is that very few people are now working on spectroscopy of the broad emission lines. The reasons for the paucity of researchers are complex but one of them is that some people moved away from the field because of a sense of frustration about the diversity of AGN spectra and the very few strong line related correlations that had been found. Eigenvector 1 is likely to change that. Obviously we are overstating the E1 – HR analogy here, and a lot of work still remains to be done on the interpretation – as well as on testing whether the same scenario may still be valid at higher redshift and source luminosity. But if the domain occupation and correlation in E1 proves to be robust

Figure 5: Model grid of the expected distribution of RQ population A sources superimposed on the E1 optical plane. Model assumes that L/M (\propto dimensionless accretion rate) is the principal physical driver (convolved with effects of source orientation). Grid is shown in steps of $L/M = 0.1$ over an inclination range of 10 – 40 degrees for a $\log M = 8.0$ black hole. BAL quasars are boxed symbols.



with larger and high-quality data samples then the analogy will have been justified.

7. Acknowledgements

We are indebted to several colleagues who took part in the work involving ESO data and who helped us to gain access to northern-hemisphere observing time (D. Dultzin-Hacyan, T. Zwitter, M. Moles). We also acknowledge financial support from the Italian Ministry of University and Scientific and Technological Research (MURST) through grants Cofin 98 – 02 – 32 and Cofin 00 – 02 – 004. J.S. acknowledges with gratitude hospitality and support from Osservatorio Astronomico di Padova, Brera and Merate where parts of the work were carried out.

References

- Brinkmann, W., Yuan, W., and Siebert, J. 1997, *A&A*, **319**, 413.
 Boroson, T. A., and Green, R. F. 1992, *ApJS*, **80**, 109 (BG92).
 Kellermann K. I., Sramek R., Schmidt M., Shaffer D. B. and Green R. 1989, *AJ*, **98**, 1195.
 Marziani, P., Sulentic, J. W., Dultzin-Hacyan, D., Calvani, M., & Moles, M. 1996, *ApJS*, **104**, 37.
 Marziani, P., Sulentic, J. W., Zwitter T., Dultzin-Hacyan D., and Calvani, M., 2001, *ApJ*, in press.
 Sulentic, J. W., Marziani, P., Zwitter, T. and Calvani, M., 1995a, *ApJ*, **438**, 1.
 Sulentic, J. W., Marziani, P. Dultzin-Hacyan, D., Calvani, M. and Moles, M., 1995b, *ApJ*, **445**, 85.
 Sulentic, J. W., Marziani, P. and Dultzin-Hacyan, D. 2000a, *ARA&A*, **38**, 521.
 Sulentic, J. W., Zwitter, T., Marziani, P., and Dultzin-Hacyan, D. 2000b, *ApJL*, **536**, L5.
 Wang T, Brinkmann W., Bergeron J. 1996, *A&A* **309**, 81–86.

Disk Orientations in PMS Binary Systems Determined Through Polarimetric Imaging With UT1/FORS

J.-L. MONIN¹, F. MÉNARD^{2,1}, and N. PERETTO³

¹LAOG, Observatoire de Grenoble, Grenoble, France

²Canada-France-Hawaii Telescope Corporation, Kamuela, USA

³Université Joseph Fourier, Grenoble, France

Summary

Photons are an expensive product of astronomical telescopes. The wide wavelength and instrumental techniques coverage offered by the VLT allows astronomers to dissect the incident radiation in many ways: spectroscopy and imagery are well-known observing techniques to VLT observers. A maybe less well-known technique is polarimetry. The IPOL mode of FORS on UT1 allows to measure high-quality polarimetric images on a wide field of view. We used this instrument during period 65 to determine the respective orientation of circumstellar disks in pre-Main-Sequence binaries. In this paper, we present our method and first results obtained with FORS/IPOL. Thanks to the top-quality assistance of the VLT and FORS teams, our run was remarkably successful and the instrument appears extremely well adapted to fine polarimetric measurements on large fields of view. Our first results suggest that circumstellar disks tend to be aligned in PMS binaries.

Introduction

Our current understanding of low-mass stellar formation has to take into account two very different yet complementary constraints. On one hand, when we consider individual stars, the current model put forward for embedded Young Stellar Objects (YSOs) includes a central stellar core, surrounded by an equatorial accretion disk and a remnant infalling envelope. This stage is frequently associated with energetic bipolar molecular outflows, perpendicular to the disk and tracing the symmetry axis of the whole system (Fig. 1a).

On the other hand, we also know that a large fraction of T Tauri stars (TTS) form in binary or multiple ($N > 2$) systems. This ubiquitous property of the stellar formation process has a potentially enormous influence on the previous one because the circumstellar environment of the individual components of a multiple system can be deeply modified by the presence of a companion. The study of individual disks in PMS binary systems and in particular their relative orientations can provide

strong constraints on the star-formation process (Fig. 1b).

Strictly speaking, a full 3-D orientation determination of the rotation axes of both components requires the knowledge of 2 angles: the inclination on the line of sight and the orientation in the plane of the sky. The former angle can be obtained through the combination of the projected rotational velocity, $v \sin i$, the rotational period, and an estimate of the stellar radius. This determination is quite indirect and can induce large uncertainties. Polarimetry can give access to the disk orientation in the plane of the sky, provided the disk is far enough from pole-on, a condition met in more than 50% of the cases.

Method

The presence of a disk, even if spatially unresolved, can be traced in large parts by the thermal emission of its dust. This dust, and especially its small particles, also polarises the starlight in the optical and near-infrared in a fashion that depends on the scattering geometry. Numerical simulations show

that unresolved aperture linear polarimetry can be used to extract information about the geometry of the scattering medium.

Models of bipolar reflection nebulae by Bastien and Ménard (1990) have shown that the position angle of the integrated linear polarisation of the scattered starlight is parallel to the equatorial plane of the disk, provided the inclination is sufficiently large (see Fig. 2). The method is thus likely to give good results when circumstellar disks are present around the two stars in the binary, i.e. when both are Classical TTS (CTTS). We have chosen our targets so that at least one of the components can be classified as an active T Tauri star. Previous observations of PMS binary stars have shown that most of the time, if one of the components of a young binary system has an active disk, so has the other.

Caveat

One of the main problems of polarimetric measurements in young systems is that such stars are often deeply

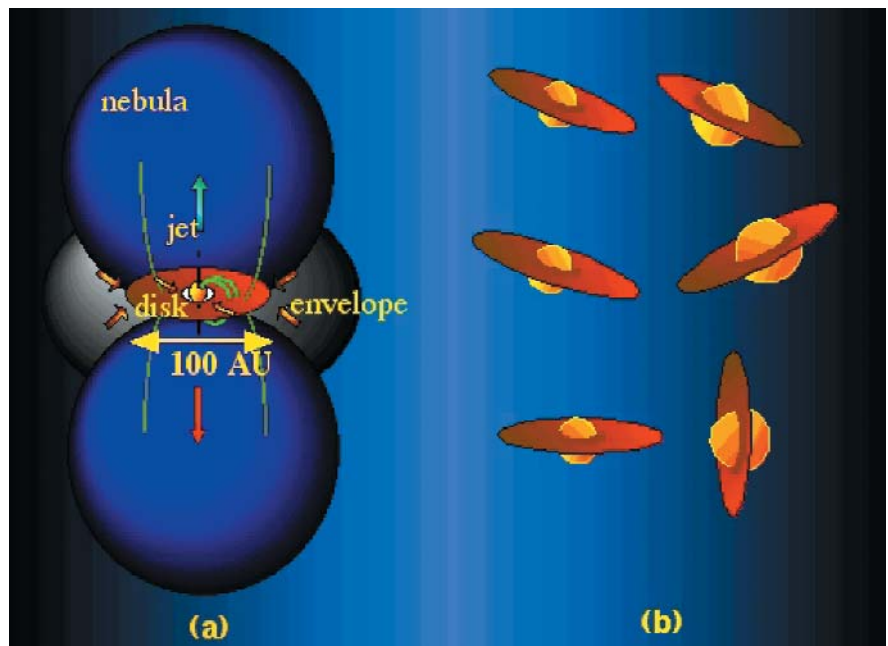


Figure 1: "Standard" TTS model including a circumstellar disk, an envelope and a nebula (a). When it comes to a binary (the most probable outcome in a young stellar object formation), the determination of the respective orientation of both disks (b) can bring new constraints on the stellar formation process.

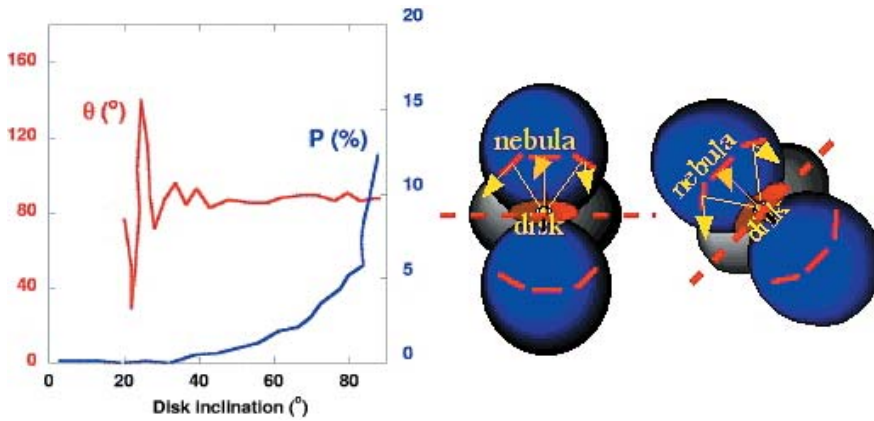


Figure 2: The circumstellar dust structure present around a TTS polarises the stellar light. Left: models by Bastien & Ménard (1990) show that if the disk is more than 45 degrees from pole-on, the polarisation direction reliably traces the disk orientation. Right: in a binary, the relative orientation of the disks can be determined from their polarisation.

embedded in molecular clouds and subject to interstellar medium polarisation. When we measure two different polarisation directions in a binary system, we can be fairly sure that they are actually different, but if they are similar, there is a chance that this identity is due to a common interstellar polarisation. This is why a large-field polarimetric imaging system like the one available with FORS/IPOL on UT1 is essential in this context. We are now able to measure *at the same time*, the polarisation on the central system and on a large number of nearby field stars (Fig. 3). These ‘outsiders’ measurements bring very valuable information on the large-scale interstellar polarisation pattern, providing a kind of ‘calibration’ of the central binary measurement.

Instrument

Most of the observer information can be found in the ESO FORS user manual. The basic method of linear polarisation measurements uses a transmission polariser (also called analyser in such a case) in the incident beam, so that the system measures the projected intensity going through. When using different positions of the polariser, one can reconstruct the level of polarisation and the position angle of the polarisation direction. One of the main difficulties of this method is that we want to estimate small fluctuations (typically 1%) over a large signal that remains constant when the analyser is rotated. Any transparency variation in the incident beam can be wrongly interpreted as a polarisation signal. To overcome this difficulty (as in many polarimeters), the FORS instrument is equipped with a Wollaston prism that splits the beam into two different directions with orthogonal polarisation states, the so-called *ordinary* (O) and *extraordinary* (E) beams. A stepped half-wave plate retarder is placed at the entrance of the incident beam and can be rotated at

various angles multiple of 22.5° (16 positions in a complete rotation), making the incident polarisation rotate. For each position of the plate, a CCD image is recorded. The separation of the two O and E beams on the CCD is performed via the Wollaston prism, using a focal 9-slit mask, so that a given polarisation state (E or O) occupies half of

the focal plane image. The total field of view of the instrument is $6.8' \times 6.8'$ in the Standard Resolution (SR) mode with a focal scale of $0.2''/\text{pixel}$. In this mode, the slits are $20''$ wide on the CCD. One could theoretically extract the polarisation information (Stokes parameters Q & U, hence the polarisation level P and its position angle θ) with 2 positions of the half wave plate. In practice, 4 positions are often necessary. The FORS/IPOL observing blocs allow to choose 4, 8 or 16 positions, leading to 4, 8 or 16 images stored. Then a Fourier series is computed to extract P and θ from the data.

Data Reduction

We have written a dedicated data reduction pipeline using NOAO/IRAF. The first step concerns of course bias, bad pixels and flat-field corrections. Then the images go through a polarisation pipeline. Two options are available: P and θ can be estimated on a pixel per pixel basis, a useful possibility to map extended structures like reflection nebulosities, at the cost of a loss of accuracy on point sources when the image quality (FWHM) changes during a rota-

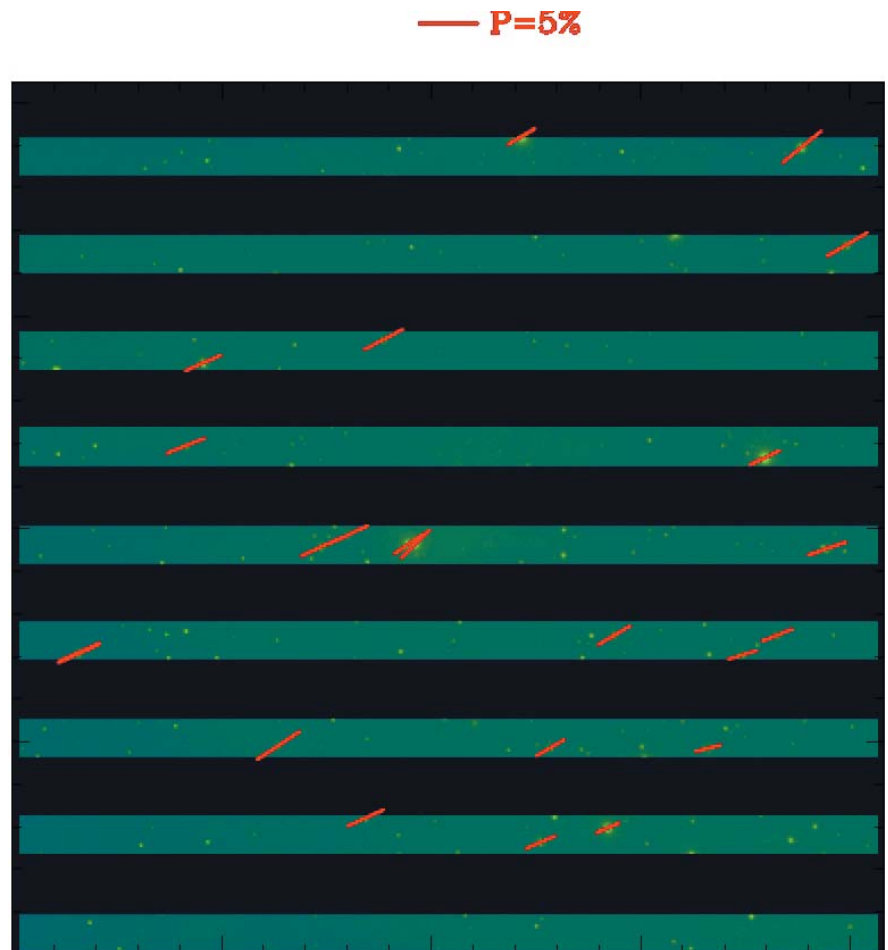


Figure 3: Resulting polarisation map on a $6.8' \times 6.8'$ field of view around the SZ 60 binary. We can trace the local interstellar polarisation on a large number of surrounding field stars. These supplementary measurements are of great importance to finally determine the intrinsic polarisation on the central object.

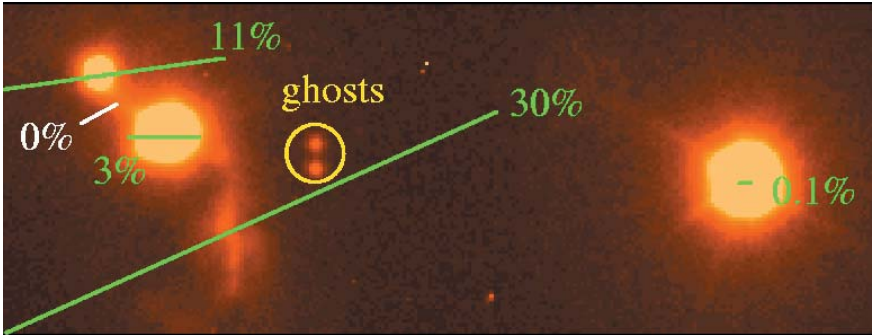


Figure 4: I band image and polarisation map of WSB 42 and its associated – strongly polarised – reflection nebula.

tion acquisition. Another possibility uses aperture photometry to estimate precise polarisation measurements on point-like objects. Indeed, the individual CTTS components and their disks in our binaries are most of the time spatially unresolved, and the disk orientation information is obtained via aperture photometry. When using aperture photometry, we can account for any FWHM change if a large enough aperture is used. Both techniques are available in our pipeline on request, to estimate the polarisation of point sources and extended features alike (see Fig. 4).

We measure the errors using two independent methods: first from the statistical photon noise on the E & O beams separately, and then propagating the errors up to U, Q, P and θ ; second, measuring the standard deviation on the 4, 8 or 16 images from the half-wave plate rotation. Both estimations are consistent except in some pathological cases, and this second method is extremely useful to consistently check our results. Our conclusion on the observing strategy is that it is strongly recommended to systematically record 16 images using all the available $\lambda/2$ plate positions. The result is without question worth the time investment. Most of the time, the residual error is less than $\Delta P = 0.1\%$ (absolute value) when the binary components are well separated (≥ 1.3 arcsec). Our programme also includes tight binaries for which we have to adjust and subtract a PSF; depending on the contrast and separation, the errors can at worse reach $\Delta P = 0.25\%$, a value well within our goal.

Instrumental Polarisation

Of crucial importance is the determination of the instrumental polarisation. We have carefully measured it against nearby unpolarised targets. We have observed GJ 781 and GJ 781.1, two high proper-motion stars (so quickly moving indeed since the time our finding chart was made, that the VLT image pointing recognition system could not

lock at first sight!). As the close solar neighbourhood is remarkably devoid of dust, the interstellar polarisation of near-Earth objects can be considered null. The average of our 4 measurements on both GJ objects gives $P_{\text{inst}} = 0.02\% \pm 0.03\%$. Even if bad luck could have made the instrumental polarisation just cancel the possible intrinsic polarisation of these test stars, we independently found some of our low-polarisation scientific targets to present linear measurements very close to previously published measurements. We believe that FORS/IPOL (+ incident optics) instrumental polarisation is actually very low, well below 0.1%, so we considered it as negligible for practical purposes and we did not remove it from other measurements.

Preliminary Results

Figure 3 shows that the interstellar polarisation can dominate over the central object intrinsic polarisation: on this

image, all the polarisation vectors are aligned, with a possible fluctuation on the central objects. One of the great advantages of FORS/IPOL in this matter is that our wide-field polaro-imaging data allow us to carefully measure the local interstellar polarisation. We are currently working on a method to remove this “ambient” polarisation in order to study the intrinsic target polarisation. Another valuable result is that we have obtained images at different wavelengths (V, R and I bands) so that we will be able to check whether the expected λ dependence of the polarisation is recovered. For most of our sources, the result will remain unchanged, with both polarisations remaining parallel, but in a few cases, the changes can be clear, in magnitude and/or orientation.

The fact that in most binaries the disks appear to be mostly parallel (see Fig. 5) suggests that this is a result of the binary formation process. As these systems are young (1–3 Myr), it is unlikely that tidal interactions have had the time to realign the disks. If disks around the components in young binaries are coplanar, then they may provide stable favourable environments to build large planetary bodies.

Acknowledgement

None of our measurements would have been possible without the constant and extremely efficient support of the VLT and FORS/IPOL teams. We also acknowledge the help of the telescope operators, and they may recognise themselves when we say that there has been “no cause for alarm” during the run.

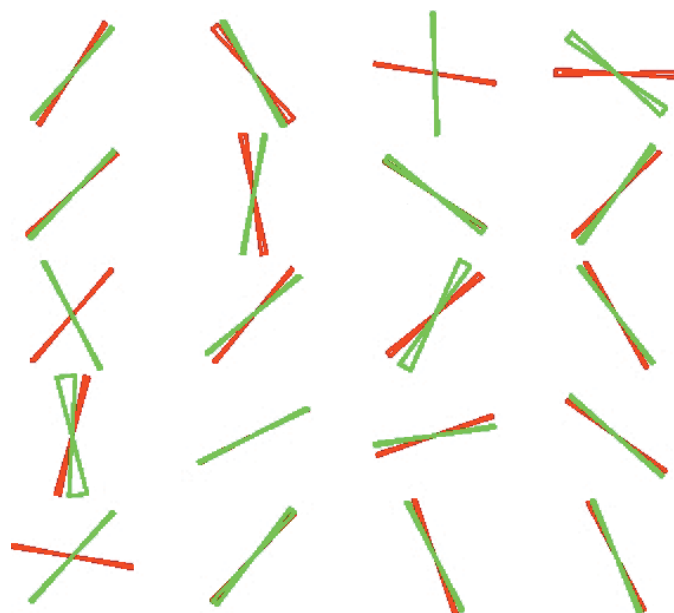


Figure 5: Orientation sketch of twenty binaries observed during our first FORS/IPOL run. The disks are figured as bow ties of constant length and a width proportional to the residual error (primary in red, secondary in green) In more than 16 objects upon 20, both disk polarisation orientations are similar, indicating that disks tend to be physically aligned.

Detecting Magnetic Fields of Upper-Main-Sequence Stars With FORS1 at ANTU

S. BAGNULO¹, T. SZEIFERT¹, G.A. WADE², J.D. LANDSTREET³ and G. MATHYS¹

¹European Southern Observatory, Santiago, Chile

²Dépt. de Physique, Université de Montréal, Canada

³Physics and Astronomy Department, The University of Western Ontario, London, Ontario, Canada

During the night between 22 and 23 March 2001, the VLT unit telescope ANTU was pointed to a 6th-magnitude A-type star to obtain several low-resolution spectra in circular polarisation with FORS1. Two nights later, the same exercise was repeated selecting a second A-type star of similar magnitude. The outcome of this experiment was the firm detection of a magnetic field in an upper-main-sequence star, HD 94660. It is the first time that a VLT unit telescope was (successfully) used to detect magnetic fields in non degenerate stars.

We will start with a quick overview about observations of stellar magnetic fields, and we will outline the theoretical fundamentals of magnetic diagnostic techniques. Then we will describe our experiment with the VLT and discuss which perspectives our results open for the observations of stellar magnetic fields with large telescopes.

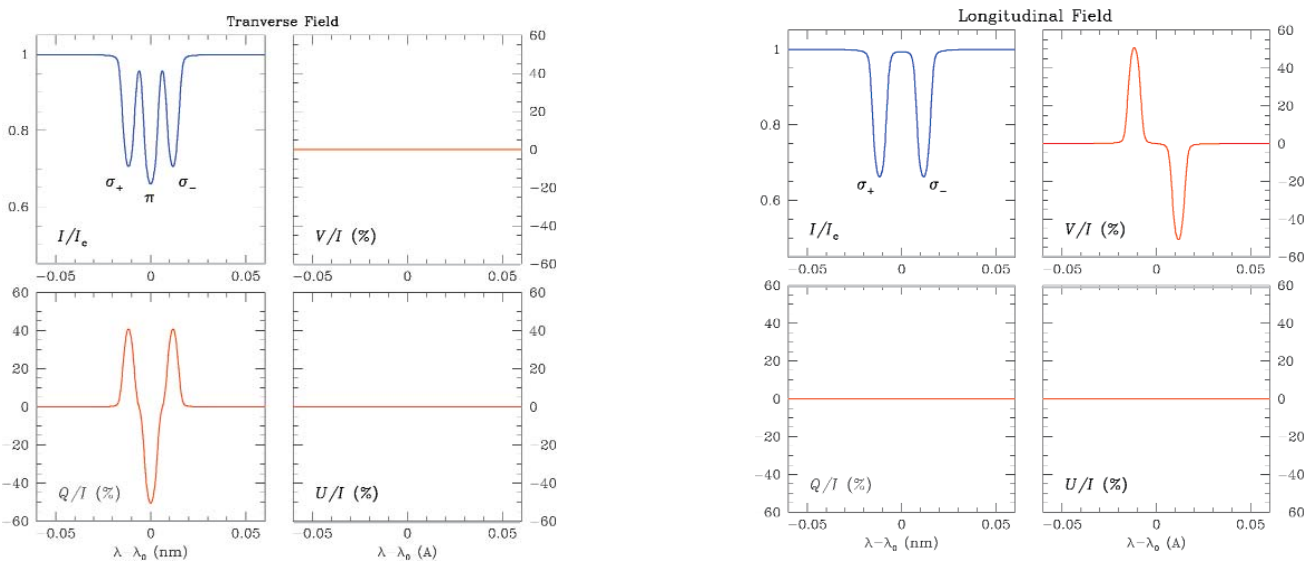
1. Some History

Magnetic fields have been firmly detected in many objects of the Hertzsprung-Russell diagram. In historical

order, obviously first comes the Sun, with the discovery made by Hale (1908) that sunspots are characterised by a magnetic field up to a few kG. The first detection of a magnetic field in a star other than the Sun was made 40 years later, with the observations of the Ap star 78 Vir by Babcock (1947). A decade later, it was clear that most of the chemically peculiar stars of the upper main sequence are characterised by a magnetic field organised on a large scale, with a typical strength of a few hundred up to a few ten thousand G (Babcock 1958). Ap stars are still the

The Zeeman Effect on Spectral Lines

Let us assume that a spectral line is formed in presence of a magnetic field perpendicular to the line of sight. The classical interpretation of the *Zeeman effect* describes an atomic oscillator split into two σ components at frequencies $\nu_0 \pm \nu_L$, and into a π component at frequency ν_0 , where ν_0 is the unperturbed frequency of the oscillator, and ν_L is the Larmor frequency. The σ components appear polarised in the direction perpendicular to the magnetic field vector, the π component is polarised in the direction parallel to the magnetic field. In case of a longitudinal field, the spectral line will be split into two σ components at frequencies $\nu_0 \pm \nu_L$, circularly polarised in opposite directions. Above some critical regime, about 1 MG, the quadratic Zeeman effect becomes important, and line formation can be explained only in terms of quantum-mechanics. For $B > 50$ MG, magnetic field and Coulomb forces are of comparable strength, and only few numerical calculations have been performed to explore the physics of line formation in this regime. These complications should be taken into account for objects such as (some) magnetic white dwarfs, or cataclysmic variables, but can be safely neglected in non degenerate stars. For a 10 kG magnetic field, the Stokes profile of a *metallic* line originated by a single stellar surface element appears as in the left lower panels for a transverse field, and as in the right lower panels for a longitudinal field. Stokes I represents the well-known 'intensity', Stokes V measures the circular polarisation, Stokes Q and U the linear polarisation. Typically one prefers to plot the ratio Stokes V/I , Q/I , and U/I , i.e., we normalise the polarisation to the intensity (sometimes the continuum intensity), and we express this ratio in percent units, as in these panels. Note that for a transverse field, the circular polarisation is zero (left panels). Note also the different signs of Stokes Q in the π and σ components – which correspond to a linear polarisation parallel to the field in the π components, and perpendicular to the field in the σ components. (The fact that Stokes U is null depends uniquely on the reference system adopted for the measurement of the linear polarisation.) For a longitudinal field (right panels), the linear polarisation is zero.



For a field vector arbitrarily oriented, the line components are 'elliptically' polarised, see for instance the top panels on page 33, which refer to a 10 kG field tilted at an angle of 45° with respect to the line of sight, and with an azimuth angle of 30°.

most popular targets for studying stellar magnetic fields (except the Sun, of course): their strong and smooth field produces a signal of polarisation on the spectral lines that can relatively easily be detected even through disk-integrated observations. In comparison, the value of the disk-averaged solar magnetic field is extremely low: from 3 G at solar minimum to 20 G at solar maximum. Most of it is concentrated in discrete magnetic elements of mixed polarity, so that the net, disk-averaged component of the field along the line of sight is much smaller than those values. In particular, the circular polarisation of spectral lines due to several magnetic flux tubes of different polarities would mostly cancel out if the sun were observed as a star. Most main-sequence late-type stars have probably a solar-like magnetic morphology, which as such escaped all attempts of detection until the eighties, when Robinson et al. (1980) detected a phenomenon of magnetic intensification in the spectral lines of ξ Boo A and 70 Oph A.

Amongst the objects outside the main sequence, magnetic white dwarfs are the 'easiest' targets: as in the Ap stars, the magnetic field of white dwarfs is generally characterised by a smooth morphology, but with a strength which can measure up to several hundred megagauss! However, white dwarfs are very faint objects (typically $V > 13$), therefore only middle- and large-size telescopes are suitable for their observations. The first detection of a magnetic white dwarf was made 30 years ago (Kemp et al. 1970), and large surveys have been carried out in the last decade (Schmidt & Smith 1995; Putney 1997).

Thanks to refined studies of magnetic intensification of spectral lines, or the use of more modern and exotic techniques such as the LSD (this means Least Square Deconvolution, Donati et al. 1997), magnetic fields are nowadays commonly observed also in pre-main-sequence stars, and in various evolved objects such as RS CVn stars.

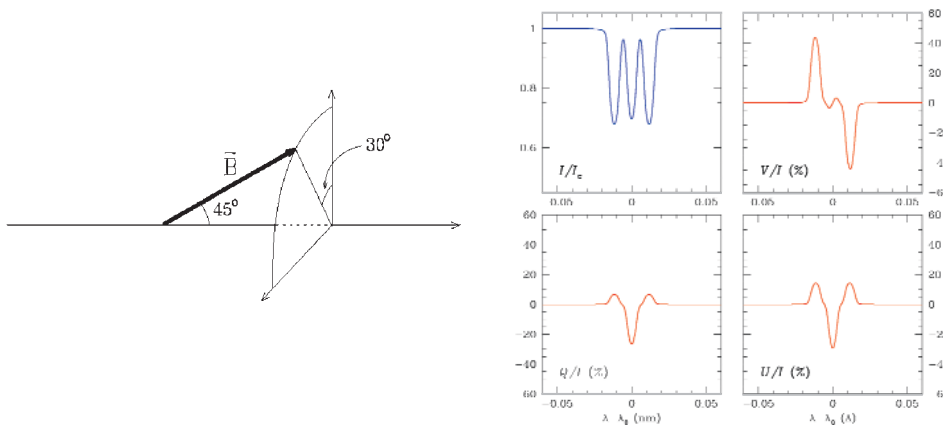
As we will show next, the VLT has also the capability of playing a central role in the studies of stellar magnetic

fields, not only for observations of extremely faint objects that would be simply invisible to middle-size-class telescopes, but also for highly sensitive detections of magnetic fields in relatively bright stars.

2. Theoretical and Observational Basis

The most direct method for detection of magnetic fields in non degenerate stars is based on the analysis of the Zeeman effect in the Stokes parameters of the spectral lines.

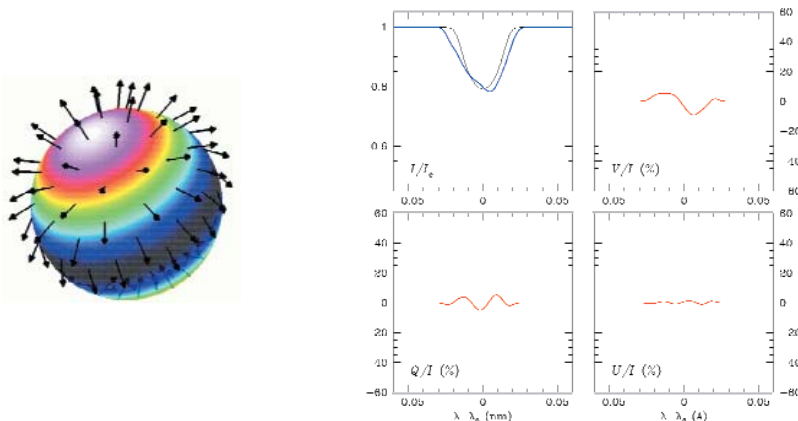
Spectral lines formed in presence of a magnetic field may be split into several (polarised) components. In the optical range, the Zeeman splitting is of the order of about 1 km s^{-1} per kG, which means for instance that the splitting of spectral lines of a star characterised by a mean field strength of 10 kG is comparable to the effect of rotational broadening if the star rotates with projected rotational equatorial velocity $v \sin i = 10 \text{ km s}^{-1}$. It is clear that rotational broadening is going to wash out



The stellar case is a bit more complicated, as one has to integrate the contributions from all stellar surface elements, taking into account a magnetic field which changes across the stellar surface: the polarisation signal is noticeably diluted, since contributions to the polarisation signal coming from different stellar regions tend to cancel out. The right panels in the figure below show the Stokes profiles calculated for a 10 kG dipole oriented as shown in the left panel, and for a star that rotates with $v \sin i = 10 \text{ km s}^{-1}$. Note that Zeeman splitting in Stokes I is washed out by the rotational broadening, whereas polarisation in spectral lines can typically be observed in stars that rotate with $v \sin i$ up to a few tens of km s^{-1} . (In faster rotators, also Stokes Q , U , and V become 'invisible'.) For 'real' magnetic morphologies, which are in general much more complex than the dipolar one, detection of stellar magnetic fields may be quite challenging!

Note that the Zeeman effect is also responsible for a broadening of the spectral lines, which depends upon the magnetic strength, but – to first order, not on the field orientation. The contributions from different stellar regions do *not* cancel out, and spectral lines formed in presence of a magnetic field appear always slightly broader than what expected in the same physical conditions but without magnetic field.

(For comparison, the black thin solid line represents the spectral line formed without the presence of a magnetic field.)



One of the worst enemies of the polarisation in spectral lines is the instrumental blurring. The Stokes profiles shown in the figure would be considerably smeared out if they were observed with a spectral resolution as low as 40,000 (!) and would be reduced to a level nearly consistent with noise at spectral resolutions lower than 10000. High resolution is mandatory for spectropolarimetry of metallic lines. Clearly, for Hydrogen lines, the resolution requirements are considerably relaxed.

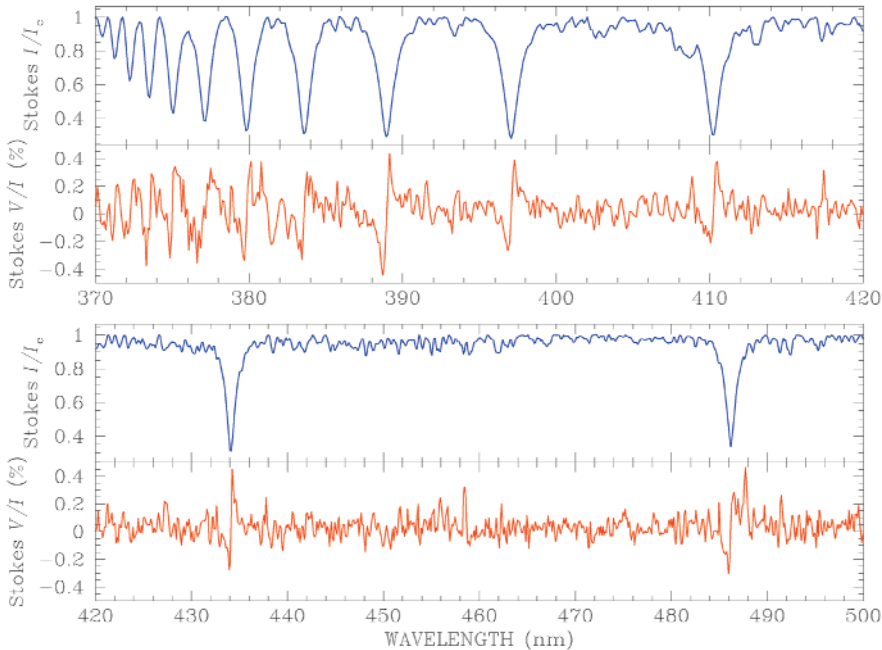


Figure 1: The polarised spectrum of the magnetic Ap star HD 94660.

the Zeeman splitting in most stars, except those that are very slow rotators and which possess a very strong magnetic field. Although these kinds of objects do exist, and Zeeman splitting has been detected indeed in several magnetic Ap stars (see Mathys et al. 1997), most magnetic stars can be disclosed as such only through the use of polarimetric techniques. (The Zeeman effect on spectral lines is illustrated in the box below.)

Indeed, most of our knowledge of stellar magnetic fields comes from the detection of *circular* polarisation of metallic lines. The theory of line formation in a magnetic field shows that the measurement of the first-order moment of Stokes V about the line centre of metallic lines is proportional to the component of the magnetic field along the line of sight averaged over the stellar disk, i.e., the *mean longitudinal magnetic field* (e.g., Mathys 1991; this technique is equivalent to the measurement of the splitting of a spectral line observed in both senses of circular polarisation, which is what Babcock did in his pioneering work in the 50's). An extensive campaign of spectropolarimetry of Ap stars was carried out by Mathys (1991) at ESO with CASPEC at the 3.6-m telescope. Since CASPEC was decommissioned, no high-resolution spectroscopy in circular polarisation is currently possible at ESO.

An alternative technique for the detection of stellar magnetic fields was developed in the 70's by Angel & Landstreet (1970; see also Borra & Landstreet 1980), based on the detection of circular polarisation on the Hydrogen Balmer lines (and in some hot stars, also He Balmer lines). The H Balmer lines are so broad that they can

be easily detected even at low resolution. In fact, what for instance Borra & Landstreet (1980) used was rather a *photopolarimetric* technique, which made use of two 5 Å wide filters centred on the wings of the H β . Similarly to the measurement of the first-order moment of Stokes V about the line centre, the measurement of the difference between the circular polarisation observed in the red and blue wings of H β permits one to derive the mean longitudinal field. In principle, we thought the same technique could be used with a low-resolution spectropolarimeter such as FORS1, with which, in addition, several Balmer lines could have been observed. In the past, spectropolarimetry of the H α and H β Balmer lines was repeatedly applied for detection of strong magnetic fields of white dwarfs. The question was whether the same technique could have been used for detection of weaker stellar fields, such as those of magnetic Ap stars. The theoretical examples shown in the box refer to sharp metallic lines, and do not account for instrumental blurring. What happens with the (very broad) H lines observed at the low resolution of FORS1 ?

Under reasonable approximations, one can show that for H lines

$$\frac{V}{I} = 4.67 \times 10^{-13} \lambda^2 \frac{dI}{d\lambda} \frac{1}{I} \langle B_z \rangle \quad (1)$$

where I is the usual (unpolarised) intensity, V is the Stokes parameter which measures the circular polarisation, λ is the wavelength expressed in Å, and $\langle B_z \rangle$ is the mean longitudinal field expressed in G. The precision of this expression is certainly arguable, the reader can find more details e.g., in

Mathys (1989). However, there is no doubt that it does permit us to give a first rough estimate of the longitudinal field $\langle B_z \rangle$ – caution should be used however for detailed modelling purposes. A simple numerical exercise shows where the major problems come from. Take a star with a 1 kG longitudinal field, be aware that for H Balmer lines of A and B stars $dI/d\lambda \times 1/I$ is typically $< 0.1 \text{ \AA}^{-1}$, and find that the expected value of the circular polarisation is about 0.1%. This means that for a firm detection of a 1 kG magnetic field, we need to count at least 10^6 photons. For a 100 G field we expect a polarisation of 0.01%, i.e., we want to obtain a S/N ratio of 10^4 ! Clearly, such a S/N ratio need not be per pixel, but integrated over the direction perpendicular to the dispersion, and over all the various observed Balmer lines. With the GRISM 600B (which covers the interval range between 3450 and 5900 Å, i.e., including all Balmer lines from H β on), the signal that we want to detect is spread over approximately 10^3 pixels. Therefore, we estimated that 10^5 was the order of magnitude of photons per pixel that we should try to reach – something safely possible by setting the readout mode to low gain, and with the help of multiple exposures. (Multiple exposures are anyway mandatory in polarimetric mode: to minimise the effect of cross-talk, exposures have to be taken with the retarder waveplate set at different angles.)

3. Results

Thanks to DDT 266.D-5649, we were able to test this technique with FORS1 at ANTU. The observations were carried out with the Grism 600B. With a 0.4 arcsec slit we obtained a spectral resolution of about 2000. As a target for our experiment we selected a well studied magnetic Ap star, HD 94660, which is known to have a very long rotational period (≈ 2800 d) and a moderately strong magnetic field. For comparison, we also decided to observe a non magnetic star of similar spectral type and magnitude, HD 96441. Figure 1 shows the observed spectrum of HD 94660 in 'natural' light (Stokes I), normalised to the (pseudo) continuum, together with the spectrum of the circular polarised radiation. The S/N as measured from the rms around the continuum is about 1500 per pixel (binned in the direction perpendicular to the dispersion). A dozen Balmer lines are clearly visible, and what looks like noise is due in fact to the contributions of many metallic lines: it should be recalled that chemically peculiar stars are characterised by overabundances (with respect to the solar case) of iron peak and rare-earth elements. All H Balmer lines appear clearly polarised up to a maximum level of about 0.4%. Note the characteris-

tic S-shape of Stokes V profiles of Balmer lines; the fact that the circular polarisation is negative in the blue wings and positive in the red wings tells us that the mean longitudinal field is negative, i.e., points away from the observer.

Like Stokes I , also Stokes V looks very noisy. A fraction of the ‘noise’ is probably due to the polarisation coming from the metallic lines, as it appears clear from a comparison with the observations of HD 96441, the non-polarised star that was selected for a comparative test (see Fig. 2). Here the signal of circular polarisation is consistent with a null detection, and what we see in Stokes V is real noise.

A more quantitative overview of the results of our experiment is shown in Figure 3. A least-square technique was used to derive the longitudinal field via Eq. (1), allowing also for a constant contribution of instrumental polarisation. The validity of Eq. (1) is in fact limited to unblended H lines. Clearly, our spectrum includes zillion metallic lines, many of them blended with H lines. Still, Eq. (1) was empirically shown to be a reasonable assumption. We first applied a least-square technique including *all* data points (i.e., including all H Balmer lines and all metallic lines); then we repeated the calculations considering only the wavelength intervals around the Balmer lines. The results from the two experiments were found consistent among themselves, and for HD 94660 we derived a longitudinal field of -2110 ± 50 G (Figure 3 refers to the H Balmer lines only). This value is fully consistent with what is known from

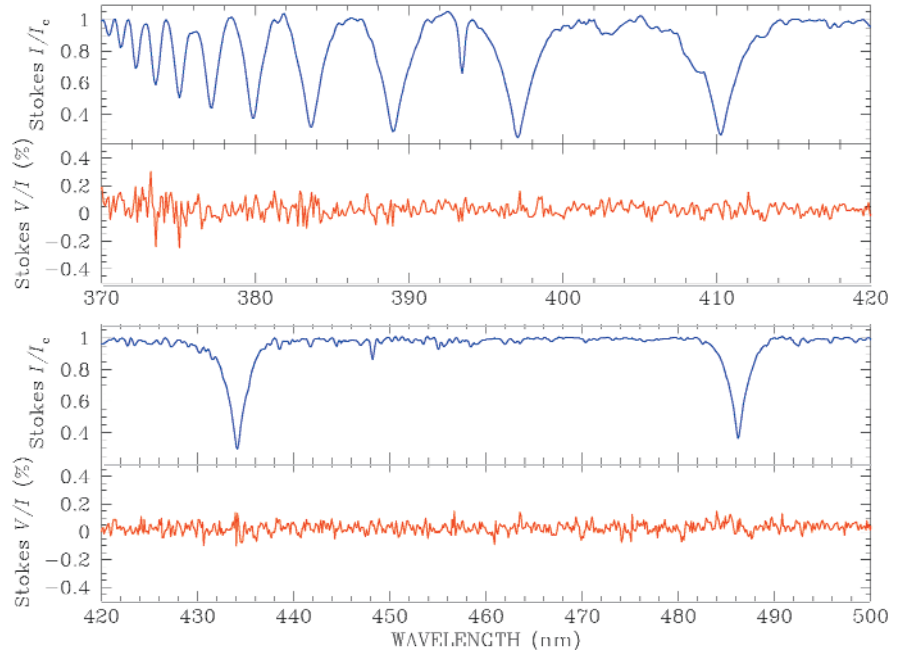


Figure 2: The unpolarised spectrum of the non magnetic A star HD 96441.

previous studies of the same star. As a matter of fact, Balmer lines dominate the observed Stokes I and Stokes V . However, the *real* error associated to our estimate of $\langle B_z \rangle$ is probably larger than the *formal* error obtained via the least-square technique: it should be recalled that Eq. (1) permits us to obtain the mean $\langle B_z \rangle$ only as a first approximation. The estimate of the mean longitudinal field of HD 96441 was found consistent with zero. The contribution due to instrumental polarisation was found about -0.03% .

4. A Comparison with the Previous Techniques

The magnetic target selected for our experiment was a very bright star: $V = 6$. Our choice was due to the fact that most of the known magnetic stars are very bright. Clearly, the actual exposure time was very short (about 30 seconds, split in several exposures). We roughly estimate that 200–300 G fields can be detected with an exposure time of about 2 hours in a 13th magnitude star. (The limit magnitude that we can reach

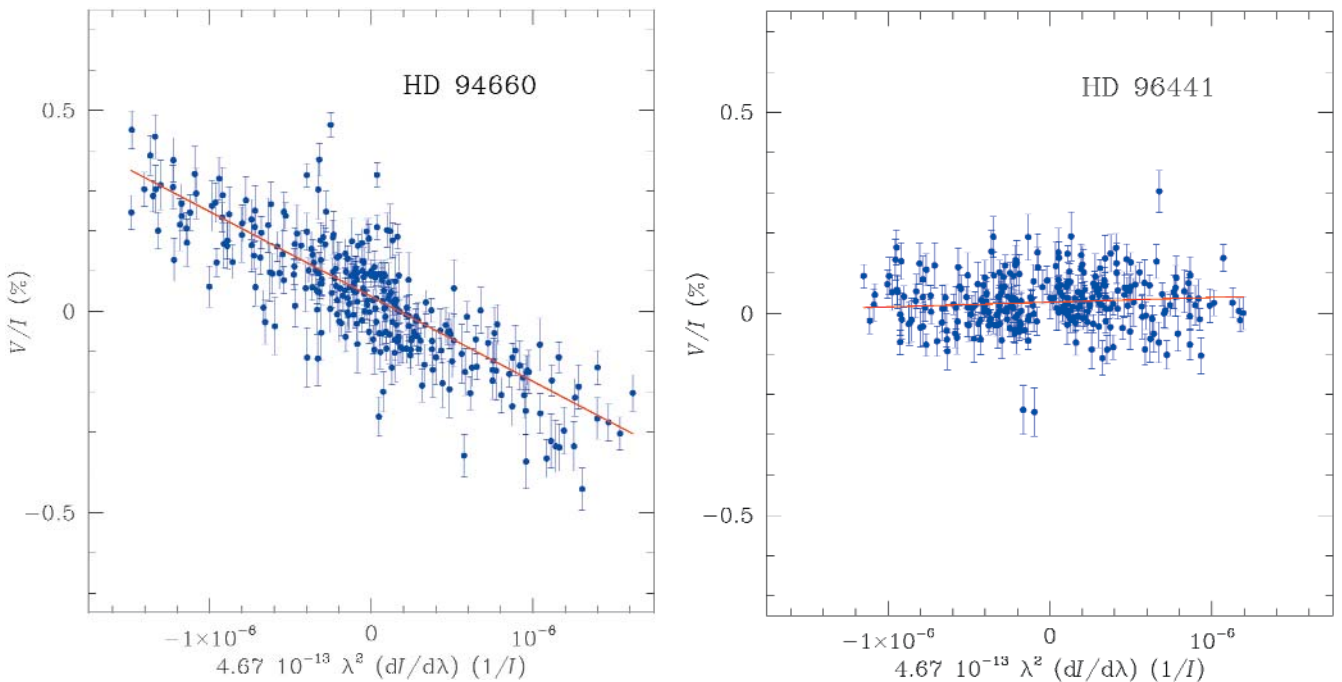


Figure 3: The slope of the red line (obtained via a least-square technique to the observed data) is proportional to the stars’ mean longitudinal field. For the magnetic star HD 94660 (left panel) we measured $\langle B_z \rangle = -2110 \pm 50$ G. For the non magnetic star HD 96441 (right panel) there is no magnetic field detection.

is in fact strictly related to the precision that we want to obtain: stronger field can be detected in fainter stars.)

Practically, what is the advantage of using FORS1 + ANTU to detect stellar magnetic fields, compared to the use of the previous techniques at the small- and middle-size-class telescopes? Do we just save telescope time and/or observe fainter stars?

Compared to the photopolarimetric technique of H β , the capability of observing several Balmer lines reflects in a substantial gain in terms of S/N, thus in terms of limit magnitude of the star that one wants to observe, even assuming an identical size for the collecting area.

A proper comparison with the technique based on high-resolution spectropolarimetry of metallic lines is less straightforward. With this technique, and in the cooler early-type stars, one can easily detect hundred metallic lines, thus obtaining a very high S/N per pixel is not a critical issue. One could suspect that the sole advantage of using FORS1 at the VLT is due to the large collecting area of the telescope, and that high-resolution spectropolarimetry of metallic lines would be still the best-choice to study stellar magnetic fields. This is certainly true for detailed *modelling* of magnetic fields in *slower* rotators, but low-resolution spectropolarimetry of H Balmer lines will remain the best-choice for *surveys* of magnetic stars, and for studying magnetic field's *faster* rotators, even when high-resolution spectropolarimetric capabilities will be available at the large-size-class telescopes.

The polarisation of H Balmer lines is well detectable also in relatively fast rotators, maybe up to 150 km s⁻¹. This represents a major advantage with respect to high-resolution spectropolarimetry of metallic lines, a technique which can successfully be applied only to stars that rotate with $v \sin i < 30\text{--}40$ km s⁻¹. Furthermore, the multi-object capability of FORS1 is available also in spectropolarimetric mode, which may substantially increase the efficiency of the telescope time.

On the whole, the use of a technique based on *low-resolution* spectropolarimetry on large-size-class telescopes such as FORS1 at the VLT opens the very interesting opportunity to study magnetic fields in upper main sequence stars fainter and faster rotating that it was possible before. Why do we care about this possibility?

5. Scientific Applications

Chemically peculiar stars do not represent a restricted class of objects, but a consistent fraction of all upper main sequence stars – about 20%. Understanding their physics is a compulsory step in order to have a comprehensive view of general stellar physics and evolution. For the time being, the physics of the atmospheres of magnetic Ap stars is far from being well understood. We believe that their chemical anomalies result from the influence of the magnetic field on the diffusing ions, possibly in combination with the influence of a weak, magnetically-directed wind (Michaud 1970; Babel 1992). The magnetic field is itself probably a fossil remnant, either of a field swept up by the star during formation, or possibly generated during pre-main-sequence evolution. In fact, it is unknown *when* the magnetic field of these stars forms. Does the magnetic field characterise their entire life on the main sequence, or does the magnetic field pop up at the surface at some stage? The results of some studies suggest that the magnetic fields and chemical anomalies in Ap stars originated at the moment when young Ae/Be stars arrive on the zero-age line, when the gaseous dust envelopes surrounding them dissipate and accretion ceases, i.e., magnetic Ap stars form at the ZAMS. On the other hand, Hubrig et al. (2000) have recently argued that magnetic stars are concentrated toward the centre of the main sequence band (for stellar masses $\leq 3 M_{\odot}$). Summarising, there are no firm conclusions about the role played by the magnetic field in the evolution of Ap stars (nor other non-peculiar stars). We do not know either whether all Ap stars

pass through a magnetic phase, or just some of them. This is due mainly to a single difficulty: due to their weird spectral energy distributions, it is not possible to locate Ap stars on a precise position along the main sequence strip (and hence derive their ages). Systematic errors seem to be very important. This is also illustrated by recent studies using Hipparcos data (Gomez et al. 1998; Hubrig et al. 2000) which draw apparently contradictory conclusions about the general evolutionary state of magnetic A stars.

The use of a FORS1 at the VLT opens the possibility to search for magnetic stars in open clusters, sampling the stellar evolution across the main sequence, and correlating the presence of magnetic fields with age. This is a task that has been unsuccessfully attempted in the past, being virtually out of reach of small and middle-size telescopes. With FORS1 used in multi-object spectropolarimetric mode it may become a feasible and interesting research field.

References

- Angel J.R.P., Landstreet J.D., 1970, *ApJ* **160**, L147.
Babcock H.W., 1947, *ApJ* **105**, 105.
Babcock H.W., 1958, *ApJS* **3**, 141.
Babel J., 1992, *A&A* **258**, 449.
Borra E.F., Landstreet J.D., 1980, *ApJS* **42**, 421.
Donati J.-F., Semel M., Carter B. D., Rees D.E., Cameron A.C., 1997, *MNRAS* **291**, 658.
Gomez A.E., Luri X., Grenier S., et al. 1998, *A&A* **336**, 953.
Hale G.E., 1908, *PASP* **20**, 220.
Hubrig S., North P., Mathys G., 2000, *ApJ* **539**, 352.
Kemp J.C., Swedlund J.B., Landstreet J.D., Angel J.R.P., 1970, *ApJ* **161**, 77.
Mathys G., 1989, *Fundamentals of Cosmic Physics*, **113**, p.143.
Mathys G., 1991, *A&AS* **89**, 121.
Mathys G., Hubrig S., Landstreet J.D., Lanz T., Manfroid J., 1997, *A&AS* **123**, 353.
Michaud G., 1970, *ApJ* **160**, 641.
Putney A., 1997, *ApJS* **112**, 527.
Robinson R.D., Worden S.P., Harvey J.V., 1980, *ApJ* **236**, L155.
Schmidt G.D., Smith P.S., 1995, *ApJ* **448**, 305.

Colour composite of the spiral galaxy M83 in the visible. This mosaic is a composite of WFI images taken in the B, V, and R filters (3 × 200 sec in each filter). It shows the structure of the spiral galaxy M83 in great detail, especially its regions of active star formation and clusters. Such deep wide-field images of nearby galaxies are also very valuable for the search of low-surface-brightness companions to the central galaxy and of faint tidal structures in its outer regions. This colour composite was constructed by D. Froebrich and A. Scholz at Thüringer Landessternwarte Tautenburg from test data taken by J. Eislöffel and R. Mendez. ►



ANNOUNCEMENTS

PRELIMINARY ANNOUNCEMENT

ESO-CERN-ESA Symposium on Astronomy, Cosmology and Fundamental Physics

Garching, Germany
March 4–7, 2002

The connections between Astronomy, Cosmology and Fundamental Physics are well known, and become closer every day. Recent exciting developments in these fields include the structures in the cosmic background radiation, evidence for an accelerating Universe, searches for dark matter candidates, evidence for neutrino oscillations, space experiments on fundamental physics, and discoveries of extrasolar planets. ESO, CERN and ESA are thus involved in scientific endeavours and technologies which overlap considerably, and the importance of close communication and co-operation between them is clear.

This joint Symposium is the first to be co-organised and co-sponsored by all three organisations. Topics will include scientific areas of interest to the communities of the three organisations: astronomy from ground and space, cosmology and astro-particle physics, and fundamental physics in a wider context. It is meant to give a broad overview, and to highlight the contributions of the three organisations, their plans, and the synergies between them. The programme will consist largely of invited reviews and discussion, although there will also be some shorter contributed papers and posters.

Scientific Organising Committee:

R. Battiston (Univ. of Perugia), R. Bender (Univ. of Munich), A. de Rujula (CERN), L. DiLella (CERN), C. Fabjan (CERN), A. Gimenez (ESA), M. Jacob (CERN), F. Pacini (Arcetri), A. Renzini (ESO), P. Shaver (ESO; chair), M. Spiro (Saclay), B. Taylor (ESA), P. van der Kruit (Univ. of Groningen), S. Vitale (Univ. of Trento), S. Volonté (ESA), M. Ward (Univ. of Leicester)

More details and a registration form will be posted at:

<http://www.eso.org/gen-fac/meetings/symp2002>

or contact symp2002@eso.org for further information

Symposium secretaries: Christina Stoffer and Britt Sjoeborg
European Southern Observatory, Karl-Schwarzschild-Str. 2, 85748 Garching bei Muenchen, Germany
Fax: +49 89 32006 480
E-Mail: symp2002@eso.org

International Conference on Light Pollution

There will be a Conference on Light Pollution held in La Serena, Chile, on the 5th to 7th of March 2002. The aim of the meeting is the open discussion and dissemination of information about light and radio frequency pollution with the emphasis on its effects on astronomy.

International experts will give invited talks on research, modelling, engineering, and legal aspects of light pollution and its control; lighting engineering and light pollution control associations (IDA, OTPC, OPCC, CIE, IESNA, etc.) will report on their activities and we solicit contributed talks and posters from individuals involved in the subject; there will be visits to local astronomical observatories (CTIO, ESO, OCIW, Mamalluca), the photometric laboratory of the University of Valparaíso, and to the 3rd Millennium Cross of Coquimbo, a successful light control project, as well as a conference dinner and press conference.

For more information on this conference, please visit the following web sites:

www.opcc.cl

www.iau.org/IAU/News

www.darksky.org/ida/ida_2/index.html

ESO VACANCY

Applications are invited for the position of

HEAD OF ADMINISTRATION

ESO employs in total approximately 500 staff members, and the Administration Division comprises the Administration at the Headquarters in Garching near Munich and the Administration in Santiago in Chile. The successful candidate will be supported by some 50 qualified staff members. As a member of the ESO Management Board the Head of Administration contributes essentially to the development of the overall policy, strategic planning, relations to the members of personnel and maintains professional contacts at highest level outside the Organisation. The main task is to provide efficient administrative services and advice to the Director General, Division Leaders and to staff members in the scientific and technical areas in the fields of financial planning and accounting, personnel management, purchasing, legal and contractual matters, information systems and building and site maintenance.

Beside an appropriate professional qualification, the ideal candidate will have substantial management and leadership experience within a scientific organisation, preferably international. Knowledge of administrative, legal, financial and personnel procedures are required. Excellent communication skills and a very good knowledge of English are essential. Knowledge of German would be an important asset. Additional knowledge of other European languages, in particular Spanish, would be an advantage.

We offer an attractive remuneration package including a competitive salary (tax free), comprehensive social benefits and financial help in relocating your family. The initial contract is for a period of three years with the possibility of a fixed-term extension. Serious consideration will be given to outstanding candidates willing to be seconded to ESO on extended leaves from their home institutions. Either the title or the grade may be subject to change according to qualification and the number of years of experience.

If you are interested in working in a stimulating international research environment and in areas of frontline science and technology, please consult our homepage <http://www.eso.org> for details and forward your résumé (in English) to ESO, Mr. Roland Block, Head of Personnel Department, Karl-Schwarzschild-Str. 2, D-85748 Garching, Germany, Tel +49 89 320 06-589, e-mail: rblock@eso.org.

PERSONNEL MOVEMENTS

International Staff

(1 April – 30 June 2001)

ARRIVALS

EUROPE

KOKE, Thomas (D), Adm. Software Syst. Specialist
LI CAUSI, Gianluca (I), Associate
MARTEAU, Stéphane (F), Operations Support Scientist

CHILE

DAHLEM, Michael (D), Operations Staff Astronomer
IVANOV, Valentin (I), Fellow
KONTINEN, Samu (SF), Associate SEST
NIELBOCK, Markus (D), Fellow
PRITCHARD, John (NZ), Operations Staff Astronomer
SAVIANE, Ivo (I), Fellow

DEPARTURES

EUROPE

BROADHURST, Thomas (GB), User Support Astronomer
DAY, Philippa (GB), Technical Documentation Archivist
MIRALLES, Joan-Marc (I), Associate
MOUREAU, Serge (B), Electronic Technical Engineer
SPOON, Henrik (NL), Student

CHILE

FRANCOIS, Patrick (F), Astronomer
SEKIGUCHI, Tomohiko (J), Student

Local Staff

(1 April – 30 June 2001)

ARRIVALS

SALGADO IBARRA, Fernando, Electronics Engineer, Paranal
AUBEL NAVARRETE, Karla Renata, Telescope Instruments
Operator, La Silla

DEPARTURES

MORALES OSORIO, David, Accounting Clerk, Santiago
TIGHE CULLEN, Roberto, Óptico, La Silla

Scientific Preprints

(April–June 2001)

1413. S. Hubrig, D. Le Mignant, P. North and J. Krautter: Search for Low-Mass PMS Companions Around X-Ray Selected Late B Stars. *A&A*.
1414. F. Patat et al.: The Metamorphosis of SN 1998BW. *ApJ*.
1415. W. Hummel et. al.: H α Emission Line Spectroscopy in NGC 330. *A&A*.
1416. M. Bellazzini, F.R. Ferraro, E. Pancino: A Step Toward the Calibration of the RGB Tip as a Standard Candle. *ApJ*.
1417. G. Andreuzzi, G. De Marchi, F.R. Ferraro, F. Paresce, L. Pulongone and R. Buonanno: VLT Observations of the Peculiar Globular Cluster NGC 6712. II. Luminosity and Mass Functions. *A&A*.

ESO, the European Southern Observatory, was created in 1962 to "... establish and operate an astronomical observatory in the southern hemisphere, equipped with powerful instruments, with the aim of furthering and organising collaboration in astronomy ..." It is supported by nine countries: Belgium, Denmark, France, Germany, Italy, the Netherlands, Portugal, Sweden and Switzerland. ESO operates at two sites. It operates the La Silla observatory in the Atacama desert, 600 km north of Santiago de Chile, at 2,400 m altitude, where several optical telescopes with diameters up to 3.6 m and a 15-m submillimetre radio telescope (SEST) are now in operation. In addition, ESO is in the process of building the Very Large Telescope (VLT) on Paranal, a 2,600 m high mountain approximately 130 km south of Antofagasta, in the driest part of the Atacama desert. The VLT consists of four 8.2-metre and three 1.8-metre telescopes. These telescopes can also be used in combination as a giant interferometer (VLTI). The first two 8.2-metre telescopes (called ANTU and KUEYEN) are in regular operation, and the other two will follow soon. Over 1200 proposals are made each year for the use of the ESO telescopes. The ESO Headquarters are located in Garching, near Munich, Germany. This is the scientific, technical and administrative centre of ESO where technical development programmes are carried out to provide the La Silla and Paranal observatories with the most advanced instruments. There are also extensive astronomical data facilities. In Europe ESO employs about 200 international staff members, Fellows and Associates; in Chile about 70 and, in addition, about 130 local staff members.

The ESO MESSENGER is published four times a year: normally in March, June, September and December. ESO also publishes Conference Proceedings, Preprints, Technical Notes and other material connected to its activities. Press Releases inform the media about particular events. For further information, contact the ESO Education and Public Relations Department at the following address:

EUROPEAN
SOUTHERN OBSERVATORY
Karl-Schwarzschild-Str. 2
D-85748 Garching bei München
Germany
Tel. (089) 320 06-0
Telefax (089) 3202362
ips@eso.org (internet)
URL: <http://www.eso.org>
<http://www.eso.org/gen-fac/pubs/messenger/>

The ESO Messenger:
Editor: Marie-Hélène Demoulin
Technical editor: Kurt Kjær

Printed by
J. Gotteswinter GmbH
Buch- und Offsetdruck
Joseph-Dollinger-Bogen 22
D-80807 München
Germany

ISSN 0722-6691

1418. H. Jerjen and M. Rejkuba: Tip of the Red Giant Branch Distance for the Sculptor Group Dwarf ESO 540-032. *A&A*.
1419. F. Poli, N. Menci, E. Giallongo, A. Fontana, S. Cristiani, S. D'Odorico: The Evolution of the Luminosity Function in Deep Fields: A Comparison with CDM Models. *ApJ Letters*.
1420. J.U. Fynbo et al.: Detection of the Optical Afterglow of GRB 000630: Implications for Dark Bursts. *A&A*.
1421. E. Le Floch, I.F. Mirabel, O. Laurent, V. Charmandaris, P. Gallais, M. Sauvage, L. Vigroux, and C. Cesarsky: Mid-Infrared Observations of NGC 1068 with the Infrared Space Observatory. *A&A*.
1422. J.U. Fynbo, P. Møller and B. Thomsen: Deep Imaging of Q2112+059: A Bright Host Galaxy but no DLA Absorber. *A&A*.
1423. F. Comerón and J. Torra: Near-Infrared Imaging of Compact HII Regions in Cygnus. *A&A*.
1424. F. Patat and G. Carraro: Star Clusterings in the Carina Complex: *U BV RI* Photometry of Bochum 9, 10 and 11. *MNRAS*.
1425. T.-S. Kim, S. Cristiani and S. D'Odorico: The Ly α Forest at $1.5 < z < 4$. *A&A*.
1426. P. Saracco, E. Giallongo, S. Cristiani, S. D'Odorico, A. Fontana, A. Iovino, F. Poli, E. Vanzella: Deep Near-IR Observations of the Chandra Deep Field and of the HDF South. *A&A*.
1427. P. Møller and J.U. Fynbo: Detection of a Redshift 3.04 Filament. *A&A*.
1428. J.U. Fynbo et al.: The Optical Afterglow and Host Galaxy of RGB 000926. *A&A*.
1429. J.U. Fynbo, P. Møller and B. Thomsen: Probing the Faint End of the Galaxy Luminosity Function at $z = 3$ with Ly α Emission. *A&A*.
1430. G.A. Wade, S. Bagnulo, O. Kochukhov, J.D. Landstreet, N. Piskunov, M.J. Stiff: LTE Spectrum Synthesis in Magnetic Stellar Atmospheres. The Interagreement of three Independent Polarised Radiative Transfer Codes. *A&A*.

Contents

C. Cesarsky: Successful First Light for the VLT Interferometer	1
--	---

TELESCOPES AND INSTRUMENTATION

A. Glindemann et al.: Light at the End of the Tunnel – First Fringes with the VLT	2
F. Paresce: Scientific Objectives of the VLT Interferometer	5
H. Jones, E. Pompei and the 2p2 Team: 2p2 Team News	7
L. Wisotzki, F. Selman and A. Gilliotte: Commissioning the Spectroscopic Mode of the WFI at the MPG/ESO 2.2-m Telescope at La Silla	8
C. Urrutia, T. Paz, E. Robledo, F. Gutierrez, D. Baade, F. Selman, F. Sanchez, J. Brewer and M. Scodreggio: VLT-Style Observing with the Wide Field Imager at the MPG/ESO 2.2-m Telescope at La Silla	14
J. Manfroid, F. Selman and H. Jones: Achieving 1% Photometric Accuracy with the ESO Wide Field Imager	16
R. Hook: Scisoft – a Collection of Astronomical Software for ESO Users	20
LATEST NEWS: C. Madsen: ESO High-Level Presentation in Porto	21

REPORTS FROM OBSERVERS

L. VANZI, L. Hunt and T. Thuan: SOFI and ISAAC Pierce the Obscured Core of SBS 0335-052	22
J.W. Sulentic, M. Calvani and P. Marziani: Eigenvector 1: An H-R Diagram for AGN?	25
J.-L. Monin, F. Ménard and N. Peretto: Disk Orientations in PMS Binary Systems Determined Through Polarimetric Imaging With UT1/FORS	29
S. Bagnulo, T. Szeifert, G.A. Wade, J.D. Landstreet and G. Mathys: Detecting Magnetic Fields of Upper-Main-Sequence Stars With FORS1 at ANTU	32
Colour composite of the spiral galaxy M83 in the visible	37

ANNOUNCEMENTS

Preliminary Announcement of an ESO-CERN-ESA Symposium on "Astronomy, Cosmology and Fundamental Physics"	38
International Conference on Light Pollution	38
ESO Vacancy "Head of Administration"	39
Personnel Movements	39
Scientific Preprints (April–June 2001)	39